UNIVERSIDADE ESTADUAL DE CAMPINAS
FACULDADE DE ENGENHARIA ELÉTRICA E DE COMPUTAÇÃO

John Willihans Cruz Condemaita

N-1 MULTI-CONTINGENCY TRANSIENT STABILITY CONSTRAINED OPTIMAL POWER FLOW WITH DISCRETE CONTROLLERS USING AN AC BRANCH FLOW MILP MODEL

UM MODELO DE PLIM PARA O FLUXO DE POTÊNCIA ÓTIMO COM RESTRIÇÕES DE ESTABILIDADE TRANSITORIA MULTI-CONTINGENCIA N-1 COM CONTROLES DISCRETOS UTILIZANDO A ABORDAGEM DE FLUXO EM RAMOS

CAMPINAS
2019

UNIVERSIDADE ESTADUAL DE CAMPINAS
Faculdade de Engenharia Elétrica e de Computação

John Willihans Cruz Condemaita

N-1 MULTI-CONTINGENCY TRANSIENT STABILITY CONSTRAINED OPTIMAL POWER FLOW WITH DISCRETE CONTROLLERS USING AN AC BRANCH FLOW MILP MODEL

UM MODELO DE PLIM PARA O FLUXO DE POTÊNCIA ÓTIMO COM RESTRIÇÕES DE ESTABILIDADE TRANSITORIA MULTI-CONTINGENCIA N-1 COM CONTROLES DISCRETOS UTILIZANDO A ABORDAGEM DE FLUXO EM RAMOS

Dissertation presented to the School of Electrical and Computer Engineering of the State University of Campinas in partial fulfillment of the requirements for the degree of Master in Electrical Engineering, in the area of Electrical Energy

Dissertação apresentada à Faculdade de Engenharia Elétrica e de Computação da Universidade Estadual de Campinas como parte dos requisitos exigidos para a obtenção do título de Mestre em Engenharia Elétrica, na área de Energia Elétrica

Supervisor/*Orientador*: MARCOS JULIO RIDER FLORES

ESTE EXEMPLAR CORRESPONDE À VERSÃO FINAL DISSERTAÇÃO DEFENDIDA PELO ALUNO JOHN WILLIHANS CRUZ CONDEMAITA, E ORIENTADA PELO PROF. DR. MARCOS JULIO RIDER FLORES

Prof. Dr. Marcos Julio Rider Flores

CAMPINAS
2019

Ficha catalográfica
Universidade Estadual de Campinas
Biblioteca da Área de Engenharia e Arquitetura
Rose Meire da Silva - CRB 8/5974

C889n

Cruz Condemaita, John Willihans, 1993-
N-1 Multi-contingency transient stability constrained optimal power flow with discrete controllers using an AC branch flow MILP model / John Willihans Cruz Condemaita. – Campinas, SP : [s.n.], 2019.

Orientador: Marcos Julio Rider Flores.
Dissertação (mestrado) – Universidade Estadual de Campinas, Faculdade de Engenharia Elétrica e de Computação.

1. Sistema de energia elétrica - Estabilidade. 2. Programação não-linear inteira mista. 3. Programação linear inteira mista. 4. Fluxo de carga elétrica. 5. Otimização não linear. I. Rider Flores, Marcos Julio, 1975-. II. Universidade Estadual de Campinas. Faculdade de Engenharia Elétrica e de Computação. III. Título.

Informações para Biblioteca Digital

Título em outro idioma: Um modelo de PLIM para o fluxo de potência ótimo com restrições de estabilidade transitória multi-contingencia N-1 com controles discretos utilizando a abordagem de fluxo em ramos
Palavras-chave em inglês:
Electric power system - Stability
Mixed integer non-linear programming
Mixed integer linear programming
Power flow
Non-linear optimization
Área de concentração: Energia Elétrica
Titulação: Mestre em Engenharia Elétrica
Banca examinadora:
Marcos Julio Rider Flores [Orientador]
Daniel Dotta
Leonardo Nepomuceno
Data de defesa: 30-07-2019
Programa de Pós-Graduação: Engenharia Elétrica

Identificação e informações acadêmicas do(a) aluno(a)
- ORCID do autor: https://orcid.org/0000-0002-1799-529X
- Currículo Lattes do autor: http://lattes.cnpq.br/4474001740609385

COMISSÃO JULGADORA – DISSERTAÇÃO DE MESTRADO

Candidato: John Willihans Cruz Condemaita. RA: 192689

Data da Defesa: 30 de julho de 2019

Título da Dissertação: "*N-1* Multi-contingency Transient Stability Constrained Optimal Power Flow with Discrete Controllers using an AC Branch Flow MILP Model Approach / Um Modelo De PLIM Para O Fluxo De Potência Ótimo Com Restrições De Estabilidade Transitória Multi-Contingencia N-1 Com Controles Discretos Utilizando A Abordagem De Fluxo Em Ramos."

Membros da banca:

Prof. Dr. Marcos Julio Rider Flores (Presidente, FEEC/UNICAMP)

Prof. Dr. Daniel Dotta (Membro interno, FEEC/UNICAMP)

Prof. Dr. Leonardo Nepomuceno (Membro externo, FE/UNESP-Bauru)

A ata de defesa, com as respectivas assinaturas dos membros da Comissão Julgadora, encontra-se no processo de vida acadêmica do aluno.

This dissertation is dedicated to God, to my parents,
Luzmila and Victor, and my sister, Carmen.

ACKNOWLEDGEMENTS

Thank you, God, for everything in my life.

I would like to thanks to my advisor, Professor Marcos Julio Rider Flores for his support and his knowledge applied to this research work.

I must express my profound gratitude to my parents, Luzmila and Victor, my sister, Carmen, to my grandparents, Sebastian, Evangelina, Leonardo and Alejandrina, to the rest of my family, to my friends, Saul, Benjamin and Anibal, and to my little piece of heaven, for their unconditional support.

I would like to thank my friends who accompanied me in this master's project, especially to Fransk, Paolo, Jose, Pavel, Hever, Claudia, Javier, Erik, Luis Ugarte, Camilo and Luigi, my friends from LE–23 and LE–19, my friends from the GOU beraká and from the entrepreneurial league, muchas gracias amigos.

This study was financed in part by the Coordenação de Aperfeiçoamento de Pessoal de Nível Superior - Brasil (CAPES) - Finance Code 001.

"A calm and humble life will bring more happiness
than the pursuit of success and the constant
restlessness that comes with it"
Albert Einstein

ABSTRACT

This work presents a mixed integer non-linear programming (MINLP) model for the N-1 multi–contingency transient stability constrained optimal power flow using an AC branch flow model. Transformers with on-load tap changers (OLTC) and switchable shunt elements are considered as discrete controls. The objective is to minimize the power generation and load shedding costs during steady-state operation. The implicit trapezoidal integration rule is used to integrate the time-domain differential equations used to represent the classical transient stability model of synchronous machines. Through linearization techniques, the original MINLP model is approximated into a mixed integer linear programming (MILP) model. The use of a MILP model guarantees convergence to optimality by using convex commercial solvers. In order to validate the approximations, the steady-state operating points and the transient stability results obtained by the proposed methodology are compared to those obtained using an exact AC power flow algorithm and a transient stability program. The 9–Bus/3–Generator WSCC, 14–Bus/5–Generator IEEE, 39–Bus/10–Generator New England and 68–Bus/16–Generator IEEE systems are used to show the efficiency of the proposed method. Results show that the proposed model provides transient stable solutions at a minimum generation cost.

Keywords*: AC branch flow model, N-1 multi–contingency analysis, optimal power flow with discrete controls, transient stability assessment, mixed integer linear programming.*

RESUMO

Neste trabalho apresenta-se um modelo de programação não linear inteira mista (PNLIM) para o fluxo de potência ótimo com restrições de estabilidade transitória N-1 multi–contingencia utilizando o modelo AC de fluxo em ramos. Transformadores com comutadores de taps em carga e elementos shunts comutáveis são considerados como variáveis discretas. A função objetivo é a minimização do custo de geração e corte de carga durante a operação em estado estacionário. A regra trapezoidal implícita é utilizada para a integração das equações diferencias no domínio do tempo utilizadas para representar o modelo clássico da máquina síncrona para estudos de estabilidade transitória. Por meio de técnicas de linearização o modelo PNLIM original é aproximado em um modelo de programação linear inteira mista (PLIM). A utilização de um modelo PLIM garante a convergência num ponto ótimo utilizando solvers convexos comerciais. A fim de validar os resultados das aproximações, os pontos de operação de estado estável obtidos e os resultados da estabilidade transitória são comparados com os obtidos por um programa de fluxo de carga AC exato e um programa de estabilidade transitória. Os sistemas da WSCC 9–nós/3–Geradores, IEEE 14–nós/5–Geradores, Nova Inglaterra 39–nós/10–Geradores e IEEE 68–nós/16–Geradores são utilizados para mostrar a eficiência da metodologia proposta. Os resultados mostram que o modelo proposto proporciona soluções estáveis a um mínimo custo.

Palavras-chave*: Fluxo em ramos AC, analise N-1 multi–contingencia, fluxo de potência ótimo com controles discretos, avaliação de estabilidade transitória, programação linear inteira mista.*

LIST OF FIGURES

LIST OF TABLES

NOTATION

Sets:

Ω_{B}	Set of buses
Ω_{L}	Set of branches
$\Omega_{\mathrm{L}^{\mathrm{red}}}$	Set of branches of the reduced network
Ω_{C}	Set of plausible contingencies
Ω_{G}	Set of generators

Parameters:

a_i^{g}	Quadratic coefficient of production cost at bus i
b_i^{g}	Linear coefficient of production cost at bus i
c_i^{g}	Constant coefficient of production cost at bus i
c^{ls}	Load Shedding cost
g_i^{sh}	Shunt conductance at bus i
b_i^{sh}	Shunt Susceptance at bus i
$B_{m,c,t}^{\mathrm{sh,red}}$	Shunt susceptance of the reduced network at bus m, contingency c and time t
$B_{i,j}^{\mathrm{sh}}$	Half susceptance at branch ij
H_m	Inertia constant of generator m
D_m	Damping constant of generator m
V_i^0	Initial voltage magnitude at bus i
E_m^0	Initial internal voltage magnitude of generator m

$\overline{E}, \underline{E}$	Maximum and minimum internal voltage magnitudes
$G_{m,c,t}^{\mathrm{sh,red}}$	Shunt conductance of the reduced network at bus *m*, contingency *c* and time *t*
$\overline{I}_{ij}$	Maximum current magnitude at branch ij
$\overline{I}_{mn,c}^{\mathrm{red}}$	Maximum current magnitude of the reduced network at branch mn, and contingency *c*
N_{t_1}	Number of discrete time steps during fault
N_{t_2}	Number of discrete time steps during post-fault
$\overline{nt}_{ij}$	Maximum number of taps for the OLTC transformer at branch ij
P_i^0, Q_i^0	Initial active and reactive power generation at bus i
P_i^d, Q_i^d	Active and reactive power demand at bus i
P_m^m	Mechanical power input at generator *m*
$\overline{P}_i^g, \underline{P}_i^g$	Maximum and minimum active generation at bus i
$\overline{Q}_i^g, Q_i^g$	Maximum and minimum reactive generation at bus i
R_{ij}	Resistance at branch ij
X_{ij}	Reactance at branch ij
$R_{mn,c,t}^{red}$	Resistance of the reduced network at branch mn, contingency *c*, and time *t*
Reg_{ij}	Transformer regulation at branch ij
t_c^{fc}, t_c^{max}	Fault clearance and maximum simulation time in contingency *c*
$\overline{V}, \underline{V}$	Maximum and minimum voltage magnitudes
$X_{mn,c,t}^{\mathrm{red}}$	Reactance of the reduced network at branch mn, contingency *c*, and time *t*
X_{d_m}	Transient reactance of generator *m*
Z_{ij}	Impedance at branch ij

$Z_{mn,c,t}^{\text{red}}$	Impedance of the reduced network at branch mn, contingency c, and time t
$\overline{\delta}, \underline{\delta}$	Maximum and minimum rotor angle relative to the center of inertia
δ_m^0	Initial pre-fault rotor angle at generator m
$\delta_{m,c,t}^0$	Initial angle of the rotor at generator m, contingency c, and time t
θ_m^0	Initial voltage angle at bus i
$\Delta\overline{\omega}, \Delta\underline{\omega}$	Maximum and minimum deviation from the reference of the angular speed
$\Delta_{c,t}$	Length of the discrete time steps in contingency c, and time t
ω_0	System angular speed
Γ	Number of piece-wise discretization blocks

Continuous variables:

E_m, E_m^{sqr}	Internal voltage magnitude at generator m and its square equivalent
I_{ij}, I_{ij}^{sqr}	Current magnitude at branch ij and its square equivalent
$I_{mn,c,t}^{\text{red}}$	Square current magnitude of the reduced network at branch mn, contingency c, and time t
P_{ij}, Q_{ij}	Active and reactive power flow at branch ij
$P_i^{\text{g}}, Q_i^{\text{g}}$	Active and reactive power generated at bus i
$P_{m,c,t}^{\text{e}}$	Active electric power generated at bus m, contingency c, and time t
$P_{mn,c,t}^{\text{red}}$	Active power flow of the reduced network at branch mn, contingency c, and time t
r_i	Load shedding percent at bus i
$Q_{m,c,t}^{\text{e}}$	Reactive electric power generated at bus m, contingency c, and time t
$Q_{mn,c,t}^{\text{red}}$	Reactive power flow of the reduced network at branch mn, contingency c, and time t
Q_i^{sh}	Reactive power generation of the shunt element at bus i

V_i, V_i^{sqr}	Voltage magnitude at bus i and its square equivalent
$\tilde{V}_i, \tilde{V}_i^{sqr}$	Regulated voltage of the OLTC transformer at bus i and its square equivalent
$V_{ij,k}^{c}$	Auxiliary variable used for the linearization of the product between V_i^{sqr} and $t_{ij,k}$
δ_m	Pre-fault rotor angle at generator *m*
$\delta_{m,c,t}$	Angle of the rotor at generator *m*, contingency *c*, and time *t*
$\delta_{c,t}^{COI}$	Angle of the center of inertia at contingency *c*, and time *t*
$\Delta\omega_{m,c,t}$	Deviation from the reference of the angular speed at generator *m*, contingency *c*, and time *t*
θ_i	Voltage angle at bus i

Binary and Integer Variables:

h_i	Binary operation of the shunt element at bus i
nt_{ij}	Integer operation of the OLTC transformer at branch ij
$t_{ij,k}$	Binary operation of the OLTC transformer at branch ij, and tap position *k*

TABLE OF CONTENTS

CHAPTER ONE: INTRODUCTION

Optimal power flow (OPF) is used worldwide for optimizing the operation and planning of electric power systems (EPS). If carefully tuned, the OPF can provide quality control actions for the economical and reliable operation of EPS in future scenarios of generation and demand (DOMMEL and TINNEY, 1968). Including transient stability constraints (TSC) into the OPF is a natural extension, known as TSC-OPF. The solution of the TSC-OPF problem provides an economic steady-state operation in terms of production (i.e., power generation) costs and, if the EPS is subjected to a large disturbance, it should be able to guarantee transient stability in terms of the rotor angle and the angular speed of synchronous machines. However, solving the TSC-OPF is a challenging task, because transient stability assessment requires the solution of multiple time-domain differential equations which, combined with the non-linear algebraic equations used to represent the AC steady-state operation of EPS increases the computational complexity of the optimization problem (ABHYANKAR, GENG, *et al.*, 2017) (GENG, ABHYANKAR, *et al.*, 2017).

With the advent of modern optimization methods and high-performance computing, there has been an ongoing interest for modeling and solving the TSC-OPF problem. Authors in (CAI, CHUNG and WONG, 2008) proposed a differential evolution algorithm, and authors in

(JIN and XIANG, 2014) used a multi-objective parallel Non–Dominated Sorting Genetic Algorithm II (NSGA-II) to solve the TSC–OPF problem. In (SAHA, BHATTACHARYA, *et al.*, 2018) is developed a relatively new metaheuristic technique to solve the TSC-OPF based on collective decision optimization (CDO) considering a basic formulation of the transformers taps and shunt compensation, in (XIA, CHAN, *et al.*, 2015) is develop an enhanced particle swarm optimization method to solve the TSC-OPF considering a dynamic model of VAr compensators and thyristor-controlled series capacitors, to solve the dynamic transient equations by direct methods and in (CHEN, LUO, *et al.*, 2016) is solved the TSC-OPF by differential evolution considering transformers tap regulation. Although metaheuristics, such as genetic algorithms and evolutionary methods, are easy to implement and to deploy, they cannot guarantee optimality at any step of the process. On the other hand. In (ARREDONDO, CASTRONUOVO, *et al.*, 2018), the TSC-OPF is solved by a nonlinear programming solver, and the performance of three different integration methods are compared.

In (YANG, LIU, *et al.*, 2017) (YANG, LIU, *et al.*, 2018) is presented a parallel solution of the multi-contingency TSC-OPF based on the recursive reduced-order method. Another work where is presented a parallel environment are in (YANG, QIN, *et al.*, 2018) where is applied an exact optimality condition to solve the TSC-OPF.

Authors in (CHEN, TAKA and OKAMOTO, 2001) and (TONG, LING and QI, 2008) propose to the TSC–OPF problem using functional transformation techniques to convert an infinite-dimensional optimization problem into a finite-dimensional optimization problem, and solved it by standard non-linear programming (NLP) techniques, which cannot guarantee optimality. In (HISKENS and PAI, 2000), authors applied the numerical trapezoidal integration rule to obtain the trajectory sensitivities, reducing the computational burden. For small systems. Moreover, in (GAN, THOMAS and ZIMMERMAN, 2000), authors used the numerical trapezoidal integration rule and successive linear programming to solve the TSC–OPF problem, disregarding discrete controls. An approach to solve the TSC–OPF problem considering multiple contingencies was developed in (YUAN, KUBOKAWA and SASAKI, 2003), where the differential equations were integrated using the trapezoidal integration rule, included into an NLP problem which is solved through an interior point method. Hybrid methods were also used to solve the TSC–OPF problem. In (MINANO, CUTSEM, *et al.*, 2010), authors developed the TSC-OPF by reducing the original multi-machine model to a one-machine infinite-bus equivalent. Moreover, authors in (CALLE, CASTRONUOVO and LEDESMA, 2013) also developed an NLP model to represent the TSC–OPF for isolated power systems. The constraints of the OPF and transient stability constraints (integrated using the trapezoidal integration rule) were embedded into the same NLP model, but only one contingency is considered at a time. In both cases, NLP solvers were used to solve the resulting TSC–OPF problem, disregarding discrete controls.

The specialized literature lacks an efficient optimization model that combines transient stability security constraints, AC economic dispatch and discrete controls (tap regulation and shunt operation), with a low computational complexity and reasonable accuracy. Finally, in Table 1.1, the proposed model characteristics are presented against with others found in the literature.

	Optimization Model	**Solution Technique**	**AC Branch Flow**	***N - 1* Multi-contingency**	**Discrete Variables**	**Time Domain Simulation**	**Machine Model**
Proposed Method	MINLP, MILP	CPLEX	●	●	●	●	Classic
(JIN e XIANG, 2014)	NLP	NSGA-II	∘	∘	∘	●	Classic
(YUAN, *et al*, 2003)	NLP	IPM	∘	●	∘	●	Classic
(MINANO, *et al.*, 2010)	NLP	CONOPT	∘	∘	∘	●	Classic
(CALLE, *et al*, 2013)	NLP	IPM	∘	∘	∘	●	Classic
(YANG, LIU, *et al.*, 2017)	NLP	IPM	∘	●	∘	●	Classic
(SAHA, *et al.*, 2018)	MINLP	CDO	∘	∘	●	∘	Classic
(ARREDONDO, *et al.*, 2018)	NLP	IPOPT	∘	∘	∘	●	4th Order
(XIA, CHAN, *et al.*, 2015)	MINLP	PSO	∘	∘	●	∘	4th Order
(YANG, LIU, *et al.*, 2018)	NLP	IPM-MPI	∘	●	∘	●	Classic
(YANG, QIN, *et al.*, 2018)	NLP	OC	∘	●	∘	●	Classic
(CHEN, LUO, *et al.*, 2016)	MINLP	DE	∘	∘	●	∘	Classic

Yes: ●; No: ∘

Table 1.1 – Features of the proposed method and comparison to other TSC-OPF.

In this work, the *N-1* multi-contingency TSC–OPF problem is modelled using an AC branch flow model. It is initially presented as a mixed integer non-linear programming (MINLP) model that combines, within the same formulation, the differential and non-linear algebraic equations used to model the transient stability constraints and the steady-state operation. The solution to the proposed model schedules the productions of the dispatchable generators and the following discrete controls:

- On-load tap changers of the transformers.

- Switchable shunt elements.

The objective of the proposed TSC–OPF model is to minimize the power generation and load shedding costs. Pre-fault, fault and post-fault stages are integrated in the proposed model for a set of different plausible contingencies. The fault clearance time for each contingency is determined by the operation of the protection system and an average time is used to simulate a large disturbance in transient stability assessments (KUNDUR, 1994). The implicit trapezoidal integration rule for a multi-machine system is used to integrate the transient-stability constraints during fault and post-fault. Using efficient linearization techniques, the original MINLP model is approximated into a mixed integer linear programming (MILP) model that can be formulated via mathematical programming languages, such as AMPL (FOURER, GAY and KERNIGHAN, 2003), and efficiently solved using off–the–shelf commercial solvers, such as CPLEX (ILOG, 2008). The steady-state operation and the transient stability assessment obtained by the methodology are compared with those obtained using an exact AC power flow and a transient stability program. The 9–bus/3–generators WSCC system, the 14–bus/5–generators IEEE system, the 39–bus/10–generator New England system and the 68–bus/16–generators IEEE system are used to demonstrate the efficiency and scalability of the proposed method.

1.1. OBJECTIVES

The aim of this master dissertation is to find a stable and economic operation point through an optimization model, as the main core of the proposed algorithm, considering a set of plausible contingencies. To reach this goal, the following partial objectives are proposed:

- Show the non–linear AC power flow optimization model based on branch flow, and linearize it via simplifications and approximations to guarantee optimality, reduce the error and computational time.

- Present a MINLP model to solve the OPF considering discrete controls as the shunt operation and the OLTC tap changers.

- Develop a new MINLP model for the N-1 multi–contingency TSC–OPF problem with discrete controls using an AC branch flow model.

- Develop an approximate MILP model for the proposed MINLP model, obtained from the application of efficient linearization techniques.

1.2. MOTIVATION OF THE WORK

In this dissertation the branch flow model is used to represent the AC power flow, and is applied to solve the classic OPF with discrete variables. Subsequently, TSC are added into the model. This kind of problem is nonlinear, because the equations that describe the power flow are non-linear. Thus, these challenges allow to use efficient linearization techniques that guarantee the global optimum and can be solved using well-known linear programming solvers.

The TSC–OPF problem is a relatively new approach. The use of the classic OPF to find an operation point and then apply a three-phase fault to ground and evaluate the stability in a transient stability program, is one of the basic approaches. However, introducing the TSC into the OPF in the same model and solve the problem by nonlinear optimization solvers or heuristic techniques are difficult; there are other techniques that cannot guarantee the optimal solution. The TSC-OPF includes power flow nonlinear equations and transient stability differential equations, which makes the solution of this problem a challenge.

The OPF is one of the most used tools to be extended to the inclusion of TSC into the same model. It represents a difficult challenge, because the well-known transient stability equations are differential and time-variants, and the power flow equations are time-invariant, this characteristic makes this problem difficult to solve, since it is expressed through a model of optimization a problem of dynamic character.

1.3. WORK CONTRIBUTIONS

The most outstanding contributions are the following:

- A linearized AC power flow based on branch flow approach, and subsequently the OPF is developed, considering discrete controls.

- A MINLP model for the N-1 multi–contingency TSC–OPF problem with discrete controls using an AC branch flow model.

- A MILP model for the N-1 multi–contingency TSC–OPF problem with discrete controls using an AC branch flow model.

- A novel optimization methodology to solve MILP problems, by a sequence of linear programing problems.

1.4. DISSERTATION STRUCTURE

This master project consists of six chapters detailed as follows:

Chapter 1.- INTRODUCTION: This chapter attempts to explain the motivation, objectives, contributions and justification of this master's project.

Chapter 2.- AC POWER FLOW BASED ON BRANCH FLOW MODEL: Explains the mathematical and electrical characteristics of AC power flow. Based on modeling of phase transformers and transmission lines, is presented the optimization model for the AC power flow exact equations. Subsequently is developed the nonlinear AC power flow based on branch flow approach, and via linearization and approximation techniques, is obtained the linear model for the exact AC power flow. Six power flow systems are used to validate the linear model in comparison with its nonlinear counterpart.

Chapter 3.- REVIEW OF OPTIMAL POWER FLOW AND TRANSIENT STABILITY ANALYSIS: Presents the concept of transient stability and optimal power flow and a brief literature review of transient stability constrained optimal power flow (TSC–OPF). The classical transient stability evaluation and multimachine systems considerations are presented. The advantages to use the trapezoidal integration rule is also presented, finally the most common TSC–OPF is presented, considering in the same model the solution of the three stages (pre–fault, fault and post–fault).

Chapter 4.- N-1 MULTICONTINGENCY TSC-OPF MINLP MODEL BASED ON BRANCH FLOW APPROACH: Based on the previous concepts is develop the MINLP model based on branch flow approach for the N-1 multi–contingencies TSC–OPF. Is presented the nonlinear model to solve the OPF with discrete controls based on branch flow approach. The calculation of the internal voltages and angles in the pre–fault stage, required for the subsequent dynamic calculation, is expressed by its branch flow equivalent. The swing equation is solved using the trapezoidal integration rule, and the electric power input is expressed using the branch flow approach. The transient stability is evaluated in the inequality or operative constraints, calculating the center of inertia (COI).

Chapter 5.- N-1 MULTICONTINGENCY TSC-OPF MILP MODEL BASED ON BRANCH FLOW APPROACH: This chapter shows the strategies to simplify the original MINLP model, via linearization and equivalence techniques, as seen in the develop of AC power flow based on branch flow model and other simplification techniques. The MINLP model is converted into a model of mixed integer linear programming (MILP), which can be solved by commercial solvers.

Chapter 6.- TEST CASES: Four common stability and power flow cases are evaluated to prove the efficiency and the scalability of the model. The small systems are used to prove the efficiency of the model, solving various cases (number of contingencies). It is also presented a sensitive analysis, varying the limits of the rotor angles and angular speeds and a comparative analysis of the TSC–OPF without TSC.

CHAPTER TWO:

AC POWER FLOW BASED ON BRANCH FLOW MODEL

The power flow model or load flow in energy systems is the starting point for the operational analysis of electric systems. It is used to determine the state of the network, the distribution of the power flow in the branches and others quantities of the system (MONTICELLI, 1983). In this approach, the network representation does not consider the time variation. This is a static approach, considering only the algebraic equations modeling (MONTICELLI, 1983). There are different methods for the solution of this problem like the Newton Raphson, decoupling, fast decoupling, etc.

This chapter presents the characteristics and modeling of the transmission lines and phase transformers. The AC power flow is modeled like an optimization problem and solved by a nonlinear programming solver. Besides, which will be modeled as an AC power flow based on branch flow model, and presenting a linearization procedure, based on approximations and equivalences, transforming the nonlinear programming (NLP) problem into a linear programming (LP) problem. Finally, the results obtained for different load flow testing systems are presented.

2.1. AC POWER FLOW MODEL USING POLAR FORMULATION

In this section the mathematical and electrical model of the transmission lines and phase transformers is developed to solve the AC power flow via polar formulation. Then, the optimization model to solve the AC power flow using this formulation is presented.

Mathematical model of transmission lines

For the transmission lines modeling, is considered a π equivalent representation, as shown in Figure 2.1, highlighting three parameters: series resistance R_{ij}, series reactance X_{ij}, and a shunt susceptance B_{ij}^{sh} in the transmission line between the i and j buses (MONTICELLI, 1983). The series impedance is defined by $Z_{ij} = R_{ij} + jX_{ij}$, and the series admittance $Y_{ij} = G_{ij} + jB_{ij}$.

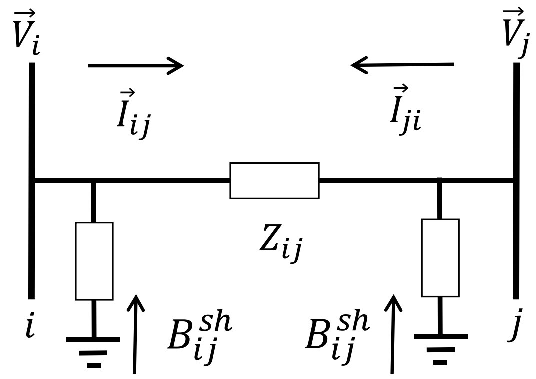

Figure 2.1 – Transmission line in π equivalent.

Where:

$$\vec{I}_{ij} = \dot{Y}_{ij}\left(\vec{V}_i - \vec{V}_j\right) + jB_{ij}^{sh}\vec{V}_j = \dot{Y}_{ij}\vec{V}_i - \dot{Y}_{ij}\vec{V}_j + jB_{ij}^{sh}\vec{V}_j \tag{2.1}$$

$$S_{ij}^{*} = P_{ij} - jQ_{ij} = \vec{V}_i^{*}\vec{I}_{ij} \tag{2.2}$$

From the equations (2.1) and (2.2) are obtained the active and reactive branch flows:

$$P_{ij}^{de} = V_i^2 G_{ij} - V_i V_j\big(G_{ij}\cos(\theta_i - \theta_j) + B_{ij}\cos(\theta_i - \theta_j)\big) \tag{2.3}$$

$$Q_{ij}^{de} = -V_i^2\big(B_{ij} + B_{ij}^{sh}\big) + V_i V_j\big(B_{ij}\cos(\theta_i - \theta_j) - G_{ij}\cos(\theta_i - \theta_j)\big) \tag{2.4}$$

$$P_{ji}^{para} = V_j^2 G_{ij} - V_i V_j\big(G_{ij}\cos(\theta_i - \theta_j) + B_{ij}\cos(\theta_i - \theta_j)\big) \tag{2.5}$$

$$Q_{ji}^{para} = -V_j^2\big(B_{ij} + B_{ij}^{sh}\big) + V_i V_j\big(B_{ij}\cos(\theta_i - \theta_j) - G_{ij}\cos(\theta_i - \theta_j)\big) \tag{2.6}$$

Mathematical model of phase transformers

The model presented in (MONTICELLI, 1983), is a general model for phase transformers $(\theta_i = \theta_p)$, as shown in the Figure 2.2, considering two buses i and j, a fictitious intermediary node p, a series admittance $Y_{ij} = G_{ij} + jB_{ij}$, an ideal autotransformer $1\!:a_{ij}$ and the relationship between the voltages V_i and V_p.

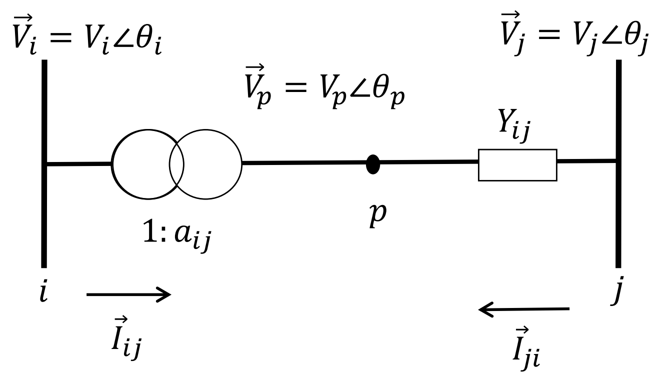

Figure 2.2 – Phase transformer.

Where the following relationship is distinguished:

$$\frac{\vec{V}_p}{\vec{V}_i} = \frac{V_p\angle\theta_p}{V_i\angle\theta_i} = a_{ij} \tag{2.7}$$

Figure 2.2 shows the model of an ideal autotransformer, this implies that the input and output powers are the same. That is, there are no active and reactive power losses as shown in (2.8):

$$\vec{V}_i\vec{I}_{ij}^* + \vec{V}_p\vec{I}_{ji}^* = 0 \tag{2.8}$$

Considering $\theta_p = \theta_i$, from the equations (2.7) and (2.8) is obtain:

$$\frac{\vec{I}_{ij}}{\vec{I}_{ji}} = -\frac{|\vec{I}_{ij}|}{|\vec{I}_{ji}|} = -a_{ij} \tag{2.9}$$

The branch current can be expressed as follows:

$$\vec{I}_{ij} = -a_{ij}Y_{ij}(\vec{V}_j - \vec{V}_p) = a_{ij}^2Y_{ij}\vec{V}_i - a_{ij}Y_{ij}\vec{V}_j \tag{2.10}$$

$$S_{ij}^* = P_{ij} - jQ_{ij} = \vec{V}_i^*\vec{I}_{ij} \tag{2.11}$$

From the equations (2.7), (2.10) and (2.11) we obtain the active and reactive power flows:

$$P_{ij}^{de} = (a_{ij}V_i)^2G_{ij} - a_{ij}V_iV_j\big(G_{ij}\cos(\theta_i - \theta_j) + B_{ij}\cos(\theta_i - \theta_j)\big) \tag{2.12}$$

$$Q_{ij}^{de} = -(a_{ij}V_i)^2B_{ij} + a_{ij}V_iV_j\,\big(B_{ij}\cos(\theta_i - \theta_j) - G_{ij}\cos(\theta_i - \theta_j)\big) \tag{2.13}$$

$$P_{ji}^{para} = V_j^2G_{ij} - a_{ij}V_iV_j\big(G_{ij}\cos(\theta_i - \theta_j) - B_{ij}\cos(\theta_i - \theta_j)\big) \tag{2.14}$$

$$Q_{ji}^{para} = -V_j^2(B_{ij} - B_{ij}^{sh}) + a_{ij}V_iV_j\big(B_{ij}\cos(\theta_i - \theta_j) + G_{ij}\cos(\theta_i - \theta_j)\big) \tag{2.15}$$

AC power flow general equations

From the above equations, the following general expressions are obtained for the active and reactive power flow in transmission lines and phase transformers.

$$P_{ij}^{de} = (a_{ij}V_i)^2 G_{ij} - a_{ij}V_iV_j \left(G_{ij}\cos(\theta_i - \theta_j) + B_{ij}\cos(\theta_i - \theta_j)\right) \tag{2.16}$$

$$Q_{ij}^{de} = -(a_{ij}V_i)^2 B_{ij} + a_{ij}V_iV_j\left(B_{ij}\cos(\theta_i - \theta_j) - G_{ij}\cos(\theta_i - \theta_j)\right) \tag{2.17}$$

$$P_{ji}^{para} = V_j^2 G_{ij} - a_{ij}V_iV_j\left(G_{ij}\cos(\theta_i - \theta_j) + B_{ij}\cos(\theta_i - \theta_j)\right) \tag{2.18}$$

$$Q_{ji}^{para} = -V_j^2 B_{ij} + a_{ij}V_iV_j\left(B_{ij}\cos(\theta_i - \theta_j) + G_{ij}\cos(\theta_i - \theta_j)\right) \tag{2.19}$$

Optimization model for the AC power flow problem

To obtain an operation point in electric power systems through an optimization problem, the equations shown above, are considered as a constraint in the model as follows:

$$\min f = \sum_{\forall\, i \in \Omega_{\mathrm{B}}, i = slack} P_i^g \tag{2.20}$$

Subject to:

$$P_i^g - P_i^d - \sum_{ij \in \Omega_{\mathrm{L}}} P_{ij}^{de} - \sum_{ji \in \Omega_{\mathrm{L}}} P_{ji}^{para} + V_i^2 g_i^{sh} = 0 \qquad \forall i \in \Omega_{\mathrm{B}} \tag{2.21}$$

$$Q_i^g - Q_i^d - \sum_{ij \in \Omega_{\mathrm{L}}} Q_{ij}^{de} - \sum_{ji \in \Omega_{\mathrm{L}}} Q_{ji}^{para} + V_i^2 b_i^{sh} = 0 \qquad \forall i \in \Omega_{\mathrm{B}} \tag{2.22}$$

$$P_{ij}^{para} = V_j^2 G_{ij} - a_{ij}V_iV_j\left(G_{ij}\cos(\theta_i - \theta_j) - B_{ij}\cos(\theta_i - \theta_j)\right) \qquad \forall ij \in \Omega_{\mathrm{L}} \tag{2.23}$$

$$P_{ij}^{de} = \left(a_{ij}V_i\right)^2 G_{ij} - a_{ij}V_iV_j\left(G_{ij}\cos(\theta_i - \theta_j) + B_{ij}\cos(\theta_i - \theta_j)\right) \qquad \forall ij \in \Omega_{\mathrm{L}} \tag{2.24}$$

$$Q_{ij}^{para} = -V_j^2\left(B_{ij} + B_{ij}^{sh}\right) + a_{ij}V_iV_j\left(B_{ij}\cos\left(\theta_i - \theta_j\right) + G_{ij}\cos\left(\theta_i - \theta_j\right)\right) \qquad \forall ij \in \Omega_L \qquad (2.25)$$

$$Q_{ij}^{de} = -\left(B_{ij} + B_{ij}^{sh}\right)\left(a_{ij}V_i\right)^2 + a_{ij}V_iV_j\left(B_{ij}\cos\left(\theta_i - \theta_j\right) - G_{ij}\cos\left(\theta_i - \theta_j\right)\right) \qquad \forall ij \in \Omega_L \qquad (2.26)$$

The objective function in (2.20) minimizes the active power generation. Constraints (2.21) and (2.22) are the equations of active and reactive power balance, respectively at i bus. Constraints (2.23)–(2.26) are the active and reactive power flows in the branches. Phase transformers and the π model of transmission lines are considered.

This power flow representation is nonlinear and nonconvex, due mainly to the presence of sines, cosines, squared variables and multiplication between variables, being suitable for the solution of this type of problems, solvers such as IPOPT (WÄCHTER and BIEGLER, 2005) and KNITRO (BYRD, J.NOCEDAL and WALTZ, 2006), and a mathematical language like AMPL (FOURER, GAY and KERNIGHAN, 2003).

2.2. BRANCH FLOW MODEL FOR AC POWER FLOW

In this section, an AC power flow using branch flow model is presented. Figure 2.3 shows a generic model of a branch in a transmission network, using the above considerations of polar model for power flow.

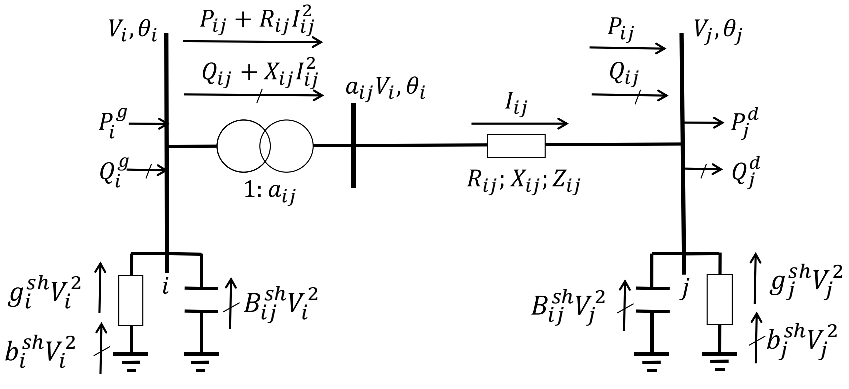

Figure 2.3 – Generic model of a branch in a transmission network.

From Figure 2.3 shown above, can be obtained a current $\vec{I}_{ij}$ as follows:

$$\vec{I}_{ij} = \left(\frac{P_{ij} + jQ_{ij}}{V_j}\right)^* \qquad \forall ij \in \Omega_{\mathrm{L}} \qquad (2.27)$$

Also, from the Figure 2.3 can be calculated a voltage drop in branch ij:

$$a_{ij}\vec{V}_i - \vec{V}_j = \vec{I}_{ij}(R_{ij} + jX_{ij}) \qquad \forall ij \in \Omega_{\mathrm{L}} \qquad (2.28)$$

From the equations (2.27) and (2.28) the following expression is calculated:

$$\left(a_{ij}\vec{V}_i - \vec{V}_j\right)\vec{V}_j^{\,*} = (P_{ij} - jQ_{ij})(R_{ij} + jX_{ij}) \qquad \forall ij \in \Omega_{\mathrm{L}} \qquad (2.29)$$

Considering that $V_i e^{j\theta_i} = V_i(\cos\theta_i + j\sin\theta_i)$, $V_j e^{j\theta_j} = V_j\left(\cos\theta_j + j\sin\theta_j\right)$ and $\theta_{ij} = \theta_i - \theta_j$, then (2.29) can be writen as:

$$a_{ij}V_iV_j\left[\cos\theta_{ij} + j\sin\theta_{ij}\right] - V_j^{\,2} = (P_{ij} - jQ_{ij})(R_{ij} + jX_{ij}) \qquad \forall ij \in \Omega_{\mathrm{L}} \qquad (2.30)$$

Identifying the real and imaginary parts in the equation (2.30) we obtain:

$$a_{ij}V_iV_j\cos\theta_{ij} = V_j^{\,2} + (R_{ij}P_{ij} + X_{ij}Q_{ij}) \qquad \forall ij \in \Omega_{\mathrm{L}} \qquad (2.31)$$

$$a_{ij}V_iV_j\sin\theta_{ij} = X_{ij}P_{ij} - R_{ij}Q_{ij} \qquad \forall ij \in \Omega_{\mathrm{L}} \qquad (2.32)$$

Adding the squares of (2.31) and (2.32), and using the trigonometric relationships, will be obtained:

$$\left[a_{ij}^2 {V_i}^2 - 2\left(R_{ij}P_{ij} + X_{ij}Q_{ij}\right)\right]V_j^2 - Z_{ij}^2\left(P_{ij}^2 + Q_{ij}^2\right) - V_j^2 = 0 \qquad \forall ij \in \Omega_{\mathrm{L}} \qquad (2.33)$$

Where can be note, that the angular difference θ_{ij} is eliminated, and it is a fourth-degree polynomial equation that calculated the voltage drop in the branch ij.

$$I_{ij}^2 = \frac{{P_{ij}}^2 - {Q_{ij}}^2}{{V_j}^2} \qquad \forall ij \in \Omega_{\mathrm{L}} \qquad (2.34)$$

From equations (2.33) and (2.34), is obtained:

$$a_{ij}^2 {V_i}^2 - 2\left(R_{ij}P_{ij} + X_{ij}Q_{ij}\right) - Z_{ij}^2 I_{ij}^2 - {V_j}^2 = 0 \qquad \forall ij \in \Omega_{\mathrm{L}} \qquad (2.35)$$

Considering branch flow model. A new the power flow model is obtained which is given by the following optimization problem.

$$\min f = \sum_{\forall\, i \,\in\, \Omega_{\mathrm{B}}, i = slack} P_i^g \qquad (2.36)$$

Subject to:

$$P_i^g - P_i^d - V_i^2 g_i^{sh} + \sum_{ji \,\in\, \Omega_{\mathrm{L}}} P_{ji} - \sum_{ij \in\, \Omega_{\mathrm{L}}} \left(P_{ij} + R_{ij} I_{ij}^2\right) = 0 \qquad \forall i \in \Omega_{\mathrm{B}} \qquad (2.37)$$

$$\begin{aligned} Q_i^g - Q_i^d + V_i^2 b_i^{sh} + \sum_{ji \,\in\, \Omega_{\mathrm{L}}} \left(Q_{ji} + B_{ji}^{sh} V_i^2\right) & \\ - \sum_{ij \in\, \Omega_L} \left(Q_{ij} - B_{ij}^{sh} V_i^2 + X_{ij} I_{ij}^2\right) = 0 & \qquad \forall i \in \Omega_{\mathrm{B}} \qquad (2.38) \end{aligned}$$

$$a_{ij}^2 {V_i}^2 - {V_j}^2 = 2\left(R_{ij}P_{ij} + X_{ij}Q_{ij}\right) + Z_{ij}^2 I_{ij}^2 \qquad \forall ij \in \Omega_{\mathrm{L}} \qquad (2.39)$$

$$V_i a_{ij} V_j \sin\left(\theta_i - \theta_j\right) = X_{ij}P_{ij} - R_{ij}Q_{ij} \qquad \forall ij \in \Omega_{\mathrm{L}} \qquad (2.40)$$

$$V_j^2 I_{ij}^2 = P_{ij}^2 + Q_{ij}^2 \qquad \forall ij \in \Omega_L \qquad (2.41)$$

The objective function (2.36) minimize the active power generation at bus i. Constraints (2.37) and (2.38) represent the active and reactive power balance in the system. Constraint (2.39) is the voltage drop in branch ij, (2.40) is the angular difference in branch ij and (2.41) is the current calculation at branch ij.

To the power flow solution, the active generation and the voltage in PV buses are constant, and the bus angle and voltage in reference bus are constant in the study period.

2.3. LINEARIZATION OF THE BRANCH FLOW MODEL FOR AC POWER FLOW

In the above model, denotes that it is a nonlinear programming problem, since there is multiplication of variables, square variables, trigonometric identities as sines and cosines. This model may be linearized using approximations and simplifications techniques.

It can be noted that in the load flow equations, the magnitudes of the current in the branches (I_{ij}) and the voltages in the nodes (V_i), appear only in the forms I_{ij}^2 and V_i^2, respectively, therefore it is convenient to consider the following variable changes:

$$V_i^{sqr} = V_i^2, V_i^{sqr} \geq 0 \qquad (2.42)$$

$$I_{ij}^{sqr} = I_i^2, I_{ij}^{sqr} \geq 0 \qquad (2.43)$$

The product V_iV_j can be linearized as follows, considering the nominal voltage magnitude (V^{nom}), the following linear equivalence can be obtained:

$$V_iV_j \approx V_j \approx (V^{nom})^2 \qquad (2.44)$$

The angular difference between two buses of a branch is normally small $\left(\theta_{ij} \approx 0\right)$, the following approximation can be made with the angles expressed in radians:

$$\sin\left(\theta_i - \theta_j\right) \cong \theta_i - \theta_j \tag{2.45}$$

The quadratic term $P_{ij}^2 + Q_{ij}^2$ can be linearized by parts such as in (2.46)–(2.53):

$$P_{ij}^2 + Q_{ij}^2 \approx \sum_{\gamma=1}^{\Gamma} m_{ij,\gamma}^S \Delta_{ij,\gamma}^P + \sum_{\gamma=1}^{\Gamma} m_{ij,\gamma}^S \Delta_{ij,\gamma}^Q \qquad \forall ij \in \Omega_{\mathrm{L}} \tag{2.46}$$

$$P_{ij}^+ - P_{ij}^- = P_{ij} \qquad \forall ij \in \Omega_{\mathrm{L}} \tag{2.47}$$

$$P_{ij}^+ + P_{ij}^- = \sum_{\gamma=1}^{\Gamma} \Delta_{ij,\gamma}^P \qquad \forall ij \in \Omega_{\mathrm{L}} \tag{2.48}$$

$$Q_{ij}^+ - Q_{ij}^- = Q_{ij} \qquad \forall ij \in \Omega_{\mathrm{L}} \tag{2.49}$$

$$Q_{ij}^+ + Q_{ij}^- = \sum_{\gamma=1}^{\Gamma} \Delta_{ij,\gamma}^Q \qquad \forall ij \in \Omega_{\mathrm{L}} \tag{2.50}$$

$$0 \leq \Delta_{ij,\gamma}^P \leq \bar{\Delta}_{ij,\gamma}^S \qquad \forall ij \in \Omega_{\mathrm{L}}, \gamma = 1 \ldots \Gamma \tag{2.51}$$

$$0 \leq \Delta_{ij,\gamma}^Q \leq \bar{\Delta}_{ij,\gamma}^S \qquad \forall ij \in \Omega_{\mathrm{L}}, \gamma = 1 \ldots \Gamma \tag{2.52}$$

$$P_{ij}{}^+, P_{ij}{}^-, Q_{ij}{}^+, Q_{ij}{}^- \geq 0 \qquad \forall ij \in \Omega_{\mathrm{L}} \tag{2.53}$$

The Figure 2.4 shows the linearization of $P_{ij}^2 + Q_{ij}^2$, where Γ represent the number of linearization blocks, $m_{ij,\gamma}^S$ is the slope of γ–th linearization block and is calculated by (2.54), $\bar{\Delta}_{ij}^S$ is upper limit of the linearization block and is show in (2.55).

$$m_{ij,\gamma}^S = (2\gamma - 1)\bar{\Delta}_{ij}^S \qquad \forall ij \in \Omega_{\mathrm{L}}, \gamma = 1 \ldots \Gamma \tag{2.54}$$

$$\overline{\Delta}_{ij}^{S} = \frac{\overline{V}\overline{I}_{ij}}{\Gamma} \qquad \forall ij \in \Omega_{\mathrm{L}} \qquad (2.55)$$

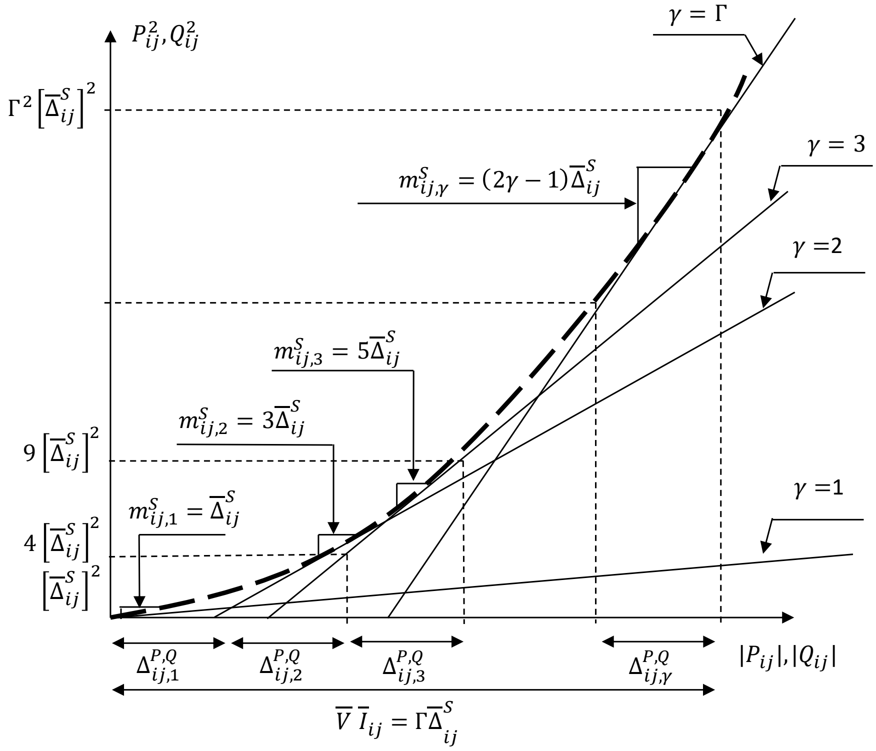

Figure 2.4 – $P_{ij}^2 + Q_{ij}^2$: Piecewise linearized.

Being the following the complete optimization model:

$$\min f = \sum_{\forall\, i \in \Omega_{\mathrm{B}}, i = slack} P_i^g \qquad (2.56)$$

Subject to:

$$P_i^g - P_i^d - V_i^{sqr} g_i^{sh} + \sum_{ji \in \Omega_{\mathrm{L}}} P_{ji} - \sum_{ij \in \Omega_{\mathrm{L}}} \left(P_{ij} + R_{ij} I_{ij}^{sqr}\right) = 0 \qquad \forall i \in \Omega_{\mathrm{B}} \qquad (2.57)$$

$$Q_i^g - Q_i^d + V_i^{sqr} b_i^{sh} + \sum_{ji \in \Omega_{\mathrm{L}}} \left(Q_{ji} + B_{ji}^{sh} V_i^{sqr}\right) - \sum_{ij \in \Omega_L} \left(Q_{ij} - B_{ij}^{sh} V_i^{sqr} + X_{ij} I_{ij}^{sqr}\right) = 0 \qquad \forall i \in \Omega_{\mathrm{B}} \qquad (2.58)$$

$$a_{ij}^2 V_i^{sqr} - V_j^{sqr} = 2\left(R_{ij}P_{ij} + X_{ij}Q_{ij}\right) + Z_{ij}^2 I_{ij}^{sqr} \qquad \forall ij \in \Omega_\mathrm{L} \quad (2.59)$$

$$a_{ij}(V^{nom})^2\left(\theta_i - \theta_j\right) = X_{ij}P_{ij} - R_{ij}Q_{ij} \qquad \forall ij \in \Omega_\mathrm{L} \quad (2.60)$$

$$(V^{nom})^2 I_{ij}^{sqr} = \sum_{\gamma=1}^{\Gamma} m_{ij,\gamma}^S \Delta_{ij,\gamma}^P + \sum_{\gamma=1}^{\Gamma} m_{ij,\gamma}^S \Delta_{ij,\gamma}^Q \qquad \forall ij \in \Omega_\mathrm{L} \quad (2.61)$$

$$P_{ij}^+ - P_{ij}^- = P_{ij} \qquad \forall ij \in \Omega_\mathrm{L} \quad (2.62)$$

$$P_{ij}^+ + P_{ij}^- = \sum_{\gamma=1}^{\Gamma} \Delta_{ij,\gamma}^P \qquad \forall ij \in \Omega_\mathrm{L} \quad (2.63)$$

$$Q_{ij}^+ - Q_{ij}^- = Q_{ij} \qquad \forall ij \in \Omega_\mathrm{L} \quad (2.64)$$

$$Q_{ij}^+ + Q_{ij}^- = \sum_{\gamma=1}^{\Gamma} \Delta_{ij,\gamma}^Q \qquad \forall ij \in \Omega_\mathrm{L} \quad (2.65)$$

$$0 \le \Delta_{ij,\gamma}^P \le \bar{\Delta}_{ij,\gamma}^S \qquad \forall ij \in \Omega_\mathrm{L}, \gamma = 1 \dots \Gamma \quad (2.66)$$

$$0 \le \Delta_{ij,\gamma}^Q \le \bar{\Delta}_{ij,\gamma}^S \qquad \forall ij \in \Omega_\mathrm{L}, \gamma = 1 \dots \Gamma \quad (2.67)$$

$$P_{ij}{}^+, P_{ij}{}^-, Q_{ij}{}^+, Q_{ij}{}^- \ge 0 \qquad \forall ij \in \Omega_\mathrm{L} \quad (2.68)$$

$$I_{ij}^{sqr} \ge 0 \qquad \forall ij \in \Omega_\mathrm{L} \quad (2.69)$$

$$V_i^{sqr} \ge 0 \qquad \forall i \in \Omega_\mathrm{B} \quad (2.70)$$

The above model, is an approximate linear programming problem for the calculate of AC power flow, where (2.56) is the objective function representing the minimization of active generation, constraints (2.57) and (2.58) represent the active and reactive power balances in the system respectively, constraints (2.59) and (2.60) represent the voltage drop and the angular difference in branch ij respectively, constraints (2.61) and (2.62)–(2.68) are the constraints of the linearization of term $P_{ij}^2 + Q_{ij}^2$, and the constraints (2.69) and (2.70) are the constraints that guarantee that the magnitudes of voltage and current squared are positive. In addition, to the constraints presented above, the active generation and the voltage in PV buses are constant, and the bus angle and voltage in reference bus are constant in all study period.

2.4. TEST AND RESULTS

The tested systems are: The 9–bus system from Western System Coordinating Council (WSCC) of the university of Illinois, used to solve problems involving the calculation of electromechanical transient, the IEEE systems of 14, 30, 57, 118 and 300 buses of the university of Washington, for the nonlinear and linear model of AC power flow, considering a step numbers for the linear model in branch flow of $\Gamma = 50$. Comparative analysis show the degree of error of the linearized model comparing the values obtained with the nonlinear model. The power flow problem was modeled in the algebraic modeling language AMPL (FOURER, GAY and KERNIGHAN, 2003). The linearized AC power flow model was solved using the off-the-shelf convex solver CPLEX (ILOG, 2008), while the exact nonlinear AC power flow was solved by KNITRO (BYRD, J.NOCEDAL and WALTZ, 2006) solver. These deviations or percentage of error were determined according to the following formulations:

$$\varepsilon_P^{loss} = \left| \frac{P_{ij}^{de} + P_{ij}^{para} - (R_{ij} I_{ij}^{sqr\approx})}{\bar{S}_{ij}} \right| \times 100 \qquad \forall ij \in \Omega_{\mathrm{L}} \tag{2.71}$$

$$\varepsilon_Q^{loss} = \left| \frac{Q_{ij}^{de} + Q_{ij}^{para} - (X_{ij} I_{ij}^{sqr\approx} - B_{ij}^{shl} V_{ij}^{sqr\approx} - B_{ij}^{shl} V_{ij}^{sqr\approx})}{\bar{S}_{ij}} \right| \times 100 \qquad \forall ij \in \Omega_{\mathrm{L}} \tag{2.72}$$

$$\varepsilon_v^{\%} = \left| \frac{V_i^{AC} + V_i^{\approx}}{V_i^{AC}} \right| \times 100 \qquad \forall i \in \Omega_{\mathrm{B}} \tag{2.73}$$

$$\varepsilon_P^{de} = \left| \frac{P_{ij}^{de} - (P_{ij}^{\approx} + R_{ij} I_{ij}^{sqr\approx})}{\bar{S}_{ij}} \right| \times 100 \qquad \forall ij \in \Omega_{\mathrm{L}} \tag{2.74}$$

$$\varepsilon_P^{para} = \left| \frac{P_{ij}^{para} - (-P_{ij}^{\approx})}{\bar{S}_{ij}} \right| \times 100 \qquad \forall ij \in \Omega_{\mathrm{L}} \tag{2.75}$$

$$\varepsilon_Q^{de} = \left| \frac{Q_{ij}^{de} - (Q_{ij}^{\approx} - B_{ij}^{shl} V_{ij}^{sqr\approx} + X_{ij} I_{ij}^{sqr\approx})}{\bar{S}_{ij}} \right| \times 100 \qquad \forall ij \in \Omega_L \quad (2.76)$$

$$\varepsilon_Q^{para} = \left| \frac{Q_{ij}^{de} - \left(-\left(Q_{ij}^{\approx} + B_{ij}^{shl} V_{ij}^{sqr\approx}\right)\right)}{\bar{S}_{ij}} \right| \times 100 \qquad \forall ij \in \Omega_L \quad (2.77)$$

Where ε_P^{loss} is the percentage deviation between the active power loss of the nonlinear exact model and the linearized model, ε_Q^{loss}, is the percentage deviation between the reactive power loss of the nonlinear exact model and the linearized model in branch ij, $\varepsilon_v^{\%}$ is the percentage deviation of the voltage magnitude of the nonlinear exact model and the linearized model, ε_P^{de} and ε_Q^{de}, are the percentage deviation between the active and reactive power flow that leave the bus i and enter the bus j, obtained from the nonlinear exact model and the linearized model respectively. ε_P^{para} and ε_Q^{para} are the percentage deviation between the active and reactive power flow, that leave the bus j and enter the bus i, obtained from the nonlinear model and the linearized model respectively, where $\bar{S}_{ij}$, is the maximum capacity of the transmission line ij.

9-bus WSCC system

In this part of the work the results obtained for the 9-bus WSCC system are presented, which has 9 branches and 3 generators, is a system commonly used for transient stability analysis.

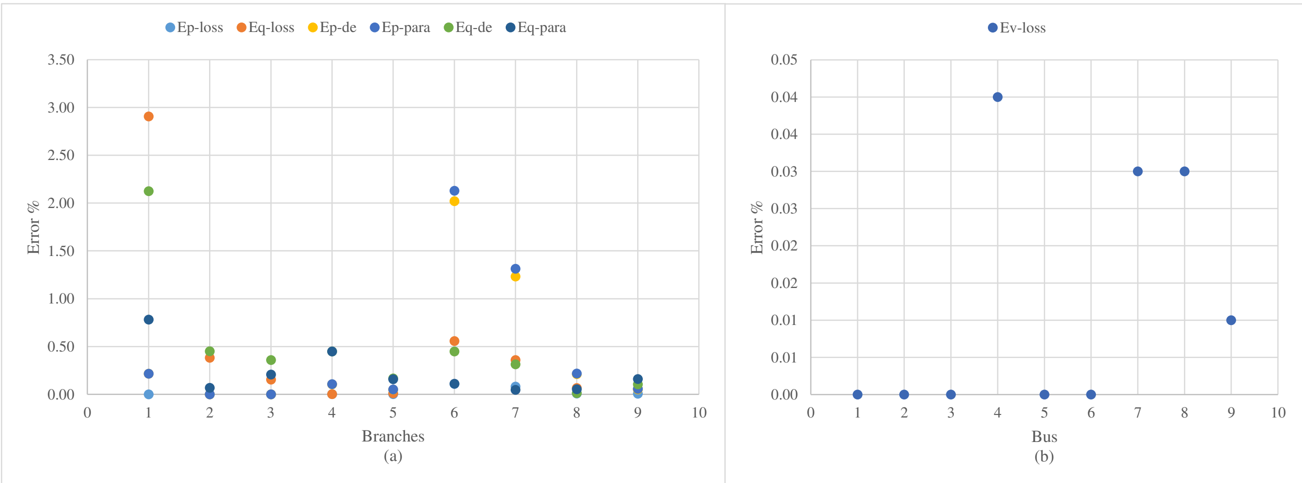

Figure 2.5– Percentage of deviations of the active and reactive power flow and voltages in the 9-bus system.

Figure 2.5 shows the percentage of deviations in each variable are small with respect to obtained by the nonlinear power flow model. In Figure 2.5(a), it can be note that the percentage deviations are smaller than 3% for the active and reactive power losses in the branches and the deviations of the power flow in the branches. In Figure 2.5(b), the percentage deviation of the voltage magnitude is less than 0.2%. The values of the losses for the nonlinear exact AC power flow and the linearized model were 4.641 MW and 4.880 MW, respectively.

14-bus IEEE system

The 14-bus IEEE system is presented, which has 20 branches and 5 generators, this system is commonly used for power flow problems.

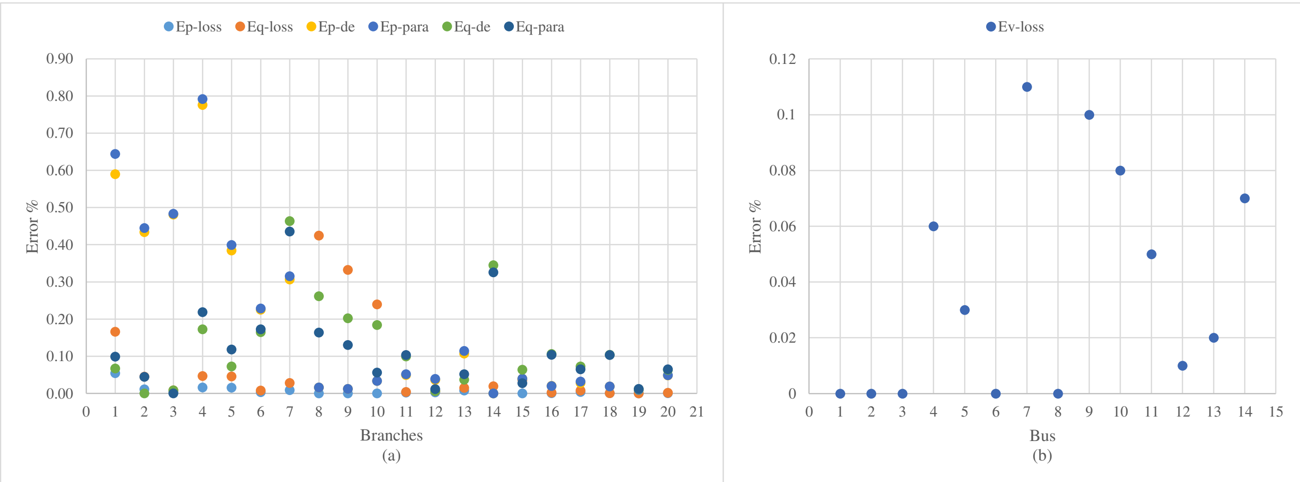

Figure 2.6 – Percentage of deviations active and reactive power flow and voltages in 14-bus system.

Figure 2.6 shows that the percentage deviations in each variable are small with respect to obtained by the nonlinear power flow model. In Figure 2.6(a) it can be seen that the percentage deviations are smaller than 0.8% for the active and reactive power losses in the branches and the deviations of the power flow in the branches. In Figure 2.6(b), the percentage deviation of the voltage magnitude is less than 0.12%. The values of the losses for the nonlinear exact AC power flow and the linearized model were 13.393 MW and 12.875 MW, respectively.

30-bus IEEE system

The 30-bus IEEE system is presented, which has 41 branches, this system is commonly used for power flow problems.

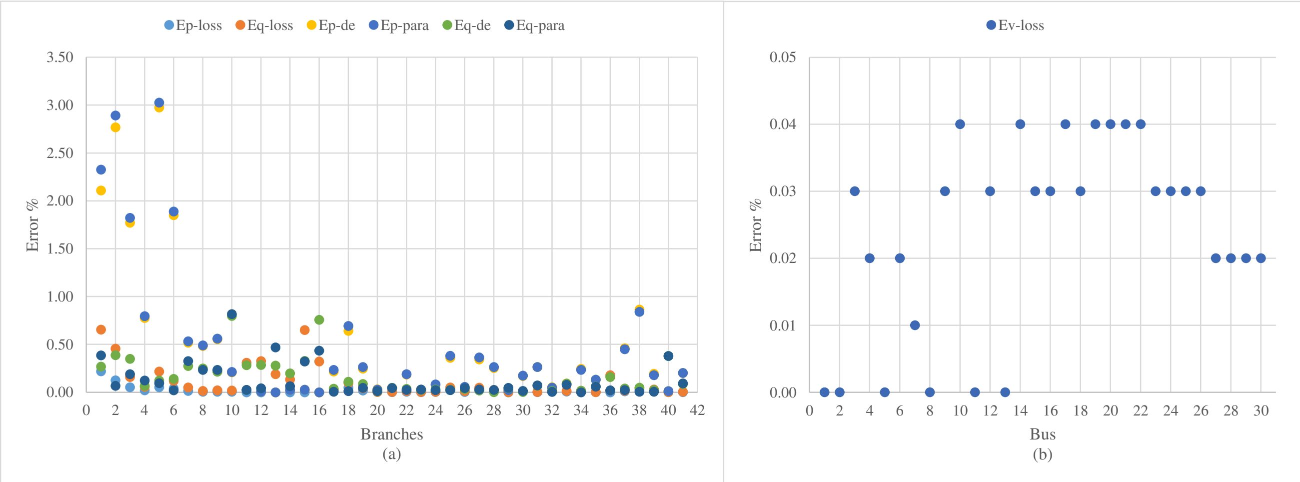

Figure 2.7 – Percentage of deviations active and reactive power flow and voltage in 30-bus system.

Figure 2.7 shows that the percentage deviations in each variable are small with respect to obtained by the nonlinear power flow model. In Figure 2.7(a) it can be seen that the percentage deviations are smaller than 3% for the active and reactive power losses in the branches and the deviations of the power flow in the branches. In Figure 2.7(b), the percentage deviation of the voltage magnitude is less than 0.045%. The values of the losses for the nonlinear exact AC power flow and the linearized model were 17.541MW and 16.796MW, respectively.

57-bus IEEE system

The 57-bus IEEE system is presented, which has 80 branches, this system is commonly used for power flow problems.

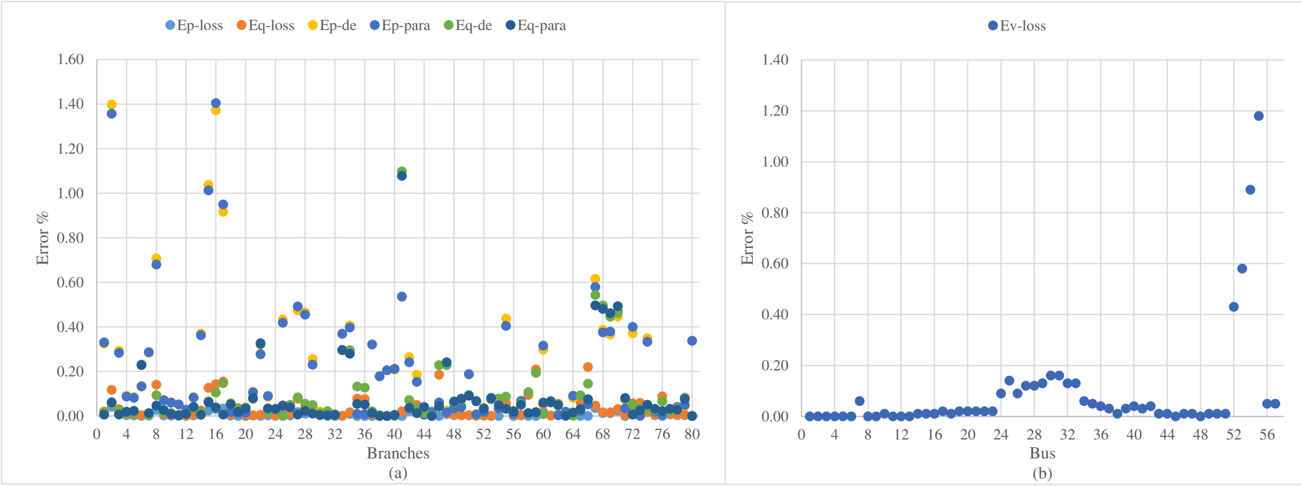

Figure 2.8 – Percentage of deviations active and reactive power flow and voltage in 57-bus system.

Figure 2.8 shows that the percentage deviations in each variable are small with respect to obtained by the nonlinear power flow model. In Figure 2.8(a) it can be seen that the percentage deviations are smaller than 1.4% for the active and reactive power losses in the branches and the deviations of the power flow in the branches. In Figure 2.8(b), the percentage deviation of the voltage magnitude is less than 1.2%. The values of the losses for the nonlinear exact AC power flow and the linearized model were 27.791MW and 27.981MW, respectively.

118-bus IEEE system

The 118-bus IEEE system is presented, which has 186 branches, this system is commonly used for power flow problems.

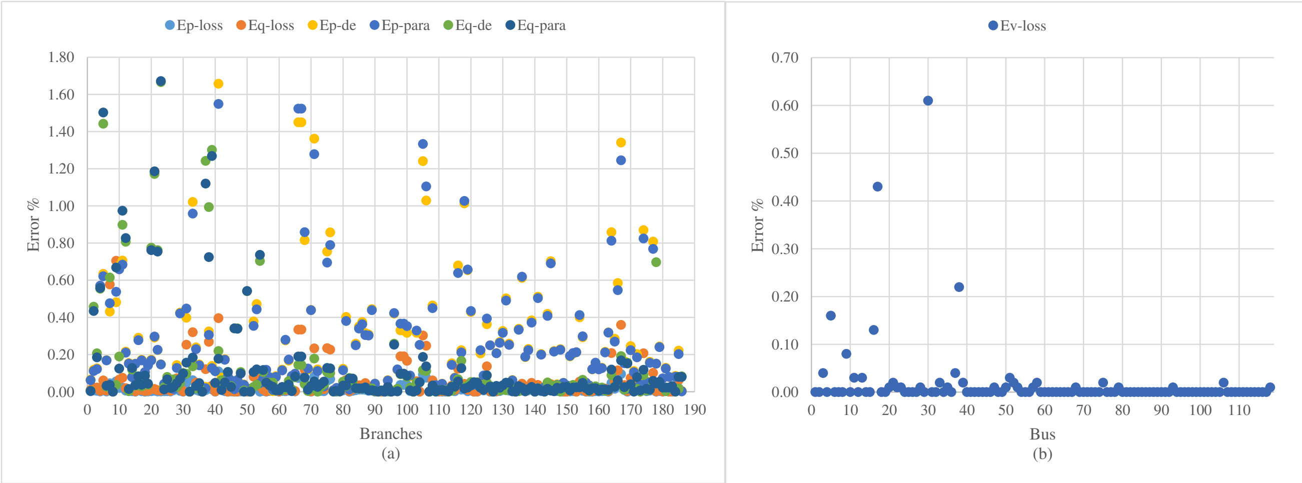

Figure 2.9 – Percentage of deviations active and reactive power flow and voltage in 118-bus system.

Figure 2.9 shows that the percentage deviations in each variable are small with respect to obtained by the nonlinear power flow model. In Figure 2.9(a) it can be seen that the percentage deviations are smaller than 1.8% for the active and reactive power losses in the branches and the deviations of the power flow in the branches. In Figure 2.9(b), the percentage deviation of the voltage magnitude is less than 0.6%. The values of the losses for the nonlinear exact AC power flow and the linearized model were 132.200MW and 131.806MW, respectively.

300-bus IEEE system

The 300-bus IEEE system is presented, which has 412 branches, this system is commonly used for power flow problems.

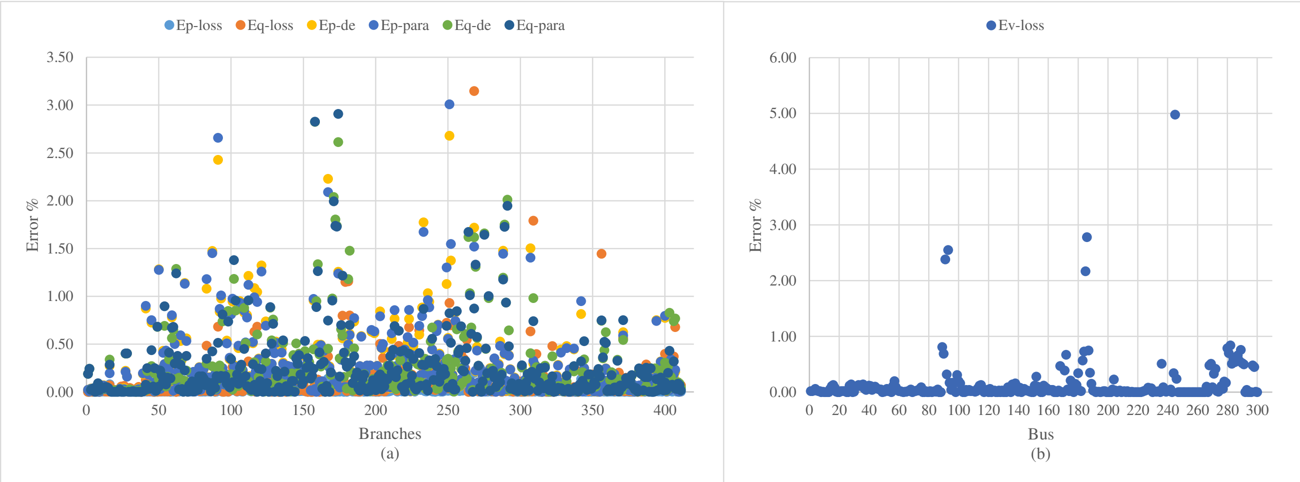

Figure 2.10 – Percentage of deviations active and reactive power flow and voltage in 300-bus system.

Figure 2.10 shows that the percentage deviations in each variable are small with respect to obtained by the nonlinear power flow model. In Figure 2.10(a) it can be seen that the average percentage deviations are smaller than 3.0% for the active and reactive power losses in the branches and the deviations of the power flow in the branches. In Figure 2.10(b), the average percentage deviation of the voltage magnitude is less than 3%. The values of the losses for the nonlinear exact AC power flow and the linearized model were 505.980MW and 503.042MW, respectively.

2.5. IMPORTANT REMARKS

In this chapter, two models were developed for the AC power flow: the exact or polar model and the power flow based on branch flow model. The branch-based power flow is easy to linearize. Both power flows were implemented in the well-known algebraic modeling language AMPL, and obtaining the results through commercial solvers such as CPLEX and KNITRO, for linear and nonlinear problems respectively.

From the results of both models, we obtained the comparisons between the exact model and the linearized model for the 9-bus WSSC system and the 14, 30, 57, 118 and 300 buses IEEE systems, which showed a good performance, obtaining errors of less than 2% for most cases, considering only a number of linearization steps of $\Gamma = 50$, emphasizing that for larger systems this number is not enough, since as the number of steps increases, the computational cost increases, but the results are more accurate. This fact makes the linearized model a good proposal for solving problems that involve the load flow.

CHAPTER THREE:

REVIEW OF OPTIMAL POWER FLOW AND TRANSIENT STABILITY ANALYSIS

In this chapter, the transient stability constrained optimal power flow (TSC–OPF) was developed as an extension of optimal power flow (OPF) with the inclusion of the time-domain differential equations which describes the behavior of the synchronous machines. The review of the literature respect to transient stability and the optimal power flow, the techniques for representing the transient stability constraints, the integration methods and the evolution of the TSC–OPF are also developed in this chapter.

3.1. OPTIMAL POWER FLOW PROBLEM

The optimal power flow (OPF) is a concept introduced in the 60's. It is cataloged as one of the most used and useful tools to solve problems of planning and operation of EPS. In the EPS operation OPF is useful to determine an optimum operating point and the appropriate control decisions and it helps to determine optimal future scenarios.

Since it is a well–studied problem in the energy systems area, it has many variations and applications, one of the most studied being the active–reactive OPF. The objective is to minimize the generation costs, considering as operational constraints, the amount of active and reactive power generation and the voltage levels. This approach is modeled as optimization problem.

The OPF is a natural extension of classic power flow, minimizing an objective function, subject to power flow equations as equality constraints and the operative constraints as the voltage and generation limits, making the OPF a non-linear programming problem, according to the following general scheme:

$$\min f(x) \tag{3.1}$$

Subject to:

$$\mathrm{G}(x) = 0 \tag{3.2}$$

$$H(x) \leq 0 \tag{3.3}$$

Where $f(x)$, is the objective function to minimize: Generation costs, active and reactive losses, etc.; $\mathrm{G}(x)$ are the equality constraints as the power flow equations, $H(x)$ are the inequality constraints as the technical and operating limits in the system.

The reference (DOMMEL and TINNEY, 1968) is one of the first works related with the OPF, in there is proposed a method based on power flow solution using the Newton method. This method is extended to yield an OPF solution, the reduced gradient procedure is used to finding the optimum and the penalty functions is used to handle functional inequality constraints. This sequence of methods is not able to guarantee convergence to the global optimum. Furthermore it is not considered the discrete variables as the OLTC regulation and shunt elements operation.

In the references (MONTICELLI, WEN-HSIUNG and LIU, 1992), (SANTOS and COSTA, 1995) and (SUN, ASHLEY, *et al.*, 1984) are used the Newton method to solve the OPF. In (MONTICELLI, WEN-HSIUNG and LIU, 1992) is proposed an adaptative method for handling movement penalties. In (SANTOS and COSTA, 1995) is proposed a Newton method to solve the OPF which operates with an augmented Lagrangian function associated with the original problem. In (SUN, ASHLEY, *et al.*, 1984), the OPF is solved by an explicit Newton method. The obtained results by these three methods have better convergence results that other techniques. However, the discrete controls are not considered.

In (ALSAC, BRIGHT, *et al.*, 1990) is present a solution of OPF via LP problems sequences, furthermore, (PHAN and KALAGNANAM, 2014) is one of the papers that includes in the OPF formulation the security constraints, where is proposed three different approaches to solve it by a global optimization algorithm based on Lagrangian duality, decomposition schemes based on Benders cuts and alternating direction method of multipliers. Other optimization techniques applied to solve the OPF are shown in (GRANVILLE, 1994) where the reactive dispatch is solved by an implementation of an interior point method; in (WU, DEBS and MARSTEN, 1994) the OPF problem is solved by a nonlinear predictor–corrector primal–dual interior point method; and in (WEI, SASAKI, *et al.*, 1997) is also developed an interior point NLP problem for the OPF.

The meta–heuristics techniques have also been used to solve the OPF. For example in (YUMBLA, RAMIREZ and COELLO, 2008), the OPF is solved using the particle swarm optimization. Authors in (BAKIRTZIS, BISKAS, *et al.*, 2002) applied an improved genetic algorithm to solve the OPF, in (H. YOSHIDA, FUKUYAMA, *et al.*, 2000) it is also applied the particle swarm optimization to solve the OPF considering a voltage security constraints, and it is presented a MINLP problem, considering as discrete variables, the automatic voltage regulator operation, the OLTC of the transformers and the reactive power control.

3.2. TRANSIENT STABILITY ANALYSIS

The transient stability is defined as the ability of an electric system to maintain the synchronism between the generator units when it is subject to a large disturbance, such as a sudden loss or increase in load or generation, or faults in the power system. This definition in general terms, describes the relationship between the electromagnetic torque and the mechanical torque in the machines, since any unbalance presented in the system can bring the loss of synchronism and the subsequent imbalance between the torques making the system unstable. Transient stability studies are developed within the following environments:

- Indirect methods or time domain simulation, refers to the solution of differential equations that describe the behavior of the synchronous machine, by using numerical integration methods. It is called an the indirect method because the obtained results are interpreted using tools that describe the evolution of state variables in the time.

- Direct methods, are based on the use of energy functions or Lyapunov functions, where the transient stability is evaluated within state space without the resolution of the differential equations, only considering the movement of the system in the attraction domain around an equilibrium point.

- Hybrid methods uses the energy function of the direct methods and the time domain simulation.

In this dissertation, the choice of the solution technique, is important since it will reveal the degree of detail of the system when subjected to a large disturbance. In this case, we use the time domain simulation, allowing to know the evolution of state variables in time, detecting the loss of synchronism between the machines, through the deviations between the angles and the angular speeds of the rotors.

Swing Equation of Synchronous Generator

In the transient stability studies, one of the most important parts is the dynamic analysis of the rotor of the machines in the transient period. Each type of transient study will have different machine models, being these phenomena mostly electromechanical. In this dissertation we use the classic model.

The swing equations are based in the mechanical laws of rotation, where the unbalance between the mechanical and electromagnetic torques are analyzed. The electromagnetic torques can be subdivided in synchronizing torque, which is in phase with the rotor angle and is equal to the sum of the electrical torque output and the electrical losses of the machine; and the damping torque that is in phase with the rotor speed.

The mechanical torque is defined as the mechanical torque delivered by the prime motor minus rotational losses (KUNDUR, 1994). Then the net torque causing acceleration or deceleration is expressed by:

$$J\frac{d\omega_{\mathrm{m}}}{dt} = T_a = T_m - T_e \tag{3.4}$$

$$H = \frac{1}{2}\frac{J\omega_{0\mathrm{m}}^2}{S_{\mathrm{BASE}}} \tag{3.5}$$

Where J is the combined moment of inertia of generator and turbine, ω_m is the mechanical angular speed of the rotor and t is the time. The equation (3.5) is the expression for the inertia constant H, defined as the kinetic energy in watt–seconds at rated speed divided by the S_{BASE} in VA.

From (3.4) and (3.5), the equation of the motion in per unit form is:

$$2H\frac{d\omega_r}{dt} = T_m - T_e \tag{3.6}$$

The relation between the electrical terms and the mechanical terms is the number of poles:

$$\omega_r = \frac{\omega_{\mathrm{m}}}{\omega_{0\mathrm{m}}} = \frac{1/p_f}{1/p_f}\frac{\omega_r}{\omega_0} = \frac{\omega_r}{\omega_0}$$

By convenience, the term ω_r that express the angular speed in electrical terms, will be denoted simply as ω.

In steady state the mechanical angle of the rotor increases uniformly in time. During the transient, an angular increment is added to the constant movement of the rotor. The expression (3.7) describes this phenomenon, note that the angular position δ of the rotor is in electrical radians whit respect to a synchronously rotating reference and δ_0 is its value at $t = 0$.

$$\delta = \omega t - \omega_0 t + \delta_0 \tag{3.7}$$

$$\frac{d\delta}{dt} = \omega - \omega_0 = \Delta\omega \tag{3.8}$$

The expression (3.8) is the time derivative of the equation (3.7). For the classic model of the machine this rotor angle is the same as the internal voltage, and by the electromechanical equation that describes the rotative movement of the machine (3.6), which relates the angular acceleration and the electromechanical torques, and solved the equations (3.6) and (3.8), is obtained the following relationship:

$$\frac{d\delta}{dt} = \omega_0 \Delta\omega \tag{3.9}$$

$$\frac{d\Delta\omega}{dt} = \frac{1}{2H}(P^m - P^e - D\Delta\omega) \tag{3.10}$$

The equations (3.9) and (3.10) describe completely the rotor dynamic when the systems are subjected to a large disturbance. The equation (3.9) and (3.10) are called the swing equation, due to its oscillatory nature over time.

Numerical Integration methods

The dynamic nature of the transient stability studies, involve the resolution of differential-algebraic equations. In this case, the transient stability analysis is reduced to the equations (3.9) and (3.10), which compose a first order non–linear differential equations system. Practically, presented as follows:

$$\frac{dx}{dt} = f(x,t) \tag{3.11}$$

Where, x is the temporal state variable, the function f represent the nonlinear differential function associated with x, assuming initial values of x and t equal to x_0 and t_0, respectively, determined in the pre-fault steady state. The numerical integration methods are used to obtain a non-analytical solution. For this purpose several approximations of the solution are made by means of point-to-point evaluations.

The equation (3.11) can be solved by numerical integration methods, which can be classified in two categories: Explicit and implicit methods. In the explicit methods, the value of state variable x at any value of t is calculated from knowledge of the previous values of t. This type of integration method, is easy to implement. Among them have: Euler, Runge Kutta of 1st, 2nd, 3rd and 4th order, which uses the Taylor series expansion to approximate the solution of (3.11). Explicit methods are considered not numerically stable.

The numerical stability is related to the consistency and the convergence of the integration methods equations. The convergence denotes the difference between the exact value of the solution of the differential equation and the approximation obtained by the integration method at any step. The consistency is defined by cut error at any step and it is expected to be zero as the integration step becomes zero. Therefore, the method should be stable in the presence of small changes or perturbations in the initial conditions producing changes in the consequent approximations.

Implicit methods use interpolation functions for solving the differential equations, in this method, to calculate the state variables is necessary evaluate the equation in future steps. The solution of (3.11) for x in $t_1 = t_0 + \Delta t$ is expressed as:

$$x(t_1) = x(t_0) + \int_{t_0}^{t_1} f\big(t, x(t)\big)\, dt \tag{3.12}$$

The most used implicit method in transient stability studies is the trapezoidal rule, which consist in a linear interpolation, calculating the area under the curve of the integral in the equation (3.12), which will be approximated by trapezium areas as shown in (3.13).

$$x_{t+1} = x_t + \frac{\Delta t}{2}[f(t+1, x_{t+1}) + f(t, x_t)] \tag{3.13}$$

Where the second term of the left side, represents the trapezium area, discretized by the predefined size of Δt, using a linear interpolation between the actual and future points in the curve.

Transient Stability modeling

For the transient stability modeling, it is necessary to take into account that the equations that describe its behavior are nonlinear differential time variant. Normally the transient stability analysis is divided in three stages, the pre-fault stage, where the system is in steady state operation, the fault stage, where the system is subjected to a large disturbance (e.g., a three-phase to ground fault) with zero voltage magnitude at the faulted bus and the post-fault stage, where the fault has been extinguished by the protection system.

In TSC–OPF modeling the classical model of the machine is usually used, since this approach is easy to implement, allows the time-domain simulation and the connection between the machines and the network be quick. This model of the synchronous machine is described in (KUNDUR, 1994) and is shown in Figure 3.1, consist in a source of internal voltage in series with the transient reactance. This is the most basic representation of the machine.

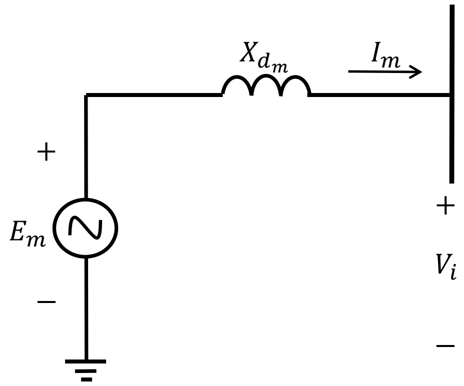

Figure 3.1 – Classical model of the synchronous machine.

In this dissertation we use the multimachine concept for the transient stability analysis based on the classic model of the machine. For this approach the following set of assumptions are made to perform the multi-machine transient stability analysis via the classical generator model based on (KUNDUR, 1994) and (ANDERSON and FOUAD, 1977):

- Mechanical power input (P_m^{m}) is constant.
- Damping or asynchronous power is negligible.
- Constant voltage in series with the transient reactance model for the synchronous machine is considered.
- The mechanical rotor angle of the machine, coincides with the angle of the internal voltage behind the transient reactance.
- Loads are represented by passive impedances and used in the reduced network calculation.

The first assumption is used for this type of analysis because the transient period is around the first 2 seconds, this type of analysis is usually called first swing analysis. The second assumption can be relaxed to linear expression of damping. The third and fourth assumptions are discussed above and shown in Figure 3.1. The assumption five is the load representation by constant impedances, this assumption allows eliminate the algebraic equations of the network. Thus, the system of equations of multimachine system is replaced to a system formed only by the algebraic differential equations. The reduced network is calculated by the next step-by-step procedure according to (KUNDUR, 1994), (ANDERSON and FOUAD, 1977):

- All variables must be expressed on a common basis, normally 100MW.

- A power flow calculation is performed so as to obtain the initial values of V_i^0, θ_i^0, P_i^0, Q_i^0. The values are to subsequently used to represent the load parameters as an impedance by: $Y_{i,\text{load}} = \frac{P_{i,\text{load}}^0 - jQ_{i,\text{load}}^0}{|V_{i,\text{load}}^0|^2}$

- The internal voltage is calculated using the value of the terminal voltage and the voltage drop in the transient reactance.

- The transient reactance and the loads are included into the original admittance matrix. Thus it is obtained the increased matrix seen from the internal nodes of the generators. In the fault stage the row and the column values associated with the bus in fault are considered zero, in the post-fault stage the admittance matrix is updated, disregarding the transmission line associated with the fault.

- The fault and post-fault increased matrix are reduced to the internal nodes of the generators by the Kron reduction. As shown in Figure 3.2, the reduced network parameters are calculated for each contingency, based on the initial power flow calculation.

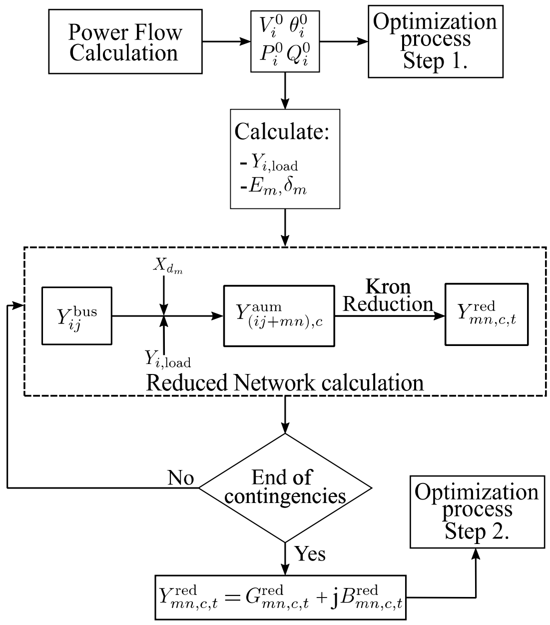

Figure 3.2 – Flowchart: Reduced Network calculation

An application example is available in (ANDERSON and FOUAD, 1977), where the 9-bus/3-generators WSCC system is evaluated to calculate the reduced matrix for one contingency, then the procedure to calculating the reduced network of this system is developed in APPENDIX B.

The graphic representation of a multimachine system is shown in the Figure 3.3. Considering the above assumptions, are derived the equations that describe the movement of the multimachine system. These assumptions allows the representation of the electric power systems according to Figure 3.3, for m generators, the nodes $1, 2, \dots m$ are referred to the internal nodes of the machines, the transmission network and the transformers are modeled as impedances. The loads, modeled as passive impedances, are also connected between the load buses and the reference bus.

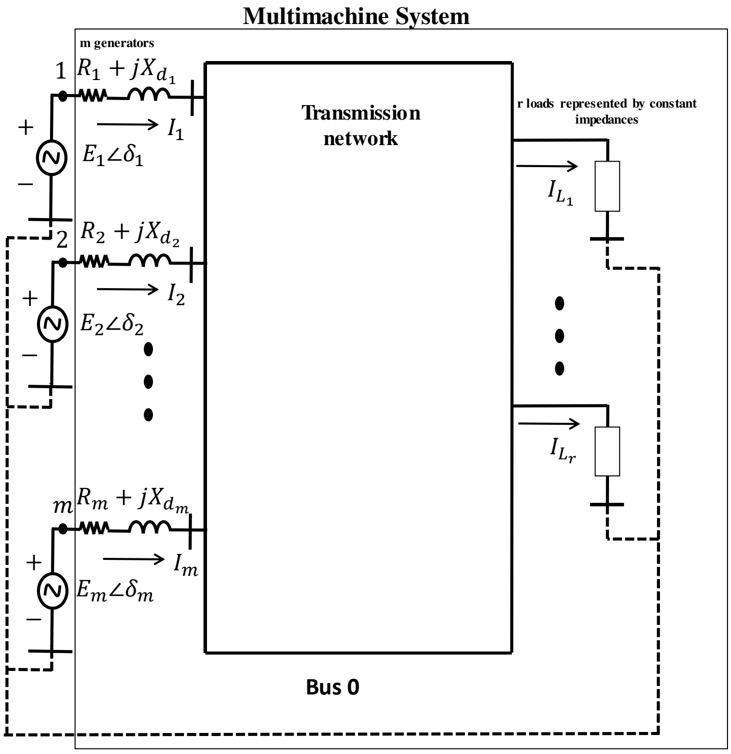

Figure 3.3 - Multimachine System

For the classical transient stability calculation it is necessary to obtain the following previous information:

- A load flow calculation in pre–fault stage, to determine the mechanical power (P_m^{m}) and the calculate the values of internal voltage and angle $\left(E_m\angle\delta_{m,t,0}\right)$ for all generators.

- The representation of the loads as passive impedances, using the calculated data of the buses of the previous load flow.

- It is necessary to have the basic dynamic data from all generators, as the inertia constant (H_m), the damping constant (D_m) and the transient reactance $\left(X_{d_m}\right)$.

- The fault allocation, the clearance time and the maximum simulation time.

3.3. TRANSIENT STABILITY CONSTRAINED OPTIMAL POWER FLOW (TSC–OPF)

The TSC–OPF, as well as the classic optimal power flow, is a powerful tool used in the operation of the electric power systems to find a stable operating point when the EPS is subjected to one or more disturbances. In EPS planning the TSC–OPF is used to determine a stable operating point in future scenarios considering the demand increase and topology changes, and it can be also used to determine stability limits.

In (CALLE, CASTRONUOVO and LEDESMA, 2013), the authors detailed the difficulties to include the Transient Stability Constraints (TSC) into OPF, and is divided in two groups:

- The inclusion of the differential equations that describe the dynamic behavior of the machine into the classical OPF. These equations can be solved by the traditional way, representing the dynamic behavior of the machine by the swing equation and solved by integration methods in time–domain simulations. Other way to solve these equations is used the direct methods such as the equal area criterion, reducing the system to a one machine infinite bus, or using the energy function such as the Lyapunov functions, the hybrid methods combining the previous two methods can also use.

- The solution of the optimization problem after the TSC inclusion, can be solved by classical nonlinear programming (NLP) methods, or using modern heuristic techniques, such as the particle swarm optimization, genetic algorithms and differential evolution.

In the literature there is a limited amount of information about the TSC-OPF, the inclusion of TSC into OPF, is used as a tool for solving common problems such as the energy dispatch, EPS planning and others, as shown in (GAN, THOMAS and ZIMMERMAN, 2000) where is solved the differential equations using the implicit integration method as the trapezoidal rule, others works where is used the trapezoidal rule are (YUAN, KUBOKAWA and SASAKI, 2003) and (LAYDEN and JEYASURYA, 2004), where the TSC–OPF is evaluated for multiple contingencies, finding a stable operation point for all cases.

The greatest difficulty is to reduce the effect of the number of integration steps. For this reason, the literature regarding the TSC–OPF shows the application of direct methods, as in

(PAI and NGUYEN, 2003), (LI, YUAN, *et al.*, 2011) and (MINANO, CUTSEM, *et al.*, 2010) where is used the simplification of the system to a one machine infinity bus, increasing the loss of information and the error.

The use of modern heuristics techniques for solving the TSC–OPF are discussed in (CHAN, LING, *et al.*, 2007), (MO, ZOU, *et al.*, 2007) and (CAI, CHUNG and WONG, 2008), where is applied the method of particle swarm optimization, genetic algorithms, and differential evolution for the TSC–OPF solution. Knowing that the obtained solutions, do not guarantee an optimal and quality solution. In addition, the large number of iterations that they consider to find those solutions.

The TSC–OPF, can be defined as optimization problem (CALLE, CASTRONUOVO and LEDESMA, 2013), as follow:

$$\min f(x_0) \tag{3.14}$$

Subject to:

$$G_0(x_0) = 0 \tag{3.15}$$

$$H_0(x_0) \leq 0 \tag{3.16}$$

$$G_t(x_t) = 0 \qquad \forall\, t \in \{0 \ldots t_c^{\max}\} \tag{3.17}$$

$$H_t(x_t) \leq 0 \qquad \forall\, t \in \{0 \ldots t_c^{\max}\} \tag{3.18}$$

The proposed TSC–OPF, is difficult to solve mainly due to the dynamic characteristics of the transient stability equations. For this reason, the discretization of the interval $\{0 \ldots t_c^{\max}\}$ is necessary, since this interval can be discretized in infinite points resulting in infinite dimensional variables and infinite equality and inequality constraints.

3.4. IMPORTANT REMARKS

The classical OPF model is developed. Based on literature review, this model, is formulated as an optimization problem. An objective function is minimized or maximized according to characteristic of the problem. The constraints are the power flow equations as equality constraints and the operative limits as inequality constraints. This model is the most basic formulation for the OPF. On the other hand, a brief review of the transient stability is developed, the three classical approaches to calculate the stability in EPS and the swing equation to solve transient stability problems that involves the classical model of the synchronous machine is also developed.

Besides, the integration methods are divided in two categories to solve differential equations, being the implicit method the most used in transient stability studies, due to easy implementation and good numerical stability. The numerical stability is directly related to the convergence and the consistency of the differential equations system.

A literature review that involves the TSC–OPF modeling is developed, highlining the difficulties to include the TSC into OPF, for its dynamic characteristics, and the use of nonlinear solvers and heuristics techniques to find an acceptable solution, since these techniques do not guarantee the global optimal solution, making this problem difficult to solve. Finally, the general form of the optimization problem of the TSC–OPF includes the dynamic constraints and the integration process is developed, embedded in the same model.

CHAPTER FOUR:

N-1 MULTI–CONTINGENCY TSC–OPF MINLP MODEL BASED ON BRANCH FLOW APPROACH

In this chapter, is presented a MINLP mathematic model for the N-1 multi–contingency TSC–OPF, based on branch flow approach, with control variables for the shunt elements in buses and the regulation of the on–load tap changers (OLTC) of phase transformers.

The AC load flow based on branch flow model, described in chapter two, is used to modeled and calculate: The OPF with discrete controls (shunt elements and OLTC regulation), the pre–fault considerations of the multimachine system (E_m and $\delta_{m,c,0}$), and the time–domain equations of the fault and the post-fault stages. This equivalence allows to solve the complete N-1 multi–contingency TSC–OPF and facilitates the application of linearization techniques, such as piecewise function. As seen in (LAYDEN and JEYASURYA, 2004), (CALLE, CASTRONUOVO and LEDESMA, 2013) and (YUAN, KUBOKAWA and SASAKI, 2003) to integrate the time-domain differential equation, the trapezoidal rule is used due to its easy implementation and good numerical stability.

4.1. OPTIMAL POWER FLOW USING THE AC BRANCH FOW MODEL

In this section, is presented an MINLP to solve the OPF with discrete controls. The voltages limits at the buses and the active and reactive power generation limits from generators, are considered as control variables, the tap regulation on the OLTC and the switchable operation of the shunt elements in the buses are also considered.

The objective function of the model proposed is the minimization of the generation costs and load shedding. The generation costs of the generators, are represented by the cost curves, which can be expressed by the polynomial form, being the quadratic representation the most used in the literature. However, it can also be expressed as a relaxed linear approximation. The quadratic representation is used in this section. The complete model of TSC–OPF is shown in (4.1)–(4.15):

$$\min \sum_{i\in\Omega_{\mathrm{B}}} \left[a_i^g \left(P_i^g\right)^2 + b_i^g P_i^g + c_i^g\right] + \sum_{i\in\Omega_{\mathrm{B}}} \left(c^{ls} P_i^d r_i\right) \tag{4.1}$$

Subject to:

$$P_i^g - P_i^d(1 - r_i) + \sum_{ji\in\Omega_{\mathrm{L}}} P_{ji} - \sum_{ij\in\Omega_{\mathrm{L}}} \left(P_{ij} + R_{ij} I_{ij}^2\right) - g_{\mathrm{i}}^{\mathrm{sh}} V_i^2 = 0 \qquad \forall i \in \Omega_{\mathrm{B}} \tag{4.2}$$

$$\begin{aligned} Q_i^g - Q_i^d(1 - r_i) &+ \sum_{ji\in\Omega_{\mathrm{L}}} \left(Q_{ji} + B_{ji}^{\mathrm{sh}} V_i^2\right) \\ &- \sum_{ij\in\Omega_{\mathrm{L}}} \left(Q_{ij} - B_{ji}^{\mathrm{sh}} V_i^2 + X_{ij} I_{ij}^2\right) - Q_i^{\mathrm{sh}} = 0 \end{aligned} \qquad \forall i \in \Omega_{\mathrm{B}} \tag{4.3}$$

$$Q_i^{\mathrm{sh}} = b_{\mathrm{i}}^{\mathrm{sh}} V_i^2 h_i \qquad \forall i \in \Omega_{\mathrm{B}} \tag{4.4}$$

$$V_i^2 \left[1 + \mathrm{Reg}_{ij} \frac{nt_{ij}}{\overline{\mathrm{nt}}_{ij}}\right]^2 - V_j^2 = 2\left(R_{ij} P_{ij} + X_{ij} Q_{ij}\right) + Z_{ij}^2 I_{ij}^2 \qquad \forall ij \in \Omega_{\mathrm{L}} \tag{4.5}$$

$$\left[1 + \mathrm{Reg}_{ij} \frac{nt_{ij}}{\overline{\mathrm{nt}}_{ij}}\right] V_i V_j \sin\left(\theta_i - \theta_j\right) = X_{ij} P_{ij} - R_{ij} Q_{ij} \qquad \forall ij \in \Omega_{\mathrm{L}} \tag{4.6}$$

$$V_j^2 I_{ij}^2 = P_{ij}^2 + Q_{ij}^2 \qquad \forall ij \in \Omega_{\mathrm{L}} \qquad (4.7)$$

$$\underline{V}^2 \leq V_i^2 \leq \overline{V}^2 \qquad \forall i \in \Omega_{\mathrm{B}} \qquad (4.8)$$

$$0 \leq I_{ij}^2 \leq \overline{I}_{ij}^2 \qquad \forall ij \in \Omega_{\mathrm{L}} \qquad (4.9)$$

$$\underline{P}_i^g \leq P_i^g \leq \overline{P}_i^g \qquad \forall i \in \Omega_{\mathrm{B}} \qquad (4.10)$$

$$\underline{Q}_i^g \leq Q_i^g \leq \overline{Q}_i^g \qquad \forall i \in \Omega_{\mathrm{B}} \qquad (4.11)$$

$$0 \leq r_i \leq 1 \qquad \forall i \in \Omega_{\mathrm{B}} \qquad (4.12)$$

$$-\overline{\mathrm{nt}}_{ij} \leq nt_{ij} \leq \overline{\mathrm{nt}}_{ij} \qquad \forall ij \in \Omega_{\mathrm{L}} \qquad (4.13)$$

$$nt_{ij} \in \mathbb{Z} \qquad \forall ij \in \Omega_{\mathrm{L}} \qquad (4.14)$$

$$h_i \in \{0,1\} \qquad \forall i \in \Omega_{\mathrm{B}} \qquad (4.15)$$

The objective function (4.1) minimizes the total operation cost. The first term represents the production cost of the active power generation for thermal units. The second term represents the load shedding cost. Constraints (4.2) and (4.3) represent the active and reactive power balance at each node, respectively. Constraint (4.4) represents the reactive power generation of the switchable shunt elements, considering its binary operation. Constraints (4.5) and (4.6) calculate the voltage magnitude drop and the angular difference in each branch ij considering the OLTC regulation, respectively. Constraint (4.7) calculates the current magnitude at each branch ij. Constraints (4.8)–(4.12) define the minimum and maximum limits for voltage magnitudes, current magnitudes, active/reactive power generations and load shedding percentage, respectively. Constraints (4.13) and (4.14) represent the discrete operation of the OLTC transformers, and (4.15) is the binary operation of the switchable shunt elements. In practice, load shedding is not always a feasible control action. However, since the unsupplied demand is heavily penalized in (4.1), having load shedding at the TSC-OPF indicates that the network is not fully capable of operate under N-1 condition, and corrective measures should be planned.

4.2. N-1 MULTI–CONTINGENCY TRANSIENT STABILITY ASSESSMENT

The term "N-1 multi–contingency", refers to a set of contingencies Ω_c, where each contingency represents a three-phase to ground fault and the output of a transmission line to clear the fault. The classical transient stability assessment involves the resolution of non-linear differential equations through numerical integration methods. The transient stability studies are conducted in three stages:

a) The pre-fault stage, where the EPS is in steady-state operation, in this stage is calculated the operation point via OPF, for all contingencies. Besides, is considered the switchable operation of the shunt elements and the OLTC tap changers.

b) The fault stage, where the EPS is subject to a large perturbation (e.g., a three-phase to ground fault) with zero voltage magnitude at the faulted bus. In this stage it is essential the clearing time definition, since the stability of the system will depend on that.

c) The post-fault stage, where the fault has been extinguished by the protection system. The system stability is evaluated in this stage according to state variables evolution over time.

For transient stability analysis, the EPS are studied as multi–machine systems, wherein the most common representation for synchronous generators in the classical dynamic model, in which an internal voltage source is connected in series to a transient reactance (KUNDUR, 1994), (ANDERSON and FOUAD, 1977).

Pre-fault AC branch flow equivalent

The swing equation of the synchronous machine defined in the previous chapter represent the dynamic behavior of the rotor angles and the deviation from the reference of the angular speed. The Figure 4.1 represents the calculation in pre-fault stage of internal voltage magnitudes

(E_m) and rotor angles (δ_m) by the equivalent AC branch flow model, necessary as one the previous conditions to transient stability evaluation. For each synchronous generator, (4.16) calculates the injected current magnitudes of the generators. Moreover, (4.17) calculates the internal voltage drop, considering the transient reactance of the generators as a branch and a unidirectional flow between the generator and the transmission network. Equation (4.18) calculates the angular difference between E_m and V_i. (4.19) represents the internal voltage magnitude limits.

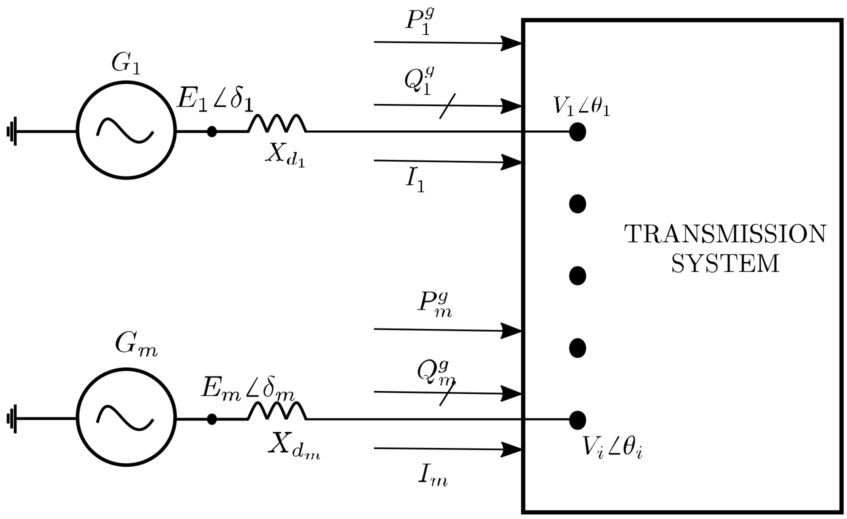

Figure 4.1 – Equivalent AC Branch flow model for the generators in pre-fault

$$V_i^2 I_m^2 = \left(P_m^g\right)^2 + \left(Q_m^g\right)^2 \qquad \forall i \in \Omega_\mathrm{B}, m \in \Omega_\mathrm{G}|_{i=m} \tag{4.16}$$

$$E_m^2 - V_i^2 = 2X_{d_m} Q_m^g + X_{d_m}^2 I_m^2 \qquad \forall i \in \Omega_\mathrm{B}, m \in \Omega_\mathrm{G}|_{i=m} \tag{4.17}$$

$$E_m V_i \sin(\delta_m - \theta_i) = P_m^g X_{d_m} \qquad \forall i \in \Omega_\mathrm{B}, m \in \Omega_\mathrm{G}|_{i=m} \tag{4.18}$$

$$\underline{E}^2 \leq E_m^2 \leq \overline{E}^2 \qquad \forall m \in \Omega_\mathrm{G}|_{i=m} \tag{4.19}$$

Fault and post-fault AC branch flow equivalent

In Figure 4.2, the electric power inputs of each generator can be calculated using a reduced transmission network during fault and post-fault stages, given by the AC branch flow model in (4.20)–(4.24). Note that all variables are time-varying and N-1 multi–contingency dependent.

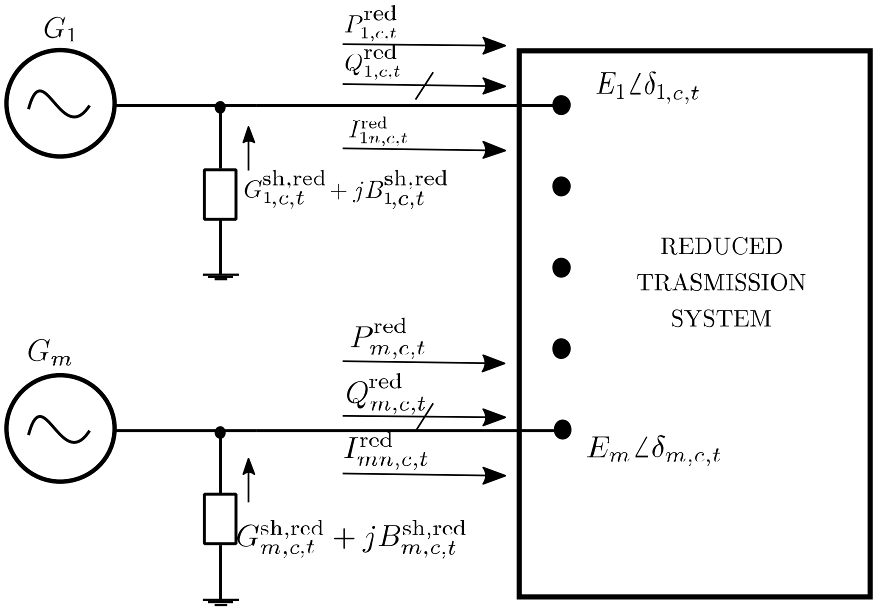

Figure 4.2 – Equivalent AC branch flow model for the reduced network for fault and post-fault situations

$$P^{e}_{m,c,t} + \sum_{nm\in\Omega_{\mathrm{L^{red}}}} P^{\mathrm{red}}_{nm,c,t} - \sum_{mn\in\Omega_{\mathrm{L^{red}}}} \left(P^{\mathrm{red}}_{mn,c,t} + R^{\mathrm{red}}_{mn,c,t}\left(I^{\mathrm{red}}_{mn,c,t}\right)^2\right) - G^{\mathrm{sh,red}}_{m,c,t}E_m^2 = 0; \qquad \forall m \in \Omega_{\mathrm{G}}, c \in \Omega_{\mathrm{C}}, t \in \left\{0 \ldots N_{t_1} + N_{t_2}\right\} \tag{4.20}$$

$$Q^{e}_{m,c,t} + \sum_{nm\in\Omega_{\mathrm{L^{red}}}} Q^{\mathrm{red}}_{nm,c,t} - \sum_{mn\in\Omega_{\mathrm{L^{red}}}} \left(Q^{\mathrm{red}}_{mn,c,t} + X^{\mathrm{red}}_{mn,c,t}\left(I^{\mathrm{red}}_{mn,c,t}\right)^2\right) - B^{\mathrm{sh,red}}_{m,c,t}E_m^2 = 0; \qquad \forall m \in \Omega_{\mathrm{G}}, c \in \Omega_{\mathrm{C}}, t \in \left\{0 \ldots N_{t_1} + N_{t_2}\right\} \tag{4.21}$$

$$E_m^2 - E_n^2 = 2\left(R^{\mathrm{red}}_{mn,c,t}P^{\mathrm{red}}_{mn,c,t} + X^{\mathrm{red}}_{mn,c,t}Q^{\mathrm{red}}_{mn,c,t}\right) - \left(Z^{\mathrm{red}}_{mn,c,t}\right)^2\left(I^{\mathrm{red}}_{mn,c,t}\right)^2; \qquad \forall mn \in \Omega_{\mathrm{L^{red}}}, c \in \Omega_{\mathrm{C}}, t \in \left\{0 \ldots N_{t_1} + N_{t_2}\right\} \tag{4.22}$$

$$E_mE_n \sin\left(\delta_{m,c,t} - \delta_{n,c,t}\right) = X^{\mathrm{red}}_{mn,c,t}P^{\mathrm{red}}_{mn,c,t} - R^{\mathrm{red}}_{mn,c,t}Q^{\mathrm{red}}_{mn,c,t}; \qquad \forall mn \in \Omega_{\mathrm{L^{red}}}, c \in \Omega_{\mathrm{C}}, t \in \left\{0 \ldots N_{t_1} + N_{t_2}\right\} \tag{4.23}$$

$$E_n^2\left(I_{\mathrm{mn,c,t}}^{\mathrm{red}}\right)^2=\left(P_{mn,c,t}^{\mathrm{red}}\right)^2+\left(Q_{mn,c,t}^{\mathrm{red}}\right)^2; \qquad \forall mn\in\Omega_{\mathrm{L^{red}}}, c\in\Omega_{\mathrm{C}}, t\in\left\{0\ldots N_{t_1}+N_{t_2}\right\} \tag{4.24}$$

Parameters that belong to set $\Omega_{\mathrm{L^{red}}}$ are calculated from the reduced network. During the fault and the post–fault stages, constraints (4.20) and (4.21) are the active and reactive electric power balance of the reduced network, respectively. Constraint (4.22) calculates the internal voltage magnitude drop between generators. Constraint (4.23) calculates the angular difference between generators, and (4.24) calculates the current magnitudes at each branch of the reduced network. Recall that all variables vary dynamically in time. The number of time steps of the model (4.20)–(4.24) is given by the time steps during the fault $\left(N_{t_1}\right)$, plus the time steps during post-fault $\left(N_{t_2}\right)$. Note that the difference between the two stages is concentrated in the parameters of the reduced network $\left(R_{mn,c,t}^{\mathrm{red}}, X_{mn,c,t}^{\mathrm{red}}, Z_{mn,c,t}^{\mathrm{red}}, G_{m,c,t}^{\mathrm{sh,red}}, \text{and } B_{m,c,t}^{\mathrm{sh,red}}\right)$, for each time step and contingency (KUNDUR, 1994), (ANDERSON and FOUAD, 1977).

Is defined the center of inertia (COI) as the angular reference of the EPS, whose formulation is shown in (4.25), the center of inertia represents the average movement of the system, and the transient stability is defined as the maximum deviation from the COI.

$$\delta_{c,t}^{\mathrm{COI}}=\frac{\sum_{m=1}^{N_g} H_m\delta_{m,c,t}}{\sum_{m=1}^{N_g} H_m} \qquad c\in\Omega_{\mathrm{C}}, t\in\left\{0\ldots N_{t_1}+N_{t_2}\right\} \tag{4.25}$$

After a large disturbance, the EPS is considered stable if the angular difference between the absolute value of rotor angle and the COI does not exceed a given security limit, as shown in (4.26) and the bound of angular speed variation, as shown in (4.27), (GAN, THOMAS and ZIMMERMAN, 2000), (CALLE, CASTRONUOVO and LEDESMA, 2013).

$$\underline{\delta}\le\delta_{m,c,t}-\delta_{c,t}^{\mathrm{COI}}\le\overline{\delta} \qquad \forall m\in\Omega_{\mathrm{G}}, c\in\Omega_{\mathrm{C}}, t\in\left\{0\ldots N_{t_1}+N_{t_2}\right\} \tag{4.26}$$

$$\Delta\underline{\omega}_m\le\Delta\omega_{m,c,t}\le\Delta\overline{\omega}_m \qquad \forall m\in\Omega_{\mathrm{G}}, c\in\Omega_{\mathrm{C}}, t\in\left\{0\ldots N_{t_1}+N_{t_2}\right\} \tag{4.27}$$

The Trapezoidal rule for the swing equation

Trapezoidal rule is used to integrate the expressions (3.9) and (3.10) from the previous chapter. As already mentioned in the previous chapter, the equation (3.13) is used to integrated the differential equations through trapezoidal rule, the expressions (4.28) and (4.29) are the calculation in time-domain of the angle of the synchronous generators $\left(\delta_{m,c,t}\right)$ and the angular speed deviation $\left(\Delta\omega_{m,c,t}\right)$, both variants for each generator, variant in time and for each contingency. The advantage of including implicit trapezoidal integration within the optimization model is the direct calculation of the angles and the angular speeds of the synchronous machines using linear expressions.

$$\delta_{m,c,t+1} = \delta_{c,m,t} + \left(\frac{\Delta_{c,t}}{2}\right)\omega_0\left(\Delta\omega_{m,c,t+1} + \Delta\omega_{m,c,t}\right)$$

$$\forall m \in \Omega_{\mathrm{G}}, c \in \Omega_{\mathrm{C}}, t \in \left\{0 \ldots N_{t_1} + N_{t_2}\right\} \quad (4.28)$$

$$\Delta\omega_{m,c,t+1} = \Delta\omega_{m,c,t} + \left(\frac{\Delta_{c,t}}{4H_m}\right)\left[2P_m^{\mathrm{m}} - P_{mc,t+1}^{e} - P_{mc,t}^{e} - D_m\left(\Delta\omega_{m,c,t+1} + \Delta\omega_{m,c,t}\right)\right]$$

$$\forall m \in \Omega_{\mathrm{G}}, c \in \Omega_{\mathrm{C}}, t \in \left\{0 \ldots N_{t_1} + N_{t_2}\right\} \quad (4.29)$$

Where:

In fault stage: $\Delta_{c,t} = \dfrac{t_c^{fc}}{N_{t_1}}, \forall c \in \Omega_{\mathrm{C}}, t \in \left\{0 \ldots N_{t_1}\right\}$

In post-fault stage: $\Delta_{c,t} = \dfrac{t_c^{\max} - t_c^{fc}}{N_{t_2}}, \forall c \in \Omega_{\mathrm{C}}, t \in \left\{N_{t_1} + 1 \ldots N_{t_2}\right\}$

Finally, the expressions (4.30)–(4.32) are the initial points for the rotor angle, angular speed variation, and mechanic power input, respectively.

$$\delta_{m,c,0} = \delta_m \qquad \forall m \in \Omega_{\mathrm{G}}, c \in \Omega_{\mathrm{C}} \quad (4.30)$$

$$\Delta\omega_{m,c,0} = 0 \qquad \forall m \in \Omega_{\mathrm{G}}, c \in \Omega_{\mathrm{C}} \qquad (4.31)$$

$$P_m^{\mathrm{m}} = P_i^{g} \qquad \forall i \in \Omega_{\mathrm{B}}, m \in \Omega_{\mathrm{G}}|_{i=m} \qquad (4.32)$$

4.3. COMPLETE MINLP MODEL

The *N-1* multi–contingency TSC–OPF problem could be modeled as a MINLP model, given by (4.33).

$$\begin{gathered} \min(4.1) \\ \text{Subject to: (4.2) - (4.32)} \end{gathered} \qquad (4.33)$$

Note that the optimization model in (4.33) is an MINLP problem due to the nonlinear relationship between continue and discrete variables. MINLP problems are non-convex and optimality can neither be guaranteed by classical optimization techniques nor by heuristic approaches. Thus, the next chapter presents a set of efficient linearization strategies used to transform the proposed MINLP into a MILP model. MILP models are desirable because there are tools (e.g., commercial solvers) available for their solution which are more efficient and scalable than the ones used for MINLP formulations.

4.4. IMPORTANT REMARKS

In this chapter the complete MINLP proposed model for the TSC–OPF is shown. The branch flow model is used to model the power flow equations in pre-fault, fault and post-fault stages. In pre-fault stage or steady state, the branch flow model is based on the equations seen in the second chapter. Thus, the switchable control of shunt elements and the OLTC tap changers are included in this model, in fault and post-fault stages, it is developed a novel assessment to model the multimachine transient stability, based on branch flow approach.

The trapezoidal rule is used as the integration method. This approach allows solving the swing equation by an implicit method, using the pre-fault solution as initial operation point. It is used in transient stability studies because it is easy to implement and has a good numerical stability, making this method ideal for this kind of problem. Therefore, the state variables as the angular speed deviation and the rotor angle, can be calculated by trapezoidal rule.

CHAPTER FIVE:

N-1 MULTI–CONTINGENCY TSC–OPF MILP MODEL BASED ON BRANCH FLOW APPROACH

In this chapter we develop a Mixed Integer Linear Programing (MILP) model, for the multi-contingency TSC–OPF, based on MINLP model developed on previous chapter. The nonlinear characteristics due to the relationship between continuous and discrete variables make this kind of problems not easy to solve. For this reason, optimality may not be assured by classical optimization techniques or by heuristic approaches. All models in the literature of TSC–OPF are NLP problems as seen in (ABHYANKAR, GENG, *et al.*, 2017), (JIN and XIANG, 2014), (MINANO, CUTSEM, *et al.*, 2010) and (CALLE, CASTRONUOVO and LEDESMA, 2013). Such problems are modeled by the classical equations of load flow calculation as seen in (MONTICELLI, 1983). The use of a branch flow model to represent the load flow equations allows the application of linearization techniques, such as the piece-wise function or linearization by parts. This approach also allows the inclusion of discrete variables as the optimal operation of shunt elements and tap regulation on OLTC.

The N-1 multi–contingency approach aims at finding an economic and stable operation point for a set of contingencies evaluated independently. This approach was tested on (YUAN, KUBOKAWA and SASAKI, 2003), although the authors do not considered discrete controls and only two contingencies are evaluated in the same simulation, by altering the parameters of the reduced network for each contingency, the trapezoidal rule is used as an integration method for the differential equations.

The branch flow model is fully developed in (FARIVAR and LOW, 2013) and (LOW and FARIVAR, 2013), where it is proposed an exact branch flow model for mesh as well as radial networks, using relaxations and convexification methods. The OPF was tested on eight systems, and the authors demonstrate that the branch flow model can be used for the analysis and optimization of mesh as well as radial networks. Also it is proposed a strategy for solving the OPF which is divided in two steps, compute a relaxed solution of OPF, by solving its conic relaxation and recover from the relaxed solution, an optimal solution of the original OPF using an angle recovery algorithm, this optimization process allows finding an optimal point whose a globally optimal solution is assumed.

5.1. LINEARIZATIONS OF THE AC BRANCH FLOW MODEL

In the previous chapter the following constraints were developed: (4.2)–(4.9), (4.16)–(4.17) and (4.20)–(4.24), voltage and current magnitudes are square. Thus, the following change in variables can be performed without loss of generality:

$$V_i^{\mathrm{sqr}} \equiv V_i^2$$
$$I_{ij}^{\mathrm{sqr}} \equiv I_{ij}^2$$
$$I_{mn,c,t}^{\mathrm{red,sqr}} \equiv \left(I_{mn,c,t}^{\mathrm{red}}\right)^2$$
$$E_m^{\mathrm{sqr}} \equiv E_m^2$$
$$I_m^{\mathrm{sqr}} \equiv I_m^2$$

Hence, the linear equivalents of (4.2)–(4.3), (4.8)–(4.9), (4.17) and (4.19)–(4.22) are shown in (5.1)–(5.9):

$$P_i^g - P_i^d(1-r_i) + \sum_{ji\in\Omega_\mathrm{L}} P_{ji} - \sum_{ij\in\Omega_\mathrm{L}} \left(P_{ij} + R_{ij} I_{ij}^{\mathrm{sqr}}\right) - g_\mathrm{i}^{\mathrm{sh}} V_i^{\mathrm{sqr}} = 0 \qquad \forall i \in \Omega_\mathrm{B} \tag{5.1}$$

$$Q_i^g - Q_i^d(1-r_i) + \sum_{ji\in\Omega_\mathrm{L}} \left(Q_{ji} + B_{ji}^{\mathrm{sh}} V_i^{\mathrm{sqr}}\right) - \sum_{ij\in\Omega_\mathrm{L}} \left(Q_{ij} - B_{ij}^{\mathrm{sh}} V_i^{\mathrm{sqr}} + X_{ij} I_{ij}^{\mathrm{sqr}}\right) - Q_i^{\mathrm{sh}} = 0 \qquad \forall i \in \Omega_\mathrm{B} \tag{5.2}$$

$$\underline{V}^{\mathrm{sqr}} \le V_i^{\mathrm{sqr}} \le \overline{V}^{\mathrm{sqr}} \qquad \forall i \in \Omega_\mathrm{B} \tag{5.3}$$

$$0 \le I_{ij}^{\mathrm{sqr}} \le \overline{I}_{ij}^{\mathrm{sqr}} \qquad \forall ij \in \Omega_\mathrm{L} \tag{5.4}$$

$$E_m^{\mathrm{sqr}} - V_i^{\mathrm{sqr}} = 2X_{d_m} Q_m^g + X_{d_m}^2 I_m^{\mathrm{sqr}} \qquad \forall i \in \Omega_\mathrm{B}, m \in \Omega_\mathrm{G}|_{i=m} \tag{5.5}$$

$$\underline{E}^{\mathrm{sqr}} \le E_m^{\mathrm{sqr}} \le \overline{E}^{\mathrm{sqr}} \qquad \forall m \in \Omega_\mathrm{G}|_{i=m} \tag{5.6}$$

$$P_{m,c,t}^e + \sum_{nm\in\Omega_{\mathrm{L}^\mathrm{red}}} P_{nm,c,t}^{\mathrm{red}} - \sum_{mn\in\Omega_{\mathrm{L}^\mathrm{red}}} \left(P_{mn,c,t}^{\mathrm{red}} + R_{mn,c,t}^{\mathrm{red}} I_{mn,c,t}^{\mathrm{red,sqr}}\right) - G_{m,c,t}^{\mathrm{sh,red}} E_m^{\mathrm{sqr}} = 0; \qquad \forall m \in \Omega_\mathrm{G}, c \in \Omega_\mathrm{C}, t \in \{0 \ldots N_{t_1} + N_{t_2}\} \tag{5.7}$$

$$Q_{m,c,t}^e + \sum_{nm\in\Omega_{\mathrm{L}^\mathrm{red}}} Q_{nm,c,t}^{\mathrm{red}} - \sum_{mn\in\Omega_{\mathrm{L}^\mathrm{red}}} \left(Q_{mn,c,t}^{\mathrm{red}} + X_{mn,c,t}^{\mathrm{red}} I_{mn,c,t}^{\mathrm{red,sqr}}\right) - B_{m,c,t}^{\mathrm{sh,red}} E_m^{\mathrm{sqr}} = 0; \qquad \forall m \in \Omega_\mathrm{G}, c \in \Omega_\mathrm{C}, t \in \{0 \ldots N_{t_1} + N_{t_2}\} \tag{5.8}$$

$$E_m^{sqr} - E_n^{sqr} = 2\left(R_{mn,c,t}^{\mathrm{red}} P_{mn,c,t}^{\mathrm{red}} + X_{mn,c,t}^{\mathrm{red}} Q_{mn,c,t}^{\mathrm{red}}\right) - \left(Z_{mn,c,t}^{\mathrm{red}}\right)^2 I_{mn,c,t}^{\mathrm{red,sqr}}; \qquad \forall mn \in \Omega_{\mathrm{L}^\mathrm{red}}, c \in \Omega_\mathrm{C}, t \in \{0 \ldots N_{t_1} + N_{t_2}\} \tag{5.9}$$

The initial values V_i^0, E_i^0 and nt_{ij}^0 are considered to be known for the products at the first term of (4.6), (4.18) and (4.23), as follows in (5.10)–(5.12):

$$\left[1 + \mathrm{Reg}_{ij} \frac{nt_{ij}}{\overline{\mathrm{nt}}_{ij}}\right] V_i V_j \approx \left[1 + \mathrm{Reg}_{ij} \frac{nt_{ij}^0}{\overline{\mathrm{nt}}_{ij}}\right] V_i^0 V_j^0 \qquad \forall ij \in \Omega_\mathrm{L} \tag{5.10}$$

$$E_m E_n \approx E_m^0 E_n^0 \qquad \forall mn \in \Omega_{\mathrm{L}^{\mathrm{red}}} \qquad (5.11)$$

$$E_m V_i \approx E_m^0 V_i^0 \qquad \forall i \in \Omega_{\mathrm{B}}, m \in \Omega_{\mathrm{G}}|_{i=m} \qquad (5.12)$$

The sine function, $\sin(\psi)$, at (4.6), (4.18) and (4.23), can be approximated around the initial angle ψ^0, by the linear function $g(\psi, \psi^0) = \sin(\psi^0) + \cos(\psi^0)\,(\psi - \psi^0)$. Note that, if $\psi^0 = 0$, then $\sin(\psi) \approx g(\psi, 0) = \psi$. Thus, (4.6), (4.18) and (4.23) are linearized as in (5.13), (5.14) and (5.15), respectively:

$$\left[1 + \mathrm{Reg}_{ij} \frac{nt_{ij}^0}{\overline{\mathrm{nt}}_{ij}}\right] V_i^0 V_j^0 g\big(\theta_i - \theta_j, \theta_i^0 - \theta_j^0\big) = X_{ij} P_{ij} - R_{ij} Q_{ij} \qquad \forall ij \in \Omega_{\mathrm{L}} \qquad (5.13)$$

$$E_m V_i g(\delta_m - \theta_i, \delta_m^0 - \theta_i^0) = P_m^g X_{d_m} \qquad \forall i \in \Omega_{\mathrm{B}}, m \in \Omega_{\mathrm{G}}|_{i=m} \qquad (5.14)$$

$$\begin{gathered} E_m E_n g\big(\delta_{m,c,t} - \delta_{n,c,t}, \delta_{m,c,t}^0 - \delta_{n,c,t}^0\big) = X_{mn,c,t}^{\mathrm{red}} P_{mn,c,t}^{\mathrm{red}} - R_{mn,c,t}^{\mathrm{red}} Q_{mn,c,t}^{\mathrm{red}}; \\ \forall mn \in \Omega_{\mathrm{L}^{\mathrm{red}}}, c \in \Omega_{\mathrm{C}}, t \in \left\{0 \dots N_{t_1} + N_{t_2}\right\} \end{gathered} \qquad (5.15)$$

During the pre-fault stage, (4.16) represents the calculate of current injection by the generators, which can be linearized using initial values for the active and reactive generation and initial voltage as shown in (5.16).

$$(V_i^0)^2 I_m^{sqr} = P_m^g P_i^0 + Q_m^g Q_i^0 \qquad \forall i \in \Omega_{\mathrm{B}}, m \in \Omega_{\mathrm{G}}|_{i=m} \qquad (5.16)$$

Constraints (4.7) and (4.24) are linearized using piece-wise approximation function. Where the accuracy of P_{ij}^2, Q_{ij}^2 and $\big(P_{mn,c,t}^{\mathrm{red}}\big)^2$, $\big(Q_{mn,c,t}^{\mathrm{red}}\big)^2$ will depend on the number of discrete steps Γ are representing by the follow equations (5.17) - (5.24) and (5.25) - (5.32) respectively:

$$\big(V_j^0\big)^2 I_{ij}^{sqr} = \sum_{\gamma=1}^{\Gamma} m_{ij,\gamma}^S \Delta_{ij,\gamma}^P + \sum_{\gamma=1}^{\Gamma} m_{ij,\gamma}^S \Delta_{ij,\gamma}^Q \qquad \forall ij \in \Omega_{\mathrm{L}} \qquad (5.17)$$

$$P_{ij}^+ - P_{ij}^- = P_{ij} \qquad \forall ij \in \Omega_{\mathrm{L}} \qquad (5.18)$$

$$P_{ij}^{+} + P_{ij}^{-} = \sum_{\gamma=1}^{\Gamma} \Delta_{ij,\gamma}^{P} \qquad \forall ij \in \Omega_{\mathrm{L}} \tag{5.19}$$

$$Q_{ij}^{+} - Q_{ij}^{-} = Q_{ij} \qquad \forall ij \in \Omega_{\mathrm{L}} \tag{5.20}$$

$$Q_{ij}^{+} + Q_{ij}^{-} = \sum_{\gamma=1}^{\Gamma} \Delta_{ij,\gamma}^{Q} \qquad \forall ij \in \Omega_{\mathrm{L}} \tag{5.21}$$

$$0 \leq \Delta_{ij,\gamma}^{P} \leq \bar{\Delta}_{ij}^{S} \qquad \forall ij \in \Omega_{\mathrm{L}}, \gamma = 1 \ldots \Gamma \tag{5.22}$$

$$0 \leq \Delta_{ij,\gamma}^{Q} \leq \bar{\Delta}_{ij}^{S} \qquad \forall ij \in \Omega_{\mathrm{L}}, \gamma = 1 \ldots \Gamma \tag{5.23}$$

$$P_{ij}{}^{+}, P_{ij}{}^{-}, Q_{ij}{}^{+}, Q_{ij}{}^{-} \geq 0 \qquad \forall ij \in \Omega_{\mathrm{L}} \tag{5.24}$$

$$\begin{aligned}(E_n^0)^2 I_{mn,c,t}^{\mathrm{red,sqr}} &= \sum_{\gamma=1}^{\Gamma} m_{mn,\gamma,c,t}^{\mathrm{S,red}} \Delta_{mn,\gamma,c,t}^{\mathrm{P,red}} \\ &+ \sum_{\gamma=1}^{\Gamma} m_{mn,\gamma,c,t}^{\mathrm{S,red}} \Delta_{mn,\gamma,c,t}^{\mathrm{Q,red}} \qquad \forall mn \in \Omega_{\mathrm{L^{red}}}, c \in \Omega_{\mathrm{C}}, t \in \{0 \ldots N_{t_1} + N_{t_2}\}\end{aligned} \tag{5.25}$$

$$P_{mn,c,t}^{+,\mathrm{red}} - P_{mn,c,t}^{-,\mathrm{red}} = P_{mn,c,t}^{\mathrm{red}} \qquad \forall mn \in \Omega_{\mathrm{L^{red}}}, c \in \Omega_{\mathrm{C}}, t \in \{0 \ldots N_{t_1} + N_{t_2}\} \tag{5.26}$$

$$P_{mn,c,t}^{+,\mathrm{red}} + P_{mn,c,t}^{-,\mathrm{red}} = \sum_{\gamma=1}^{\Gamma} \Delta_{mn,\gamma,c,t}^{\mathrm{P,red}} \qquad \forall mn \in \Omega_{\mathrm{L^{red}}}, c \in \Omega_{\mathrm{C}}, t \in \{0 \ldots N_{t_1} + N_{t_2}\} \tag{5.27}$$

$$Q_{mn,c,t}^{+,\mathrm{red}} - Q_{mn,c,t}^{-,\mathrm{red}} = Q_{mn,c,t}^{\mathrm{red}} \qquad \forall mn \in \Omega_{\mathrm{L^{red}}}, c \in \Omega_{\mathrm{C}}, t \in \{0 \ldots N_{t_1} + N_{t_2}\} \tag{5.28}$$

$$Q_{mn,c,t}^{+,\mathrm{red}} + Q_{mn,c,t}^{-,\mathrm{red}} = \sum_{\gamma=1}^{\Gamma} \Delta_{mn,\gamma,c,t}^{\mathrm{Q,red}} \qquad \forall mn \in \Omega_{\mathrm{L^{red}}}, c \in \Omega_{\mathrm{C}}, t \in \{0 \ldots N_{t_1} + N_{t_2}\} \tag{5.29}$$

$$0 \leq \Delta_{mn,\gamma,c,t}^{\mathrm{P,red}} \leq \bar{\Delta}_{mn,c,t}^{\mathrm{S,red}} \qquad \forall mn \in \Omega_{\mathrm{L^{red}}}, c \in \Omega_{\mathrm{C}}, t \in \{0 \ldots N_{t_1} + N_{t_2}\}, \gamma = 1 \ldots \Gamma \tag{5.30}$$

$$0 \leq \Delta_{mn,\gamma,c,t}^{Q,\mathrm{red}} \leq \bar{\Delta}_{mn,c,t}^{\mathrm{S,red}} \qquad \forall mn \in \Omega_{\mathrm{L^{red}}}, c \in \Omega_{\mathrm{C}}, t \in \{0 \ldots N_{t_1} + N_{t_2}\}, \gamma = 1 \ldots \Gamma \tag{5.31}$$

$$P_{mn,c,t}^{+,\mathrm{red}}, P_{mn,c,t}^{-,\mathrm{red}}, Q_{mn,c,t}^{+,\mathrm{red}}, Q_{mn,c,t}^{-,\mathrm{red}} \geq 0 \qquad \forall mn \in \Omega_{\mathrm{L^{red}}}, c \in \Omega_{\mathrm{C}}, t \in \{0 \ldots N_{t_1} + N_{t_2}\} \tag{5.32}$$

The right terms of constraints (5.17) and (5.25) represent the piece-wise linearization of (4.7) and (4.24), where Γ is the number of linearization blocks, $\overline{\Delta}_{ij}^{S}$ and $\overline{\Delta}_{mn,c,t}^{\mathrm{S,red}}$ are the upper bounds of the linearization blocks, are calculated as:

$$\overline{\Delta}_{ij}^{\mathrm{S}}=\frac{\overline{V}\,\overline{I}_{ij}}{\Gamma};\ \overline{\Delta}_{mn,c,t}^{\mathrm{S,red}}=\frac{\overline{V}\,\overline{I}_{mn,c}^{\mathrm{red}}}{\Gamma}$$

Where $\overline{I}_{mn,c}^{\mathrm{red}}$, is the maximum current in the branches of the reduced network. The terms $m_{ij,\gamma}^{S}$ and $m_{mn,\gamma,c,t}^{\mathrm{S,red}}$ is the slope of γ–th block and is calculated by:

$$m_{ij,\gamma}^{S}=(2\Gamma-1)\overline{\Delta}_{ij}^{\mathrm{S}},\qquad m_{mn,\gamma,c,t}^{\mathrm{S,red}}=(2\Gamma-1)\overline{\Delta}_{mn,c,t}^{\mathrm{S,red}}$$

The terms $\Delta_{ij,\gamma}^{P}$ and $\Delta_{mn,\gamma,c,t}^{\mathrm{P,red}}$ are the γ-th value of the P_{ij} and $P_{mn,c,t}^{\mathrm{red}}$ respectively, $\Delta_{ij,\gamma}^{Q}$ and $\Delta_{mn,\gamma,c,t}^{\mathrm{Q,red}}$ are the γ–th value of the Q_{ij} and $Q_{mn,c,t}^{\mathrm{red}}$ respectively. ${P_{ij}}^{+}, {P_{ij}}^{-}$ and $P_{mn,c,t}^{+,\mathrm{red}}, P_{mn,c,t}^{-,\mathrm{red}}$ are auxiliary variables, non-negatives, to represent $|P_{ij}|$ and $|P_{mn,c,t}^{\mathrm{red}}|$ respectively, ${Q_{ij}}^{+}, {Q_{ij}}^{-}$ and $Q_{mn,c,t}^{+,\mathrm{red}}, Q_{mn,c,t}^{-,\mathrm{red}}$ are auxiliary variables, non-negatives, to represent $|Q_{ij}|$ and $|Q_{mn,c,t}^{\mathrm{red}}|$ respectively, as seen in (5.18), (5.20), (5.26) and (5.28) respectively. To ensure that the sum of all the blocks are equal to $|P_{ij}|$, $|Q_{ij}|$, $|P_{mn,c,t}^{\mathrm{red}}|$, $|Q_{mn,c,t}^{\mathrm{red}}|$ is used the constraints (5.19), (5.21), (5.27) and (5.29). The constraints (5.22), (5.23), (5.30) and (5.31), fix the upper limits of the $|P_{ij}|$, $|Q_{ij}|$, $|P_{mn,c,t}^{\mathrm{red}}|$, $|Q_{mn,c,t}^{\mathrm{red}}|$, the constraints (5.24) and (5.32) guarantee the non-negativity of the auxiliary variables.

5.2. LINEARIZATION OF THE SWITCHABLE SHUNT ELEMENTS

Considering the change-in-variable $V_i^{\mathrm{sqr}} \equiv V_i^2$, the nonlinear constraint (4.4) is linearized using the disjunctive equivalent shown in (5.33) - (5.36):

$$\underline{V}^2(1-h_i) \le V_i^{sqr} - \frac{Q_i^{sh}}{b_i^{sh}} \le \overline{V}^2(1-h_i) \qquad \forall i \in \Omega_{\mathrm{B}}, b_i^{sh} \neq 0 \qquad (5.33)$$

$$h_i \underline{V}^2 b_i^{sh} \leq Q_i^{sh} \leq h_i \overline{V}^2 b_i^{sh} \qquad \forall i \in \Omega_{\mathrm{B}}, b_i^{sh} > 0 \tag{5.34}$$

$$h_i \underline{V}^2 b_i^{sh} \geq Q_i^{sh} \geq h_i \overline{V}^2 b_i^{sh} \qquad \forall i \in \Omega_{\mathrm{B}}, b_i^{sh} < 0 \tag{5.35}$$

$$Q_i^{sh} = 0 \qquad \forall i \in \Omega_{\mathrm{B}}, b_i^{sh} = 0 \tag{5.36}$$

Disjunctive constraints (5.33)–(5.36) represent the product $h_i V_i^{\mathrm{sqr}} b_i^{sh}$ exactly, given the binary nature of h_i. When the shunt element is capacitive, $b_i^{sh} > 0$, the constraints (5.33) and (5.34) are used. When the shunt element is inductive, $b_i^{sh} < 0$, the constraints (5.33) and (5.35). Finally, when there is no shunt element, $b_i^{sh} = 0$, the constraint (5.36) is used.

5.3. LINEARIZATION OF THE OLTC TRANSFORMERS

Considering the change-in-variable $V_i^{\mathrm{sqr}} \equiv V_i^2$, the first term of the left-side-member of (4.5) can be replaced by the auxiliary variable $\tilde{V}_i^{\mathrm{sqr}}$, which is the regulated voltage magnitude at the OLTC transformer as shown in (5.37).

$$\tilde{V}_i^{\mathrm{sqr}} = V_i^{\mathrm{sqr}} \left[1 + \mathrm{Reg}_{ij} \frac{nt_{ij}}{\overline{\mathrm{nt}}_{ij}} \right]^2 \qquad \forall ij \in \Omega_{\mathrm{L}} \tag{5.37}$$

Constraint (5.37) indicates that the regulated voltage depends on the percentage of the regulation, the tap position and the maximum number of steps. Note that the constraint (5.37) is nonlinear. Thus, to linearize it, the square integer variable nt_{ij}^2 is transformed with a binary variable $t_{ij,k}$, where $k \in 1 \ldots 2\overline{nt}_{ij}$ which represents the tap position of the OLTC transformer connected between buses i and j, and the term $nt_{ij}^2 V_i^{\mathrm{sqr}}$ is replaced through the auxiliary variable $V_{ij,k}^{\mathrm{c}}$ as shown by the linearized expression in (5.38) - (5.42):

$$\tilde{V}_i^{\mathrm{sqr}} = V_i^{\mathrm{sqr}} \left(1 - \mathrm{Reg}_{ij}\right)^2 + \sum_{k=1}^{2\overline{\mathrm{nt}}_{ij}} \frac{\mathrm{Reg}_{ij}}{\overline{\mathrm{nt}}_{ij}} \left[\frac{\mathrm{Reg}_{ij}}{\overline{\mathrm{nt}}_{ij}} (2k-1) + 2\left(1 - \mathrm{Reg}_{ij}\right) \right] V_{ij,k}^{\mathrm{c}} \qquad \forall ij \in \Omega_{\mathrm{L}} \tag{5.38}$$

$$\underline{V}^2(1-t_{ij,k}) \leq V_i^{\text{sqr}} - V_{ij,k}^{\text{c}} \leq \overline{V}^2(1-t_{ij,k}) \qquad \forall ij \in \Omega_{\text{L}}, \forall k = 1 \dots 2\overline{\text{nt}}_{ij} \qquad (5.39)$$

$$\underline{V}^2 t_{ij,k} \leq V_{ij,k}^{\text{c}} \leq \overline{V}^2 t_{ij,k} \qquad \forall ij \in \Omega_{\text{L}}, \forall k = 1 \dots 2\overline{\text{nt}}_{ij} \qquad (5.40)$$

$$t_{ij,k} \leq t_{ij,k-1} \qquad \forall ij \in \Omega_{\text{L}}, \forall k = 2 \dots 2\overline{\text{nt}}_{ij} \qquad (5.41)$$

$$t_{ij,k} \in \{0,1\} \qquad \forall ij \in \Omega_{\text{L}}, \forall k = 1 \dots 2\overline{\text{nt}}_{ij} \qquad (5.42)$$

Constraints (5.38)–(5.42) represent the linearized model for the regulated voltage magnitude. Constraint (5.38) calculates the magnitude of the regulated voltage based on the binary version of the tap position $t_{ij,k}$. Disjunctive constraints (5.39) and (5.40) define the value of the auxiliary variable $V_{ij,k}^{\text{c}}$ according to the value of $t_{ij,k}$. Constraint (5.41) guarantees the sequence of the tap position $t_{ij,k}$ within the set $k = 1 \dots 2\overline{\text{nt}}_{ij}$. Finally, (5.42) defines the binary nature of the tap position $t_{ij,k}$. The integer variable nt_{ij} can be calculate using (5.43):

$$nt_{ij} = -\overline{\text{nt}}_{ij} + \sum_{k=1}^{2\overline{\text{nt}}_{ij}} t_{ij,k} \qquad \forall ij \in \Omega_{\text{L}} \qquad (5.43)$$

Finally, the linear expression for (4.5) is given by (5.44):

$$\tilde{V}_i^{\text{sqr}} - V_j^{\text{sqr}} = 2(R_{ij}P_{ij} + X_{ij}Q_{ij}) + Z_{ij}^2 I_{ij}^{\text{sqr}} \qquad \forall ij \in \Omega_{\text{L}} \qquad (5.44)$$

5.4. PROPOSED MILP MODEL

The N-1 multi–contingency TSC–OPF problem could be modeled as an approximate MILP model, the quadratic term in (4.1) is approximated using the piece-wise approximation function as seen in (5.45)–(5.49):

$$\left(P_{\mathrm{i}}^{\mathrm{g}}\right)^2 = \sum_{\gamma=1}^{\Gamma} (m_{i,\gamma}^{\mathrm{Sg}}\, \Delta_{i,\gamma}^{\mathrm{Pg}})$$

$$P_{\mathrm{i}}^{\mathrm{g+}} - P_{\mathrm{i}}^{\mathrm{g-}} = P_{\mathrm{i}}^{\mathrm{g}} \qquad \forall i \in \Omega_{\mathrm{B}} \quad (5.45)$$

$$P_{\mathrm{i}}^{\mathrm{g+}} - P_{\mathrm{i}}^{\mathrm{g-}} = \sum_{\gamma=1}^{\Gamma} \Delta_{i,\gamma}^{\mathrm{Pg}} \qquad \forall i \in \Omega_{\mathrm{B}} \quad (5.46)$$

$$0 \le \Delta_{i,\gamma}^{P\mathrm{g}} \le \Delta_{i,\gamma}^{\mathrm{Sg}} \qquad \forall i \in \Omega_{\mathrm{B}}, \gamma = 1 \ldots \Gamma \quad (5.47)$$

$$0 \le P_{\mathrm{i}}^{\mathrm{g+}} \qquad \forall i \in \Omega_{\mathrm{B}} \quad (5.48)$$

$$0 \le P_{\mathrm{i}}^{\mathrm{g-}} \qquad \forall i \in \Omega_{\mathrm{B}} \quad (5.49)$$

Finally, the MILP model is given by (5.50):

$$\min v = \sum_{i \in \Omega_{\mathrm{B}}} \left(a_i^{\mathrm{g}} \left(\sum_{\gamma=1}^{\Gamma} \left(m_{i,\gamma}^{\mathrm{Sg}}\, \Delta_{i,\gamma}^{\mathrm{Pg}} \right) \right) + b_i^{\mathrm{g}} P_i^{\mathrm{g}} + c_i^{\mathrm{g}} \right) + \sum_{i \in \Omega_{\mathrm{B}}} \left(c^{ls} P_i^{\mathrm{d}} r_i \right)$$

Subject to:

(5.50)

Pre-fault: (4.10)–(4.13), (4.15),(5.1) –(5.6), (5.13) –(5.14), (5.16), (5.17)–(5.24), (5.33)–(5.36), (5.38)–(5.42), (5.44) and (5.45)–(5.49).

Fault and post-fault: (4.25)–(4.32), (5.7)–(5.9), (5.15), (5.25)–(5.32).

The optimization model (5.50) is a MILP problem and its optimality can be guaranteed by classical optimization techniques.

5.5. PROPOSED OPTIMIZATION METHODOLOGY

The step–by–step procedure to solve the N-1 multi–contingency TSC–OPF problem is presented as follows:

- **Step 1:** Define Ω_{C}. Based on the experience on transient stability studies, define $t_{\mathrm{c}}^{\mathrm{fc}}$, $t_{\mathrm{c}}^{\mathrm{max}}$, N_{t_1} and N_{t_2}. For each fault location and line isolated by the protection system, calculate the reduced network parameters $R_{mn,c,t}^{\mathrm{red}}, X_{mn,c,t}^{\mathrm{red}}, Z_{mn,c,t}^{\mathrm{red}}, G_{m,c,t}^{\mathrm{sh,red}}$, and $B_{m,c,t}^{\mathrm{sh,red}}$, $\forall mn \in \Omega_{\mathrm{L^{red}}}, c \in \Omega_{\mathrm{C}}, t \in \{0 \dots N_{t_1} + N_{t_2}\}$. From the data, is know $nt_{ij}^{0}, \forall ij \in \Omega_{\mathrm{L}}$. Run an AC load flow to obtained the initial values of $V_i^0, \theta_i^0, P_i^0, Q_i^0\ \forall i \in \Omega_{\mathrm{B}}$. Let $E_m^0 = V_i^0$ and $\delta_m^0 = \theta_i^0, \forall i \in \Omega_{\mathrm{B}}, m \in \Omega_{\mathrm{G}}|_{i=m}$; $\delta_{m,c,t}^0 = \delta_m^0, \forall m \in \Omega_{\mathrm{G}}, c \in \Omega_{\mathrm{C}}, t \in \{0 \dots N_{t_1} + N_{t_2}\}$ and $v^* = 0$.

- **Step 2:** Solve the relaxed version (disregarding the discrete nature of the decision variables) of the MILP model (5.50) using a commercial LP solver. Save the objective function v and obtain improved values of the initial parameters: $V_i^0 = \sqrt{V_i^{\mathrm{sqr}}}$ and $\theta_i^0 = \theta_i$, $\forall i \in \Omega_{\mathrm{B}}$, $P_i^0 = P_m^{\mathrm{g}}$ and $Q_i^0 = Q_m^{\mathrm{g}}, \forall i \in \Omega_{\mathrm{B}}, m \in \Omega_{\mathrm{G}}|_{i=m}$, $E_m^0 = E_m$ and $\delta_m^0 = \delta_m, \forall m \in \Omega_{\mathrm{G}}$, $\delta_{m,c,t}^0 = \delta_{m,c,t}, \forall m \in \Omega_{\mathrm{G}}, c \in \Omega_{\mathrm{C}}, t \in \{0 \dots N_{t_1} + N_{t_2}\}$.

- **Step 3:** If $|v - v^*| \geq \epsilon$, then let $v^* = v$ and go back to Step 2. Otherwise, continue to Step 4.

- **Step 4:** Solve the MILP model (5.50) considering the discrete controls using a commercial MILP solver. Let $v^* = v$ and obtain improved values of the initial parameters: $V_i^0 = \sqrt{V_i^{\mathrm{sqr}}}$ and $\theta_i^0 = \theta_i$, $\forall i \in \Omega_{\mathrm{B}}$, $P_i^0 = P_m^{\mathrm{g}}$ and $Q_i^0 = Q_m^{\mathrm{g}}, \forall i \in \Omega_{\mathrm{B}}, m \in \Omega_{\mathrm{G}}|_{i=m}$, $E_m^0 = E_m$ and $\delta_m^0 = \delta_m, \forall m \in \Omega_{\mathrm{G}}$, $\delta_{m,c,t}^0 = \delta_{m,c,t}, \forall m \in \Omega_{\mathrm{G}}, c \in \Omega_{\mathrm{C}}, t \in \{0 \dots N_{t_1} + N_{t_2}\}$. Using (5.43) calculate $nt_{ij}^0, \forall ij \in \Omega_{\mathrm{L}}$.

- **Step 5:** Fix the binary solution $t_{ij,k}, \forall ij \in \Omega_{\mathrm{L}}, \forall k = 1 \dots 2\overline{\mathrm{nt}}_{ij}$ and $h_i V_i \in \Omega_{\mathrm{B}}$ obtained in Step 4. Solve the relaxed version of the MILP model (5.50) using a commercial LP solver.

Save the objective function v and obtain improved values of the initial parameters: $V_i^0 = \sqrt{V_i^{\mathrm{sqr}}}$ and $\theta_i^0 = \theta_i$, $\forall i \in \Omega_{\mathrm{B}}$, $P_i^0 = P_m^{\mathrm{g}}$ and $Q_i^0 = Q_m^{\mathrm{g}}$, $\forall i \in \Omega_{\mathrm{B}}, m \in \Omega_{\mathrm{G}}|_{i=m}$, $E_m^0 = E_m$ and $\delta_m^0 = \delta_m, \forall m \in \Omega_{\mathrm{G}}$, $\delta_{m,c,t}^0 = \delta_{m,c,t}, \forall m \in \Omega_{\mathrm{G}}, c \in \Omega_{\mathrm{C}}, t \in \{0 \dots N_{t_1} + N_{t_2}\}$.

- **Step 6:** If $|v - v^*| \geq \epsilon$, then let $v^* = v$ and go back to Step 5. Otherwise, continue to Step 7.

- **Step 7:** Validate the obtained result in the time-domain simulation using a commercial stability software.

The flowchart of the Figure 5.1 shows the novel proposed optimization methodology, based on LP and MILP problems sequence, considering initial values for the principal variables obtained from AC load flow calculation.

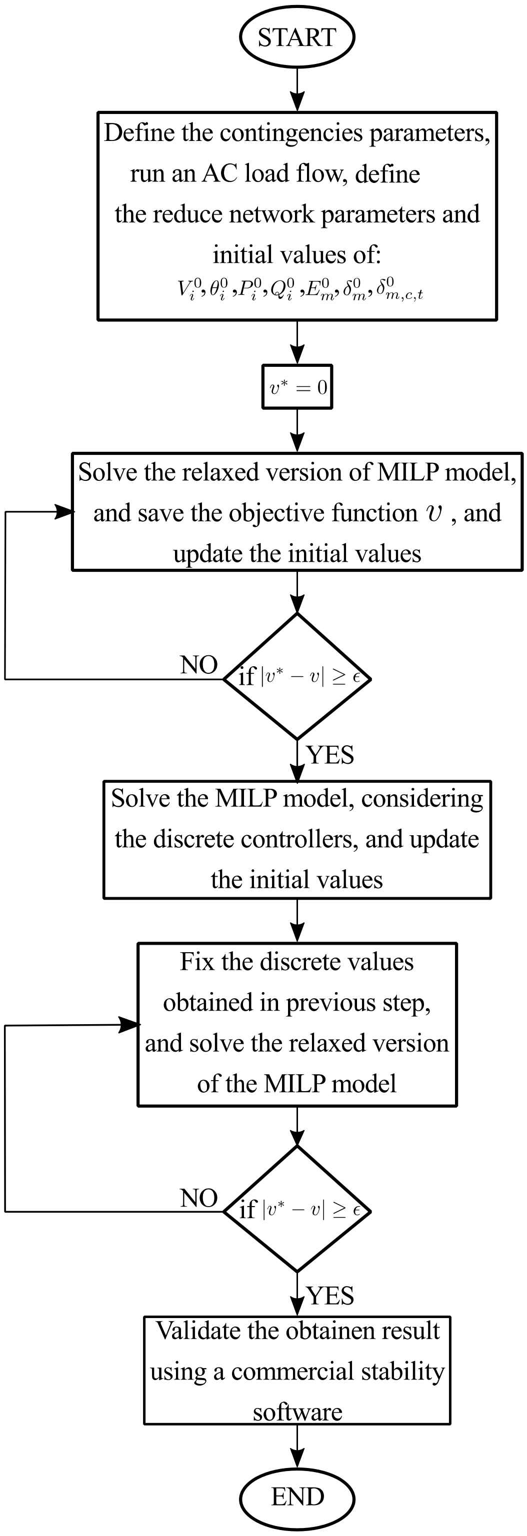

Figure 5.1 - Flowchart of the novel optimization process

5.6. IMPORTANT REMARKS

Unlike (CALLE, CASTRONUOVO and LEDESMA, 2013), this research presents besides the branch flow model, the multi-contingency assessment, where the index c indicates the set of contingencies as seen in (YUAN, KUBOKAWA and SASAKI, 2003), (LI, YUAN, *et al.*, 2011); and the discrete controls of the shunt elements and regulation of OLTC, that is enough that the model be heavier computationally. The number of contingencies based on the quantity of the index c can be more while the system is smaller.

The branch flow model, allows using linearization techniques as the piece-wise approximation (ARIAS, TABARES, *et al.*, 2018) which uses a number of blocks that according to their amount improves the response. The change of quadratic variables and the approximation of $\sin(\psi)$, are the most used and proven linearization techniques for this type of approaches, the $\sin(\psi)$ approximation serves for any angle since it uses initial values, updated in each iteration in the optimization process.

The majority of existing publication disregard an optimization process and uses as initial operating point a nonlinear version of the model, thus increasing the computational burden and only the degree of accuracy of the linear model would be checked. The novel optimization methodology shown in this dissertation improves the degree of accuracy of the MILP model through the consecutive solution of the relaxed version of the MILP model improving the response according to the predefined error.

CHAPTER SIX:

TESTS CASES

The proposed MILP model was implemented in the modeling language AMPL (FOURER, GAY and KERNIGHAN, 2003). The MILP and LP models were solved using an off–the–shelf commercial solver CPLEX (ILOG, 2008). All the tests are carried out using a 3.41GHz Intel core i7–6700 processor with 16GB of RAM. The modified 9–Bus/3–Generators WSCC, the modified IEEE 14–Bus/5–Generators, 39–Bus/10–Generators New England and the modified IEEE 68–Bus/16–Generators systems are used to show the efficiency and scalability of the proposed method.

6.1. OPF MINLP AND MILP MODEL COMPARISON

In this item is presented the performance of the MINLP and MILP models to solve the TSC–OPF without the TSC, of the 9–bus / 3–generators WSCC system, 14–bus / 5–generators IEEE system, 39–bus / 10–generators New England system and the 68–bus / 16–generators IEEE system. In Table 6.1 is shown the OPF results for the four cases systems, where the MINLP presented better results than the MILP model in terms of generation cost.

System		**Generation Cost [US$]**	**Active Power Losses [MW]**	**Time [s]**
9 Bus	OPF MINLP	2063.33	6.4830	0.06
	OPF MILP	2063.16	6.4899	0.03
14 Bus	OPF MINLP	6066.74	1.5855	17.97
	OPF MILP	6086.41	1.5096	0.94
39 Bus	OPF MINLP	93546.70	36.6551	8.14
	OPF MILP	94079.78	38.3658	1.75
68 Bus	OPF MINLP	346635.61	372.7545	86.28
	OPF MILP	349790.32	390.4930	6.23

Table 6.1 – Generation cost and active power losses of OPF

The results of Table 6.1 show the degree of precision of the MILP model and the linearization techniques adopted to presented the MILP model. Since the results are similar and with small error. The simulation time are also shown and it can be noted the difference between the models, resulting the MILP model more efficient in terms of computation time. These results can be stable or instable in transient stability terms. In the next sections, it will be shown that these obtained operating points are not necessarily stables. The main characteristic of these results is the economic operation of the EPS, finding cheap operating points in active generation terms, however this fact does not guarantee a stable operation of the EPS.

6.2. 9–BUS / 3–GENERATORS WSCC MODIFIED SYSTEM

For this system, network and dynamic data can be found in (ANDERSON and FOUAD, 1977), the production costs and generation limits were based on the study conducted in (PAI and GUYEN, 2003). This small system is commonly used in transient stability studies and has 3 generation buses and 3 loads buses.

The Table 6.2, details the technical and economic data for this system, where we observe the basic dynamic data for multimachine transient stability analysis of the EPS, the transient reactance and the inertia and damping constants. We also observe the limits of active and reactive power generation. The linear and constant coefficients of the production cost equation are presented as the economic data for this system, neglecting the quadratic coefficient because it has a small value. Table 6.3 shows the contingencies data, three N-1 contingencies whit different clearing times was tested, these contingencies are visible in Figure 6.1, the shunt compensation location and the three faults location are also visible.

Gen.	**Technical Data**							**Economic Data**		
	X_{d_g} [pu]	H_g [pu]	D_g [pu]	$\overline{P}_i^g$ [MW]	$\underline{P}_i^g$ [MW]	$\overline{Q}_i^g$ [Mvar]	$\underline{Q}_i^g$ [Mvar]	a_i^g [US^2/MW]	b_i^g [US$/MW]	c_i^g [US$]
$G1$	0.0608	23.6	0	100	0	100	-100	0.01	5.0	150
$G2$	0.1198	6.40	0	200	0	100	-100	0.01	1.2	600
$G3$	0.1813	3.01	0	90	0	100	-100	0.01	1.0	335

Table 6.2 – Technical and Economic Data 9-bus/3-generators system

Contingency	**3ϕ Fault Bus**	**Transmission Line Out**	t_i^{fc} [s]	t_i^{max} [s]
C1	7	5 – 7	0.083	2
C2	5	4 – 5	0.095	2
C3	9	6 – 9	0.080	2

Table 6.3 – *N-1* Contingencies for 9–bus/3–generators WSCC system

For this system, as seen in the Figure 6.1, three contingencies are evaluated, this selection is based on the literature and on the experience in transient stability studies. These contingencies are evaluated one independent of the other. The Table 6.4 shows the TSC–OPF considerations or operating data, as the tap regulation percentage, the number of steps of the OLTC, the limits of terminal and internal voltage, the limits of angle deviation with respect to COI, the angular speed limits, the integration steps for the fault and post fault stages are also shown, the load shedding cost, the piece-wise steps number, the angular velocity and the error of optimization process are shown.

Operating Data															
$\mathbf{Reg}_{ij}$	$\overline{\mathbf{nt}}_{ij}$	$\overline{V}$	$\underline{V}$	$\overline{E}$	$\underline{E}$	$\overline{\delta}$	$\underline{\delta}$	$\Delta\overline{\omega}$	$\Delta\underline{\omega}$	N_{t_1}	N_{t_2}	c^{ls}	Γ	ω_0	ϵ
10%	8	1.05	0.95	1.20	0.80	±45°		±0.01		25	500	30	20	377	0.001

Table 6.4 – Operating Data 9–bus/3–generators system

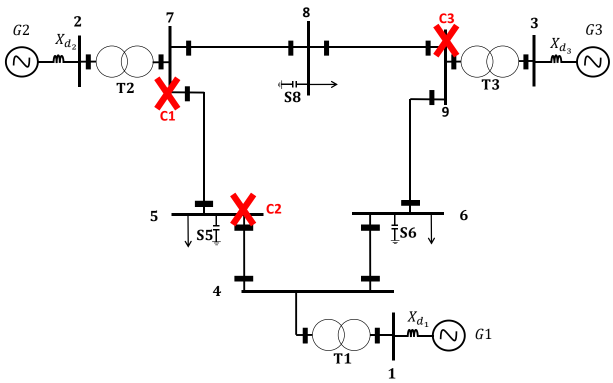

Figure 6.1 – 9–bus/3–generators system and N-1 contingencies

Evaluating contingency C1

The contingency C1, is based on (ANDERSON and FOUAD, 1977), where the disturbance initiating the transient is a three–phase fault occurring near bus 7 at the end of line 5–7. The fault is cleared in five cycles (0.083 s) by opening the line 5–7, as seen in Table 6.3.

Figure 6.2 and Figure **6.3**, show the rotor angle deviation with respect to COI and the rotor angular speed respectively. In Figure 6.2, the rotor angles deviation obtained from MILP model, are within the predefined limits, the angular speed deviation during the fault is also within the limits, and we can see the perturbation effect until the protection system clears the fault. The rotor angle of generator G2 reaches its limit in the first cycle, but in the second cycle the rotor angle is reduced, for that reason the system is stable, in addition that the model maintains that deviation within the limits.

Gen.	**Dispatch [MW]**	**OLTC**	$\boldsymbol{nt_{ij}}$	**Tap**	**Shunt**	**Status**	**Cost MILP [US$]**	**Cost MINLP [US$]**
G1	75.50	T1	-5	0.969	S5	ON	2113.82	2112.28
G2	154.30	T2	-3	0.981	S6	OFF		
G3	90.00	T3	-6	0.963	S8	OFF		

Table 6.5 – Results of the 9–bus/3–generators system, contingency C1

Also Table 6.5 shows the operating results, where we can see that the power generation of G3 is maximum, because it is the cheaper, and the rest of load, is distributed among the other two generators. The OLTC are regulated in the pre–fault stage and the tap position and the voltage values are shown. The discrete operation of the shunt elements is also shown. These two considerations are to keep the voltages in the buses within the limits. The generation cost of MILP and MINLP are also presented, highlighting a slight difference between both, the computation times were 1.27s and 45.95s, respectively.

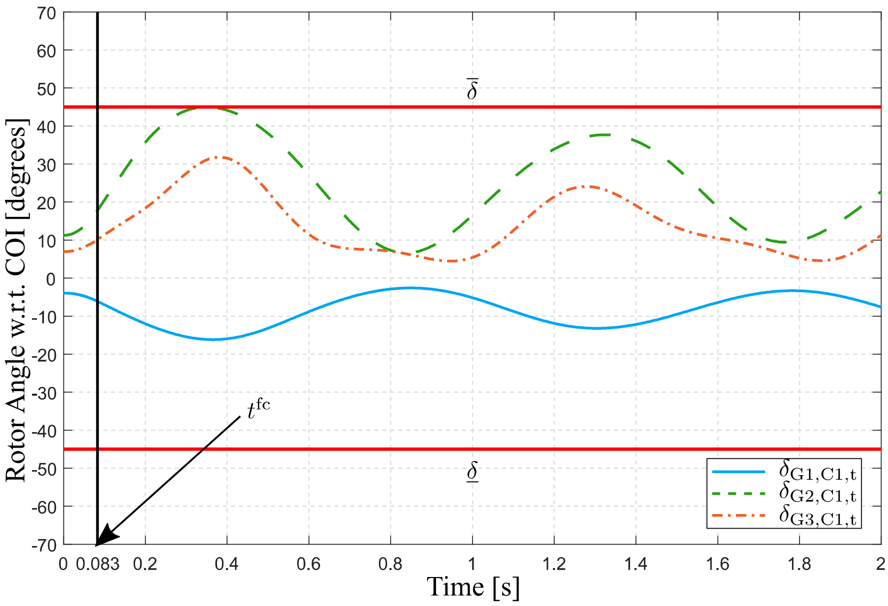

Figure 6.2 – Rotor Angle deviation w.r.t. COI 9–bus/3–generators system – Contingency C1

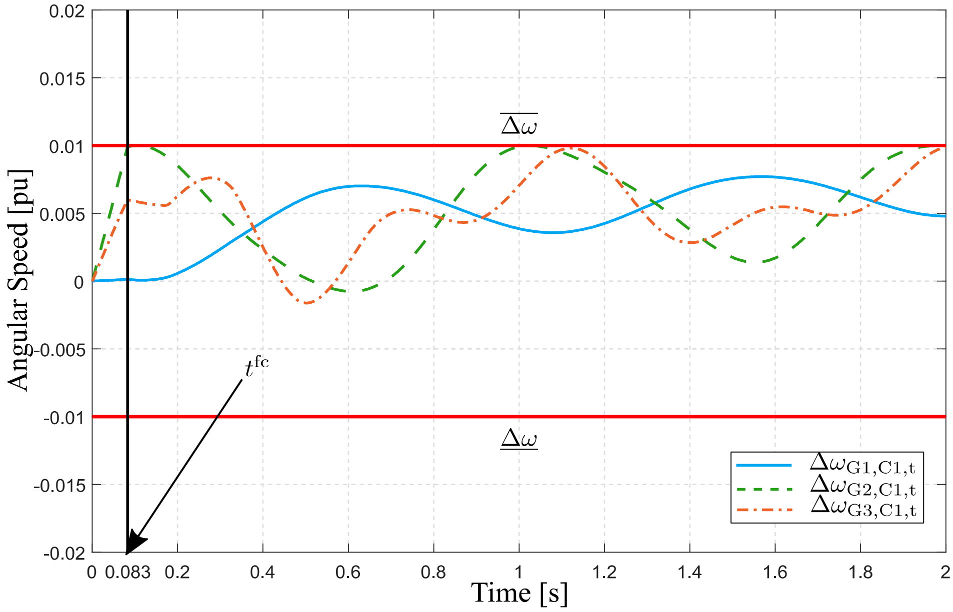

Figure 6.3 – Angular Speed 9–bus/3–generators system – Contingency C1

Evaluating contingencies C1 and C2

In this part, a new contingency is added based on transient stability studies. The operating results are shown in the Table 6.6, where, as expected the objective function (generation cost) is higher than in the previous case, because the model becomes more restricted. The computational burden increased for this reason. The computation time was 3173.92s. This increase is due to the iterative process during the minimization of the error in the optimization process. The power generation distribution is similar to the previous case, where the G3 is at its maximum capacity. The OLTC regulation and the shunt elements operation is also similar to the previous case, because the second fault is less severe than the previous case. The generation cost of the MILP and MINLP model are also presented. The MILP model results more expensive than the other one, because the approximations and simplifications require a number of steps, increasing the computational burden.

Gen.	Dispatch [MW]	OLTC	nt_{ij}	Tap	Shunt	Status	Cost MILP [US$]	Cost MINLP [US$]
G1	75.77	T1	-5	0.969	S5	ON	2114.68	2112.30
G2	154.09	T2	-2	0.988	S6	OFF		
G3	90.00	T3	-5	0.969	S8	OFF		

Table 6.6 – Results of the 9–bus/3–generators system, contingencies C1 and C2

Figure 6.4 and Figure **6.5**, show the rotor angle and rotor speed deviations. The second fault, as seen in these figures, is less severe than the other one and this is reflected in the curves. The limits are enforced, with G2 of the fault one being closest to its limit.

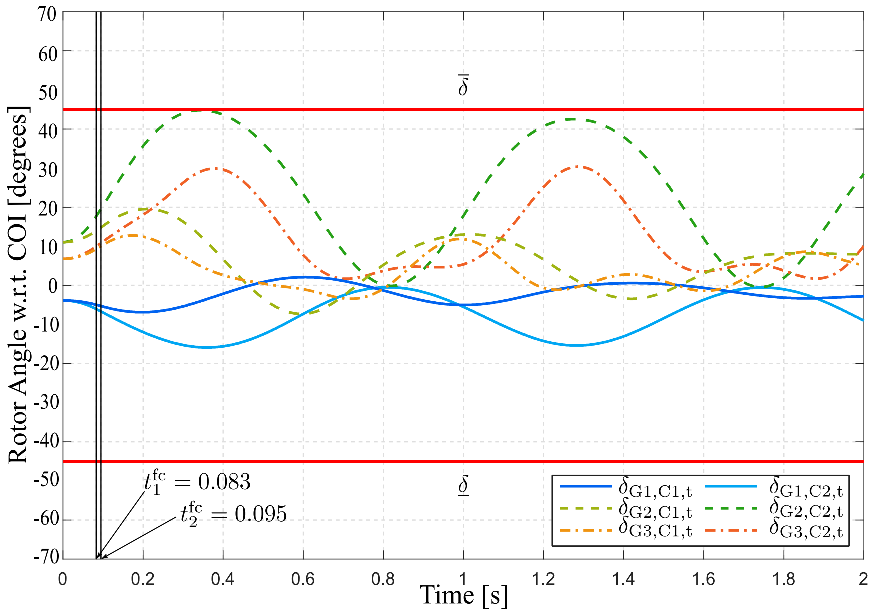

Figure 6.4 – Rotor Angle deviation w.r.t. COI 9–bus/3–generators system – Contingencies C1 and C2

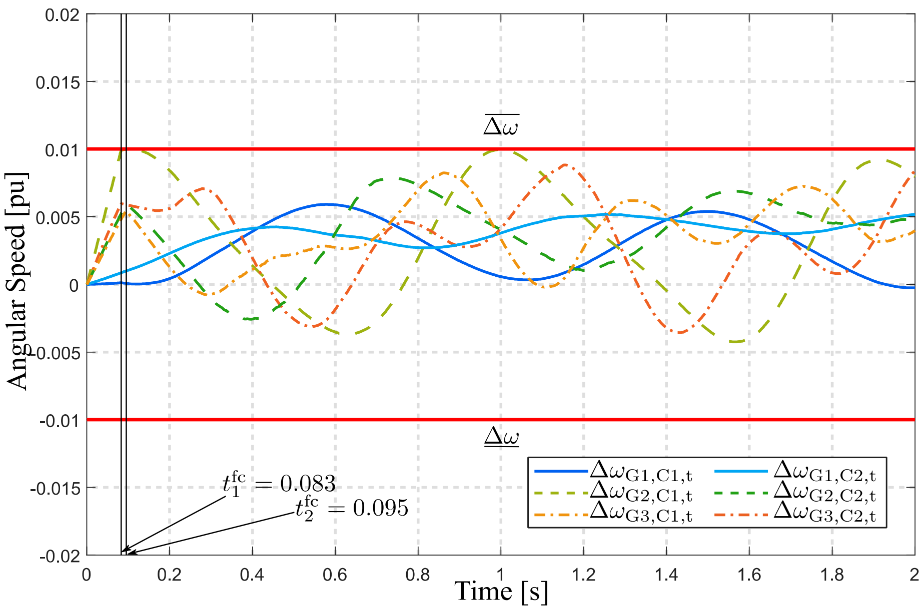

Figure 6.5 – Angular Speed 9–bus/3–generators system – Contingencies C1 and C2

contingencies C1, C2 and C3

Three contingencies are evaluated in the same model. The last contingency added to the model is similar to the first one, due to its proximity to G3. The Table 6.7 shows the operation point, the power generation is distributed among the generators and this operation point changes with reference to the other two cases, because contingency C3 is more severe than the C2. Naturally, the generation cost increases, when compared to the MINLP model. There exists a difference by the previously mentioned. The linearized version of the TSC–OPF, has an error, because it is subject to the use of linearization blocks in the application of the piecewise technique. In addition, to the other simplifications and approximations, because the model is more restrictive, the OLTC regulation and the shunt elements operation, changed with respect to previous cases.

Gen.	Dispatch [MW]	OLTC	nt_{ij}	Tap	Shunt	Status	Cost MILP [US$]	Cost MINLP [US$]
G1	81.25	T1	-5	0.969	S5	ON	2144.69	2122.75
G2	159.92	T2	-3	0.981	S6	ON		
G3	78.38	T3	-4	0.975	S8	OFF		

Table 6.7 – Results of the 9–bus/3–generators system, contingencies C1, C2 and C3

Figure 6.6 and Figure **6.7** show the rotor angle deviations and the angular speed deviations for the case involving three contingencies and the three generators. All state variables are within the predetermined limits. The Contingency C1 remains as the most severe, and the rotor angle deviation from generator G2 is around its limits. Moreover the angular speed in Figure 6.7 shows that contingencies C1 and C3 are those that most affect the system. The computational time was 3173.92s, naturally more than the previous case since the model is more restrictive.

In the previous section the Table 6.1 shows the results of the TSC–OPF without the TSC, the generation cost for this system increases respect to the obtained in Table 6.7, this is reasonable, because the TSC–OPF is more restricted than the OPF, making the generation cost more expensive.

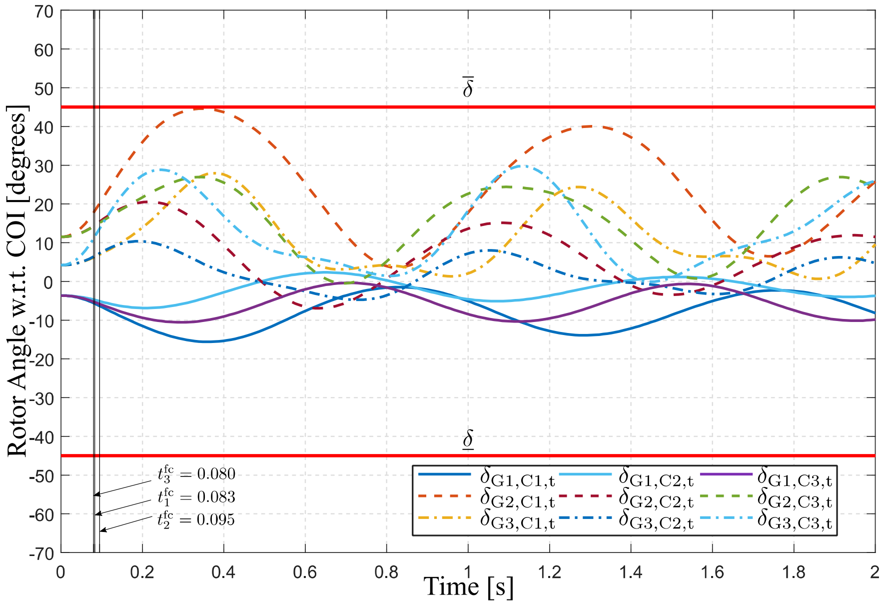

Figure 6.6 – Rotor Angle deviation w.r.t. COI 9–bus/3–generators system – Contingencies C1, C2 and C3

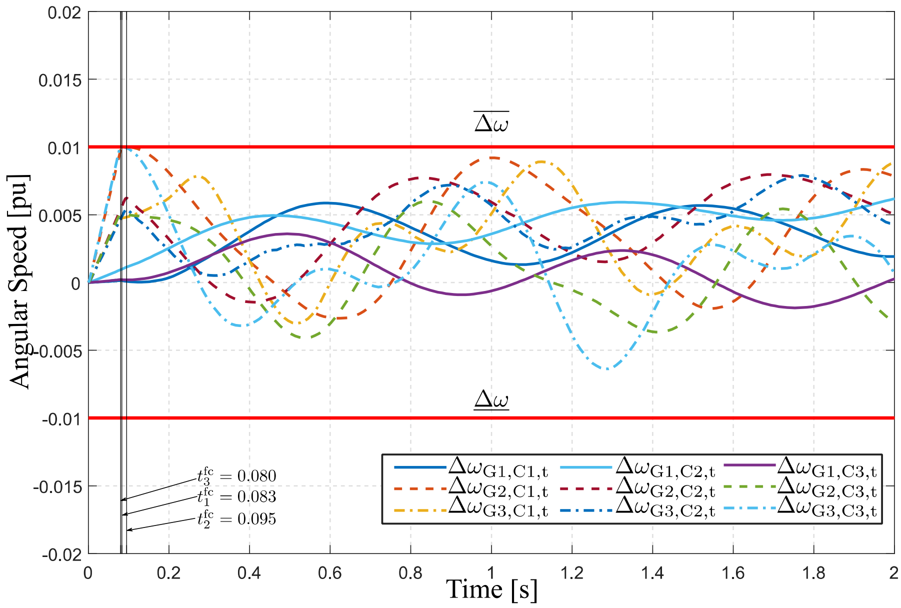

Figure 6.7 – Angular Speed 9–bus/3–generators system – Contingencies C1, C2 and C3

TSC–OPF without TSC analysis

From the TSC–OPF without the TSC constraints, an operation point is obtained, which can be stable or instable, because in the OPF analysis only the economic operation of the EPS is calculated. Figure 6.8 shows the rotor angle deviation from the COI and the angular speed trajectories of the EPS when a contingency C1 is applied, using the TSC–OPF without the TSC operation point as initial point in a MATLAB transient stability program. As seen in the figure the rotor angle and angular speed trajectories are clearly unstable in the first five cycles.

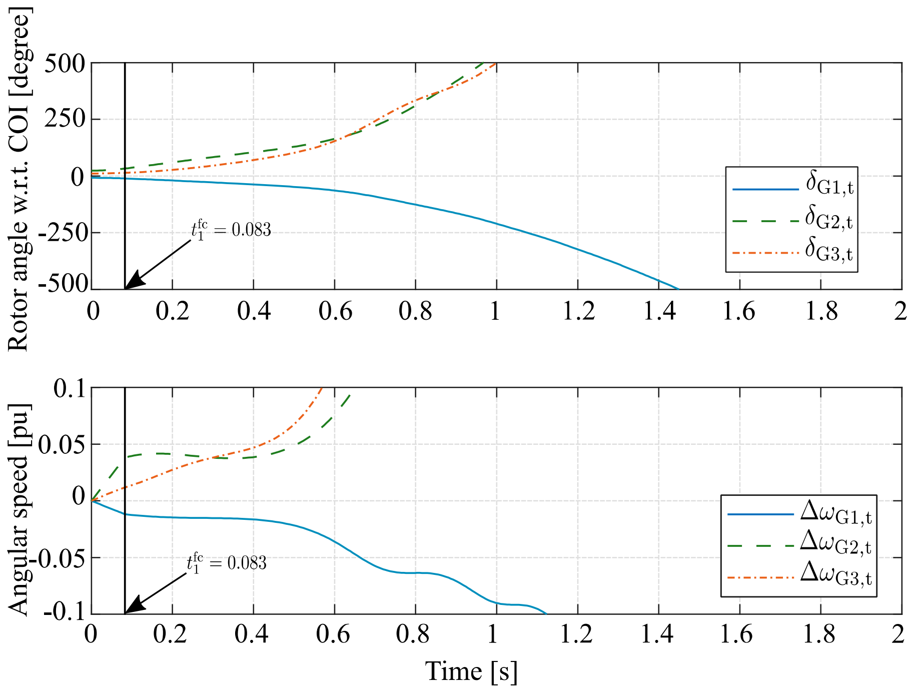

Figure 6.8 – TSC–OPF analysis without TSC 9–bus / 3–generators WSCC system

Sensitivity analysis

A sensitivity analysis over the proposed model has been performed which is summarized in Table 6.8. The generation cost and the load shedding for different transient stability limits are compared. In this case, the proposed methodology is able to identify the load shedding minimum that must be applied to the system to obtain a feasible operation.

Angle Limits $[\underline{\delta}, \overline{\delta}]$	**Generation Cost [US$]**	**Load Shedding [MW]**	**Speed Limits** $[\Delta\underline{\omega}, \Delta\overline{\omega}]$	**Generation Cost [US$]**	**Load Shedding [MW]**
90°	2144.74	0.00	0.0100	2144.69	0.00
45°	2144.69	0.00	0.0050	1902.89	95.78
30°	2176.44	4.42	0.0025	1774.96	154.85
15°	2015.83	50.07	0.0010	1716.05	191.33

Table 6.8 – 9–bus/3–generators system: Sensitive analysis

6.3. 14–BUS / 5–GENERATORS IEEE MODIFIED SYSTEM

The 14–bus/5–generators IEEE system, is commonly used in power flow analysis and optimal power flow analysis; the Table 6.9 shows the technical and economic data for the five generators of this system.

Gen.	Technical Data							Economic Data		
	X_{d_g} [pu]	H_g [pu]	D_g [pu]	$\overline{P}_i^g$ [MW]	$\underline{P}_i^g$ [MW]	$\overline{Q}_i^g$ [Mvar]	$\underline{Q}_i^g$ [Mvar]	a_i^g [US^2/MW]	b_i^g [US$/MW]	c_i^g [US$]
$G1$	0.7500	2.64	0	500	0	100	-100	0.043	40.0	100
$G2$	1.2500	9.99	0	100	0	100	-100	0.250	40.0	100
$G3$	0.7500	4.90	0	200	0	100	-100	0.010	20.0	150
$G4$	1.5000	2.64	0	100	0	100	-100	0.010	20.0	150
$G5$	1.2000	12.63	0	100	0	100	-100	0.010	20.0	150

Table 6.9 – Technical and Economic Data 14–bus/5–generators system

Network data, production costs and generation limits were based on (CHRISTIE, 1993), on the other hand, Table 6.10 shows the three contingencies. Three–phase faults are applied near to the three buses, and subsequently these faults are clarified by opening the transmission lines according to the clearance times of the protection system shows in Table 6.10.

Contingency	3ϕ Fault Bus	Transmission Line Out	t_i^{fc} [s]	t_i^{max} [s]
C1	7	7 – 9	0.070	2
C2	6	6 – 13	0.085	2
C3	1	1 – 5	0.080	2

Table 6.10 – N-1 Contingencies for 14–bus/5–generators IEEE system

The Figure 6.9 shows the N-1 contingencies which will be evaluated. The Table 6.11 shows the operating data, used to simulate the MILP model, naturally the steps number on fault and post–fault stages are less than the first case, because the generators number are increase, consequently, also the computational burden increase.

Operating Data															
$\mathbf{Reg}_{ij}$	$\overline{\mathbf{nt}}_{ij}$	$\overline{V}$	$\underline{V}$	$\overline{E}$	$\underline{E}$	$\overline{\delta}$	$\underline{\delta}$	$\Delta\overline{\omega}$	$\Delta\underline{\omega}$	N_{t_1}	N_{t_2}	c^{ls}	Γ	ω_0	ϵ
10%	8	1.10	0.90	1.20	0.80	$\pm 60°$		± 0.01		10	200	30	20	377	0.001

Table 6.11 – Operating Data 14–bus/5–generators system

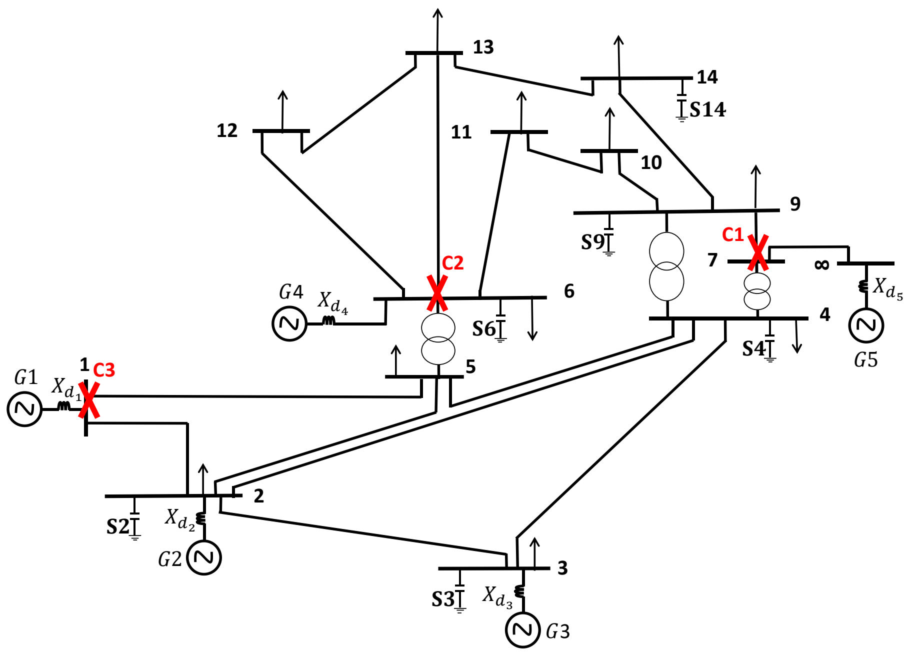

Figure 6.9 – 14–bus/5–generators system and N-1 contingencies

Evaluating contingency C1

The contingency C1, is based on experience in transient stability studies, where is applied a three–phase fault disturbance occurring near bus 7 at the end of line 7–9. The fault is cleared in 0.070s by opening the line 7–9, as seen in Table 6.9.

In Figure 6.10, the rotor angles deviation are obtained from the MILP model, in there the rotor angle deviation are into the limits, the angular speed deviation during the fault is also within the limits, and its can see the perturbation effect until the protection system clear the fault. The contingency C1 as seen in the figures is not so severe, that is reflected in the rotor angle deviations of the rotor generators, being slightly more affected the generator G3, because is the closest to the fault, besides being one of the cheapest and with less inertia constant.

Gen.	**Dispatch [MW]**	**Cost MILP [US$]**	**Cost MINLP [US$]**
G1	0.00		
G2	0.00		
G3	97.03	6086.89	6067.86
G4	75.05		
G5	88.35		

OLTC	nt_{ij}	**Tap**
T1	0	1.000
T2	0	1.000
T3	-2	0.988

Shunt	**Status**
S2	OFF
S3	ON
S4	ON
S6	ON
S9	ON
S14	OFF

Table 6.12 – Results of the 14–bus/5–generators system, contingency C1

The Table 6.12 shows the operating results, where its can see that the power generation of the generators G1 and G2 is zero, because are those that have the highest generation costs, the generators G3, G4 and G5 are distributed the total load, since they are the cheapest, and this is reflected in the generation cost, being the MILP model more expensive than the nonlinear counterpart, because the linearization techniques require a high degree of precision in the selection of piecewise block numbers; the three OLTC transformers regulation and shunt elements operation are calculated in the pre–fault stage, this to keep the voltages in the buses within the limits.

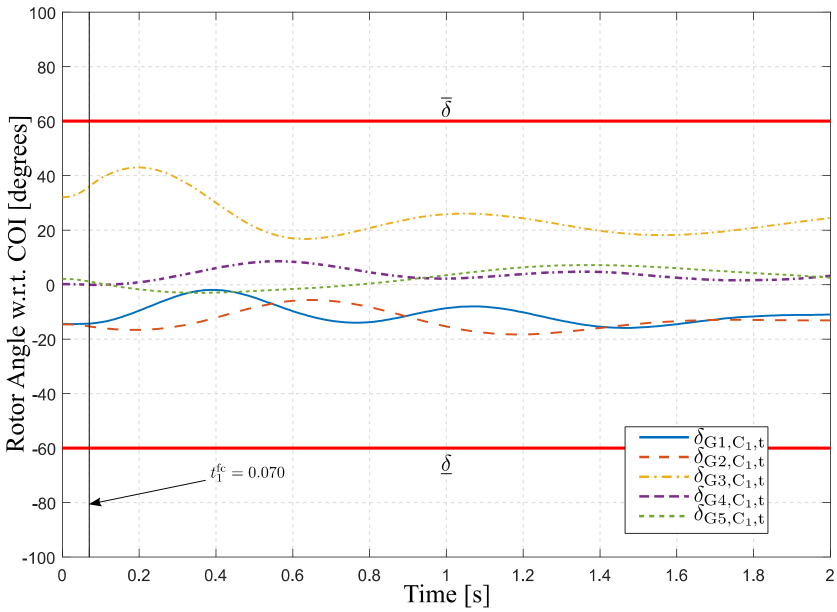

Figure 6.10 – Rotor Angle deviation w.r.t. COI 14–bus/5–generators system – Contingency C1

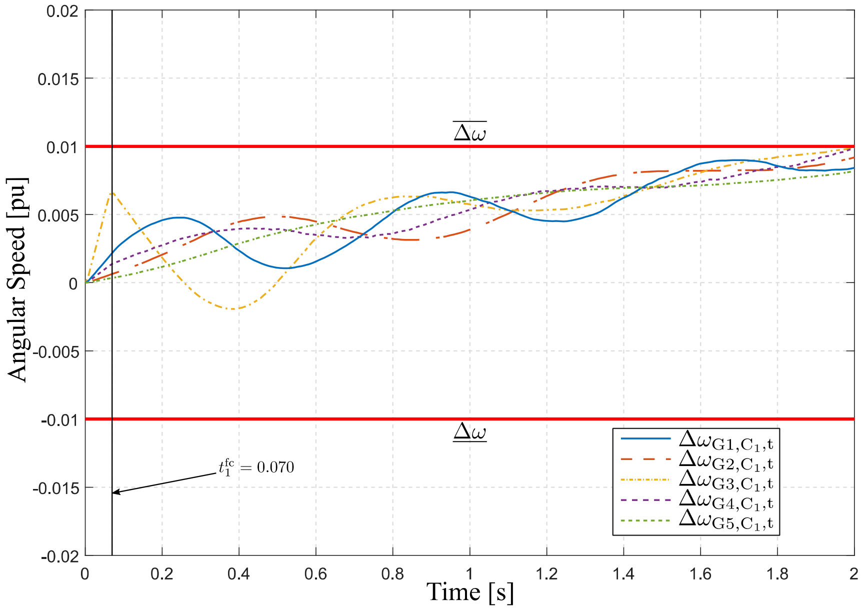

Figure 6.11 – Angular Speed 14–bus/5–generators system – Contingency C1

Evaluating contingencies C1 and C2

The contingencies C1 and C2 are evaluated in the same MLIP model, under the N-1 criteria, the operating results are shown in the Table 6.13, where, the fact of adding a new contingency does not alter too much the objective function, and is very similar to the previous case, because, besides, the model being more restricted, this second contingency is not so severe in transient stability terms, the computational time was 10098.31s, this increase is due to the iterative process during the minimization of the error in the optimization process. The power generation distribution is similar to the previous case, where the generators G3, G4 and G5 are those that distribute the load, the OLTC regulation and the shunt elements operation is also similar to the previous case, because the second fault is less severe than the previous case. Similar to the previous case the generation cost of the both models differ because the use of approximations.

Gen.	Dispatch [MW]	Cost MILP [US$]	Cost MINLP [US$]
G1	0.00		
G2	0.00		
G3	98.54	6097.25	6069.67
G4	67.21		
G5	95.00		

OLTC	nt_{ij}	Tap
T1	1	1.013
T2	1	1.013
T3	-2	0.975

Shunt	Status
S2	OFF
S3	OFF
S4	ON
S6	ON
S9	ON
S14	OFF

Table 6.13 – Results of the 14–bus/5–generators system, contingencies C1 and C2

In Figure 6.12 and Figure 6.13, the rotor angle and rotor speed deviations are shown, the second fault addition, as seen in this figures, does not alter the behavior of generator, taking as reference the previous case analysis, where the rotor angle deviations and the speed deviations of the contingency C1 and C2, are very similar and the limits are respected.

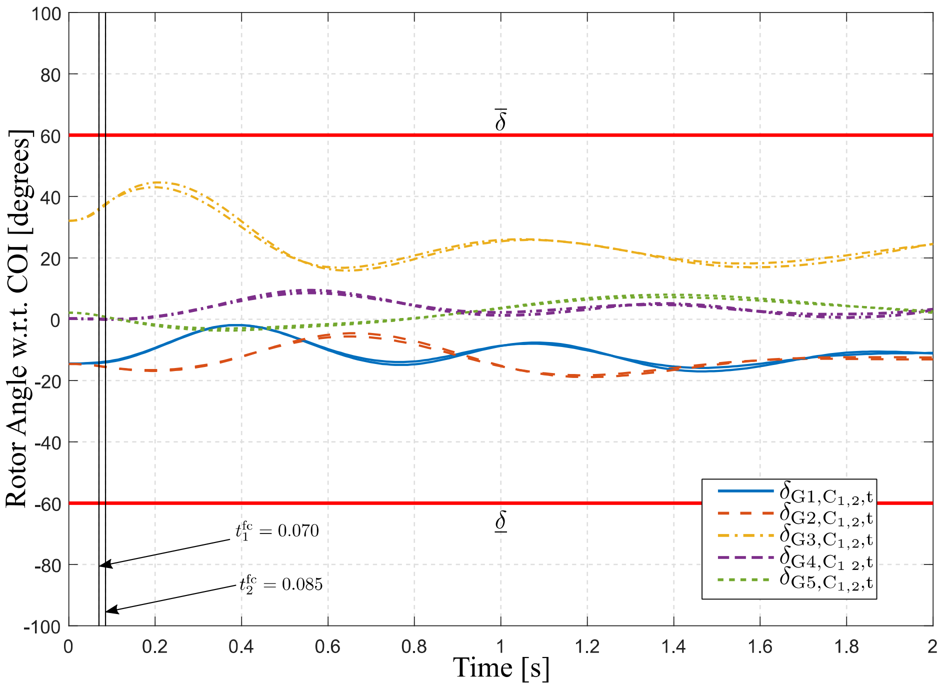

Figure 6.12 – Rotor Angle deviation w.r.t. COI 14–bus/5–generators system – Contingencies C1 and C2

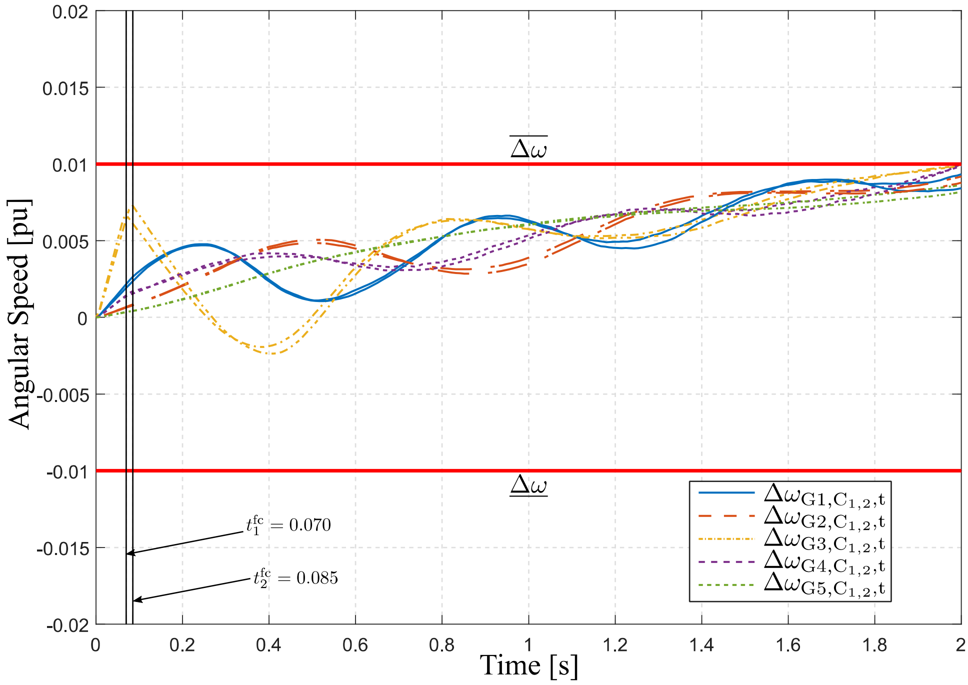

Figure 6.13 – Angular Speed 14–bus/5–generators system – Contingencies C1 and C2

Evaluating contingencies C1, C2 and C3

The results obtained by the proposed MILP model are shown in Table 6.14, the generation is distributed between the cheaper generators. The generator G3 is the most dispatched because its generation limit is greater, the generator G4 is the least dispatched because its inertia constant is smallest and the generator G5 operates at its maximum capacity.

Figure 6.14 and Figure **6.15** shown the rotor angle deviation w.r.t. COI and the angular speed deviation, as can see the predefined limits in the Table 6.11 are respected, the generator G3 is the most affected, because it has the least inertia constant as the generator G1, but this generator is no dispatched because is more expensive.

Gen.	Dispatch [MW]	Cost MILP [US$]	Cost MINLP [US$]
G1	0.00		
G2	0.00		
G3	152.81	6216.55	6118.83
G4	8.80		
G5	100.00		

OLTC	nt_{ij}	Tap
T1	6	1.0375
T2	6	1.0375
T3	4	1.0250

Shunt	Status
S2	OFF
S3	OFF
S4	ON
S6	ON
S9	ON
S14	OFF

Table 6.14 – Results of the 14–bus/5–generators system, contingencies C1, C2 and C3

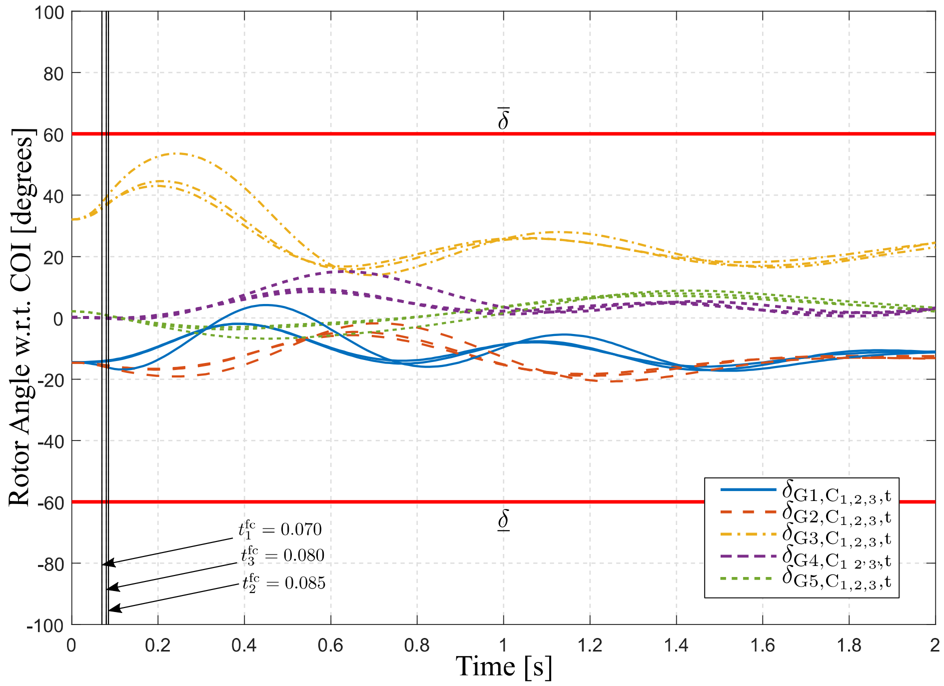

Figure 6.14 – Rotor Angle deviation w.r.t. COI 14–bus/5–generators system – Contingencies C1, C2 and C3

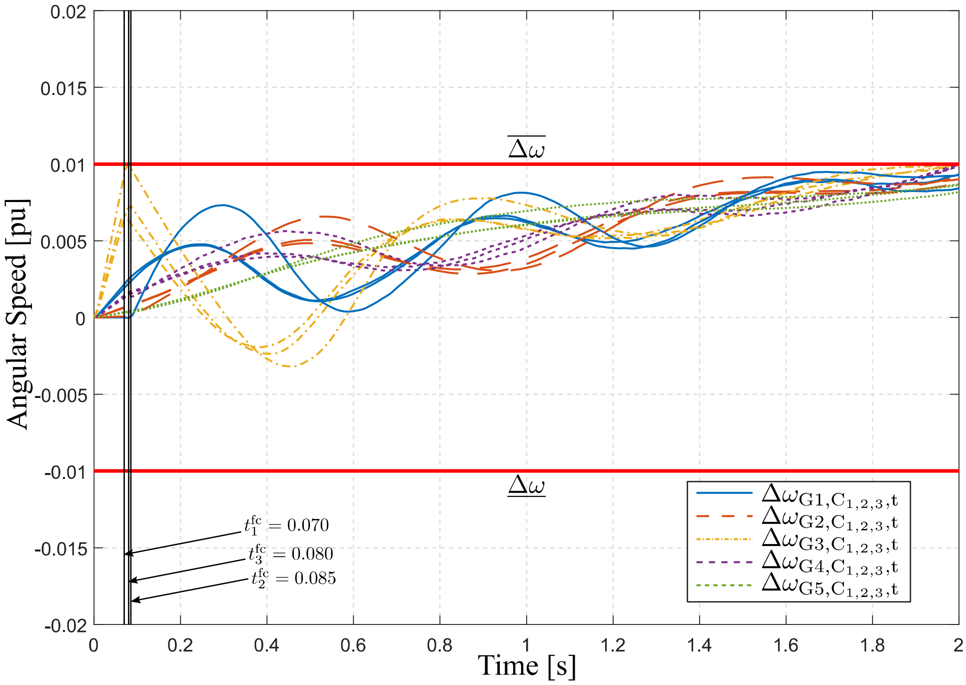

Figure 6.15 – Angular Speed 14–bus/5–generators system – Contingencies C1, C2 and C3

TSC–OPF without TSC analysis

The operating point from the TSC–OPF without the TSC, can be stable or instable, the TSC–OPF without the TSC, only calculate the best economic operation of the EPS. Figure 6.16 shows the rotor angle deviation from the COI and the angular speed of the EPS, using the obtained operation point as initial point in a transient stability program, the rotor angle and angular speed trajectories are stable, but in the previous TSC–OPF analysis it can be seen that the trajectories are within the limits and it can notice the influence of the TSC inclusion, the generator G4 is the most oscillating in the system, but it can be noted that the synchronism between the generators is maintained.

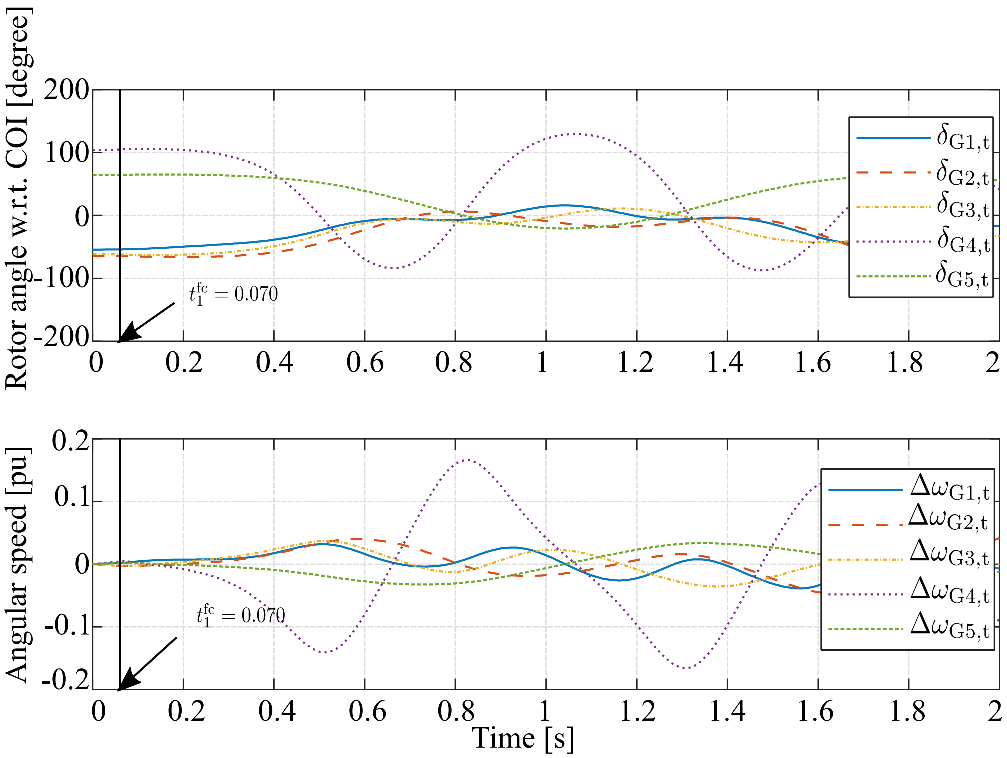

Figure 6.16 – TSC–OPF analysis without TSC 14–bus / 5–generators IEEE system

Sensitivity analysis

The proposed model was tested on different transient stability limits, the Table 6.15 shows the summary of these results. In this case, the sensitivity of the proposed methodology to the change of the angle limits does not generate load shedding, however, the speed limits changes produce a minimum load shedding, these considerations are applied to obtain a feasible operation.

Angle Limits $[\underline{\delta}, \overline{\delta}]$	**Generation Cost [US$]**	**Load Shedding [MW]**	**Speed Limits** $[\underline{\Delta\omega}, \overline{\Delta\omega}]$	**Generation Cost [US$]**	**Load Shedding [MW]**
90°	6216.55	0.00	0.0100	6216.55	0.00
45°	6101.47	0.00	0.0050	6128.04	0.00
30°	6101.47	0.00	0.0025	4732.49	65.27
15°	6411.75	0.00	0.0010	3346.30	130.89

Table 6.15 – 14–bus/5–generators system: Sensitive analysis

6.4. 39–BUS / 10–GENERATORS IEEE MODIFIED SYSTEM

For this system, network and dynamic data can be found in (GAN, THOMAS and ZIMMERMAN, 2000), Table 6.16 and Table 6.17 shows the technical and economic data and the two N-1 contingencies respectively. There are 30 discrete control variables, including 12 OLTC regulation and 18 shunt elements, it is also evaluated 10 generators active power output and terminal and internal voltages, besides the synchronism between these generators.

Gen.	Technical Data							Economic Data		
	X_{d_g} [pu]	H_g [pu]	D_g [pu]	$\overline{P}_i^g$ [MW]	$\underline{P}_i^g$ [MW]	$\overline{Q}_i^g$ [Mvar]	$\underline{Q}_i^g$ [Mvar]	a_i^g [US^2/MW]	b_i^g [US$/MW]	c_i^g [US$]
$G1$	0.03100	42.00	0	350.0	0	400.0	-400.0	0.011	15.4	240
$G2$	0.06970	30.30	0	650.0	0	200.0	-200.0	0.009	11.3	200
$G3$	0.05310	35.80	0	800.0	0	800.0	-500.0	0.009	8.8	220
$G4$	0.04360	28.60	0	750.0	0	800.0	-100.0	0.010	8.0	250
$G5$	0.13200	26.00	0	650.0	0	600.0	-600.0	0.009	11.4	220
$G6$	0.05000	34.80	0	750.0	0	300.0	-200.0	0.008	10.5	190
$G7$	0.04900	26.40	0	750.0	0	200.0	-200.0	0.009	10.0	200
$G8$	0.05700	24.30	0	700.0	0	100.0	-100.0	0.009	10.2	210
$G9$	0.05700	34.50	0	900.0	0	60.0	-50.0	0.007	7.9	230
$G10$	0.00600	500.00	0	1200	0	300.0	-300.0	0.006	8.0	220

Table 6.16 – Technical and Economic Data 39–bus/10–generators system

Two contingencies are studied, a three phase to ground fault is applied, at buses 17 and 14 and clarified by tripping the lines 17–27 and 14–15 at 0.050s and 0.085s, respectively, as shown in Table 6.17 and in the Figure 6.17.

Contingency	3ϕ Fault Bus	Transmission Line Out	t_i^{fc} [s]	t_i^{max} [s]
C1	17	17 – 27	0.050	3
C2	14	14 – 15	0.085	3

Table 6.17 – N-1 Contingencies for 39–bus/10–generators IEEE system

Table 6.18 shows the operational and stability information of the EPS. For both contingencies $N_{t_1} = 10$, $N_{t_1} = 50$, $\Gamma = 20$ and $c^{ls} = 30$US$, clearly the number of steps in fault and post–fault stages are increased, because the computational burden increases according the increase of steps number.

Operating Data										
$\mathbf{Reg}_{ij}$	$\overline{\mathbf{nt}}_{ij}$	$\overline{V}$	$\underline{V}$	$\overline{E}$	$\underline{E}$	$\overline{\delta}$	$\underline{\delta}$	$\Delta\overline{\omega}$	$\Delta\underline{\omega}$	ω_0
10%	8	1.10	0.90	1.20	0.80	$\pm 60°$		± 0.01		377

Table 6.18 – Operating Data 39–bus/10–generators system

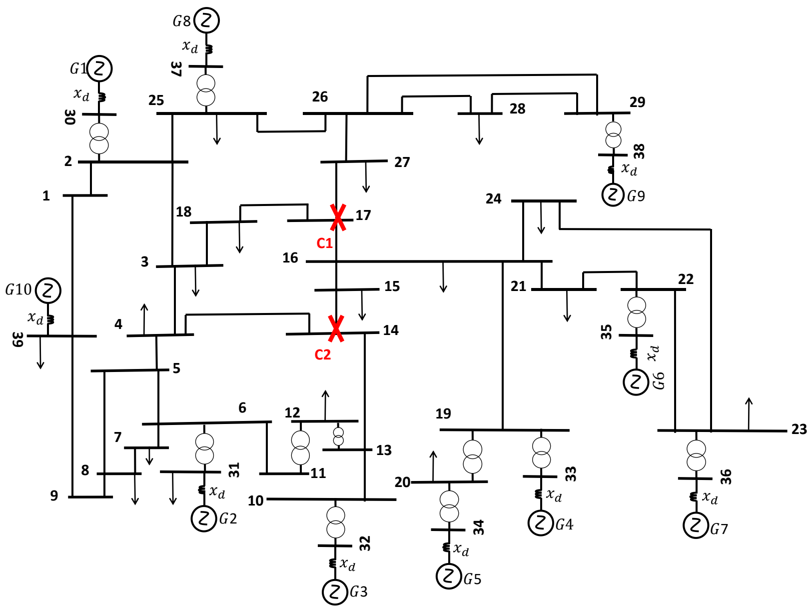

Figure 6.17 – 39–bus/10–generators system and N-1 contingencies

Evaluating contingencies C1 and C2

Table 6.19 summarizes the results considering TSC into OPF for contingencies C1 and C2. Generation cost and generation dispatch are shown and its also shown the OLTC regulation and shunt elements operation. The generation cost includes the load shedding cost, only one of the 18 shunt elements are in operation and the OLTC operation maintains the voltage profiles within the limits, the load shedding for this case was 1598MW and the total simulation time for all optimization process was 449039.32s. Note that the load shedding is deployed when considering C1 and C2.

Gen.	**Dispatch [MW]**	**Cost MILP [US$]**	**Cost MINLP [US$]**
G1	421.49	113954.8	No feasible solution (limit time acquired)
G2	167.09		
G3	246.24		
G4	558.84		
G5	257.18		
G6	459.99		
G7	391.22		
G8	419.90		
G9	523.25		
G10	1100.00		

OLTC	nt_{ij}	**Tap**
T1	8	1.050
T2	8	1.050
T3	8	1.050
T4	-6	0.963
T5	-6	0.963
T6	3	1.019
T7	3	1.019
T8	-1	0.994
T9	2	1.013
T10	0	1.000
T11	0	1.000
T12	-1	0.994

Shunt	**Status**
S4	OFF
S7	OFF
S8	OFF
S12	OFF
S15	OFF
S16	OFF
S18	OFF
S20	OFF
S21	OFF
S23	OFF
S24	OFF
S25	OFF
S26	OFF
S27	OFF
S28	OFF
S29	OFF
S31	ON
S39	OFF

Table 6.19 – Results of the 39–bus/10–generators system, contingencies C1 and C2

The Figure 6.18 shows the rotor angle deviation with respect to COI and the angular speed deviation. The obtained optimal and stable operating point are evaluated in a transient stability program, the obtained results for this N-1 scenarios, are showing in Figure 6.18; as can see the stable trajectories of rotor angles for this two contingencies, the contingency C1 is in dark green and the contingency C2 is in sky blue; the synchronism between the machines are maintained, thus, the angular speed deviation, as seem in the same figure, are stable. The main reason to the system maintains the stability, are the short fault clearance times and the load shedding.

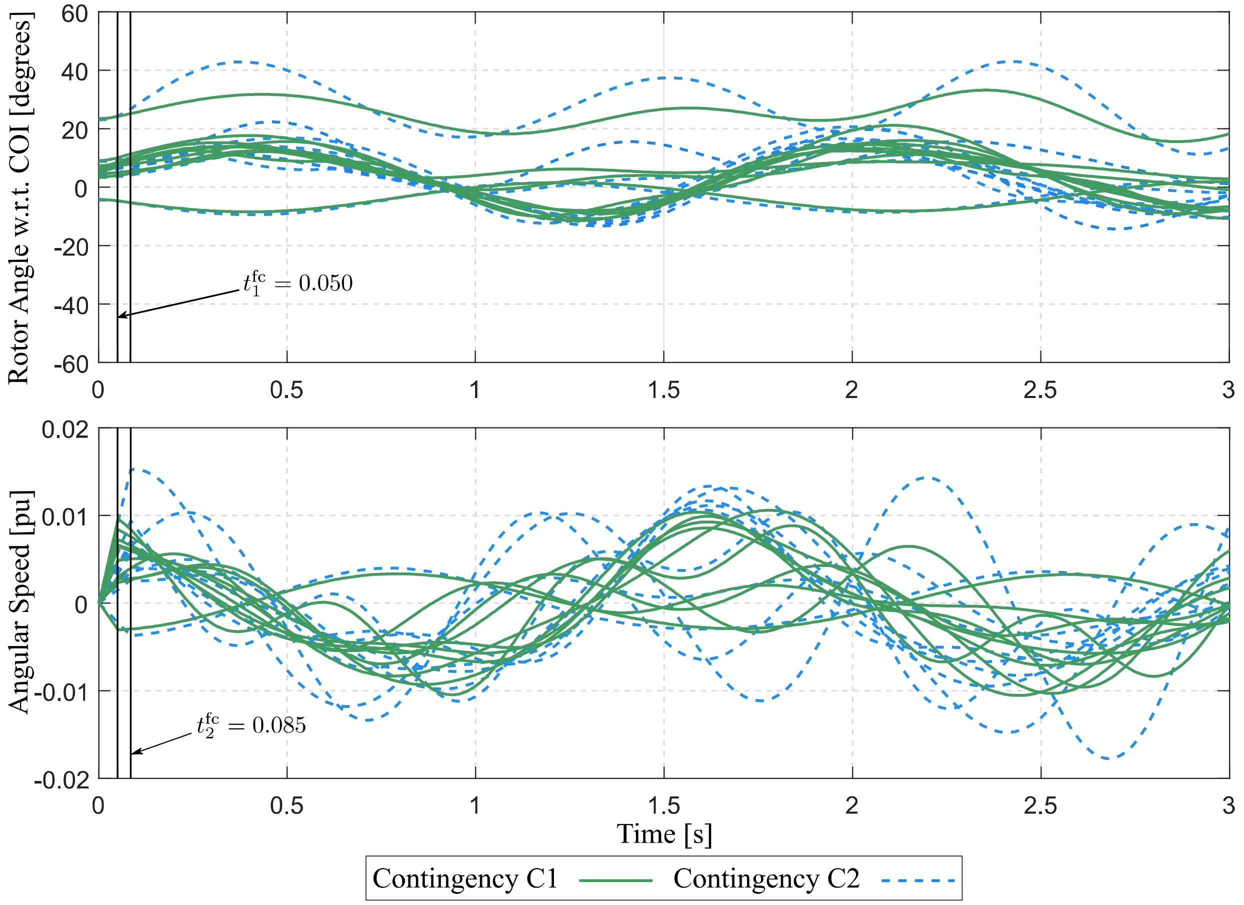

Figure 6.18– Rotor Angle and Angular Speed deviation, 39–bus/10–generators system – Two Contingencies

TSC–OPF without TSC analysis

In the Figure 6.19, the rotor angle deviation with respect to COI and the angular speed deviation are showing based on the TSC–OPF calculation without TSC, the rotor angle and angular speed trajectories are stable, but similar to the previous case, this trajectories are oscillating with the maximum deviation of the rotor angle are 80° for the contingency C1, and is noted that the TSC inclusion are influenced in this deviation, because the limits are clearly respected in the previous analysis.

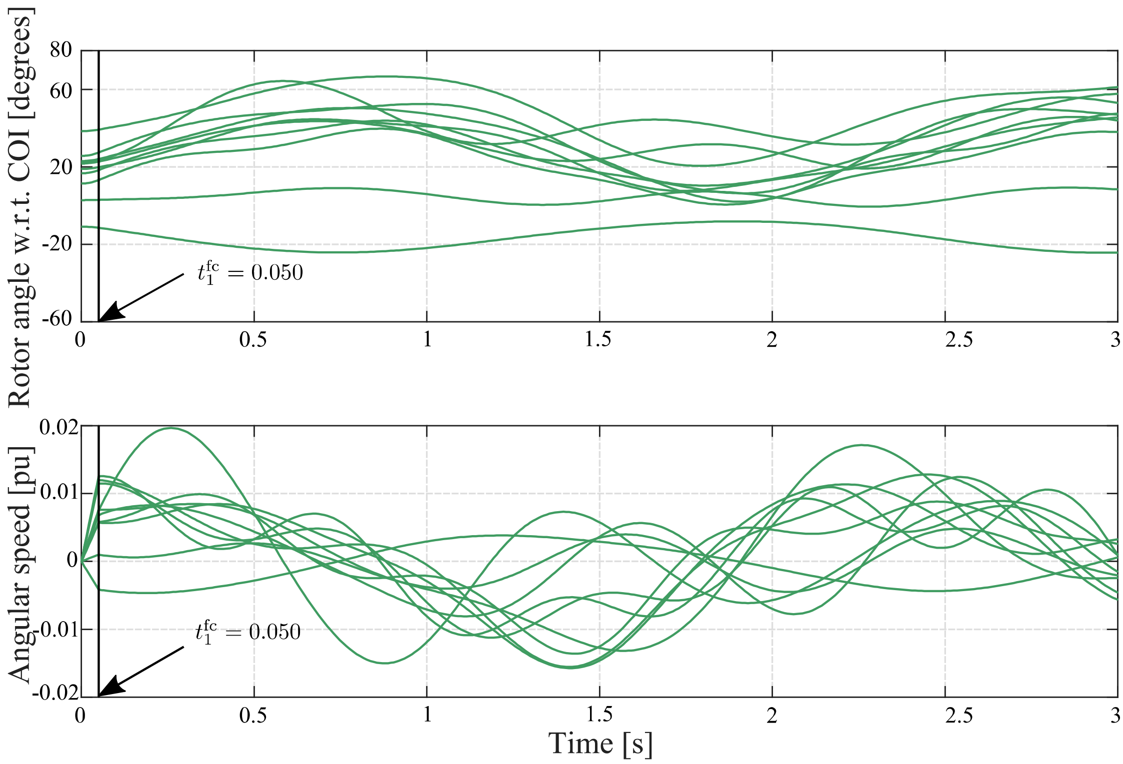

Figure 6.19 – TSC–OPF analysis without TSC 39–bus / 10–generators IEEE system

6.5. 68–BUS / 16–GENERATORS IEEE MODIFIED SYSTEM

The network and dynamic data can be found in (RAMOS, KUIAVA, *et al.*, 2014), Table 6.20 and Table 6.22 shows the one N-1 multi–contingency and the technical and economic data. This system is implemented with 33 discrete control variables, as they are 18 OLTC regulation and 15 shunt elements, 16 generators active power output and voltage are evaluated, the transient stability is also evaluated for these generators.

As show in Table 6.20 one contingency is studied, a three–phase to ground fault is applied, at bus 17 and is clarified by tripping the lines 17–36 at 0.080s.

Contingency	**3ϕ Fault Bus**	**Transmission Line Out**	**t_i^{fc} [s]**	**t_i^{max} [s]**
C1	17	17 – 36	0.080	3

Table 6.20 – N-1 Contingencies for 68–bus/16–generators IEEE system

The operational and stability data of the EPS is show in Table 6.21. For the contingency C1, is considered, $N_{t_1} = 5$, $N_{t_1} = 20$, $\Gamma = 20$ and $c^{ls} = 30\text{U\$S}$ as the number of steps in fault and post-fault stage, the linearization blocks and the load shedding cost, respectively, in this system is considered a smaller number of discretization steps, because the computational burden is increase according the number of steps is also increase.

Operating Data										
$\mathbf{Reg}_{ij}$	$\overline{\mathbf{nt}}_{ij}$	$\overline{V}$	$\underline{V}$	$\overline{E}$	$\underline{E}$	$\overline{\delta}$	$\underline{\delta}$	$\Delta\overline{\omega}$	$\Delta\underline{\omega}$	ω_0
10%	8	1.10	0.80	1.20	0.75	$\pm 60°$		± 0.01		377

Table 6.21 – Operating Data 68–bus/16–generators system

Gen.	Technical Data							Economic Data		
	X_{d_g} [pu]	H_g [pu]	D_g [pu]	$\overline{P}_i^g$ [MW]	$\underline{P}_i^g$ [MW]	$\overline{Q}_i^g$ [Mvar]	$\underline{Q}_i^g$ [Mvar]	a_i^g [US\$²/MW]	b_i^g [US\$/MW]	c_i^g [US\$]
$G1$	0.0310	42.0	0	2000.0	500.0	500.0	-500.0	0.009	8.81	220
$G2$	0.0697	30.2	0	2000.0	400.0	500.0	-500.0	0.009	8.82	200
$G3$	0.0531	35.8	0	2000.0	0.0	500.0	-500.0	0.009	8.83	220
$G4$	0.0436	28.6	0	2000.0	500.0	500.0	-500.0	0.010	8.00	250
$G5$	0.0660	26.0	0	2000.0	400.0	500.0	-500.0	0.009	8.82	220
$G6$	0.0500	34.8	0	2000.0	500.0	500.0	-500.0	0.009	8.85	220
$G7$	0.0490	26.4	0	2000.0	400.0	500.0	-500.0	0.009	8.81	220
$G8$	0.0570	24.3	0	2000.0	400.0	500.0	-500.0	0.009	8.81	220
$G9$	0.0570	34.5	0	2000.0	500.0	500.0	-500.0	0.010	8.00	250
$G10$	0.0457	31.0	0	2000.0	400.0	500.0	-500.0	0.008	8.81	190
$G11$	0.0180	28.2	0	2000.0	750.0	500.0	-500.0	0.008	8.81	190
$G12$	0.0310	92.3	0	2000.0	800.0	500.0	-500.0	0.008	8.82	190
$G13$	0.0055	248.0	0	5000.0	1500.0	1000.0	-1000.0	0.008	8.82	190
$G14$	0.0029	300.0	0	5000.0	1000.0	500.0	-500.0	0.009	8.83	220
$G15$	0.0029	300.0	0	3000.0	1000.0	500.0	-500.0	0.009	8.85	220
$G16$	0.0071	225.0	0	5000.0	1000.0	500.0	-500.0	0.009	7.00	220

Table 6.22 – Technical and Economic Data 68-bus/16-generators system

Evaluating contingency C1

Table 6.23 summarizes the results of the TSC–OPF for contingency C1. The generation costs, OLTC regulation and shunt elements operation and the generation cost that includes the load shedding cost are shown. In this system, the binary operation of the OLTC tap regulation are considering for 17 transformers, maintains the voltage profiles within the limits, the load shedding was 5702.68MW and the total simulation time for all optimization process was 373842.24s. Note that the computational burden, increases exponentially due to generators number and the system size. The load shedding is greater due to the fault characteristics, mainly the fault location.

Gen.	Dispatch [MW]	Cost MILP [US$]	Cost MINLP [US$]
G1	421.49	372017	No feasible solution (limit time acquired)
G2	167.09		
G3	246.24		
G4	558.84		
G5	257.18		
G6	459.99		
G7	391.22		
G8	419.90		
G9	523.25		
G10	1100.00		
G11	421.49		
G12	167.09		
G13	246.24		
G14	558.84		
G15	257.18		
G16	459.99		

OLTC	nt_{ij}	Tap
T1	-7	0.083
T2	3	1.038
T3	-2	0.950
T4	-1	0.975
T5	-1	0.975
T6	-8	0.800
T7	-7	0.825
T8	-4	0.900
T9	-8	0.800
T10	-8	0.800
T11	2	1.025
T12	8	1.100
T13	1	1.013
T14	8	1.100
T15	1	1.013
T16	8	1.100
T17	-3	0.925
T18	-1	0.975

Shunt	Status
S17	ON
S18	ON
S19	OFF
S21	ON
S23	OFF
S25	OFF
S27	OFF
S29	OFF
S33	OFF
S41	ON
S44	ON
S59	OFF
S60	OFF
S61	ON
S68	OFF

Table 6.23 – Results of the 68–bus/16–generators system, contingencies C1

The Figure 6.20 shows the rotor angle deviation with respect to COI and the angular speed deviation. The obtained optimal and stable operating point are evaluated in a transient stability program; as can see the stable trajectories of rotor angles for this contingency, the synchronism between the machines are maintained, thus, the angular speed deviation, as seen in the same figure, are stable. The main reason to the system maintains the stability, are the short fault clearance times and the load shedding.

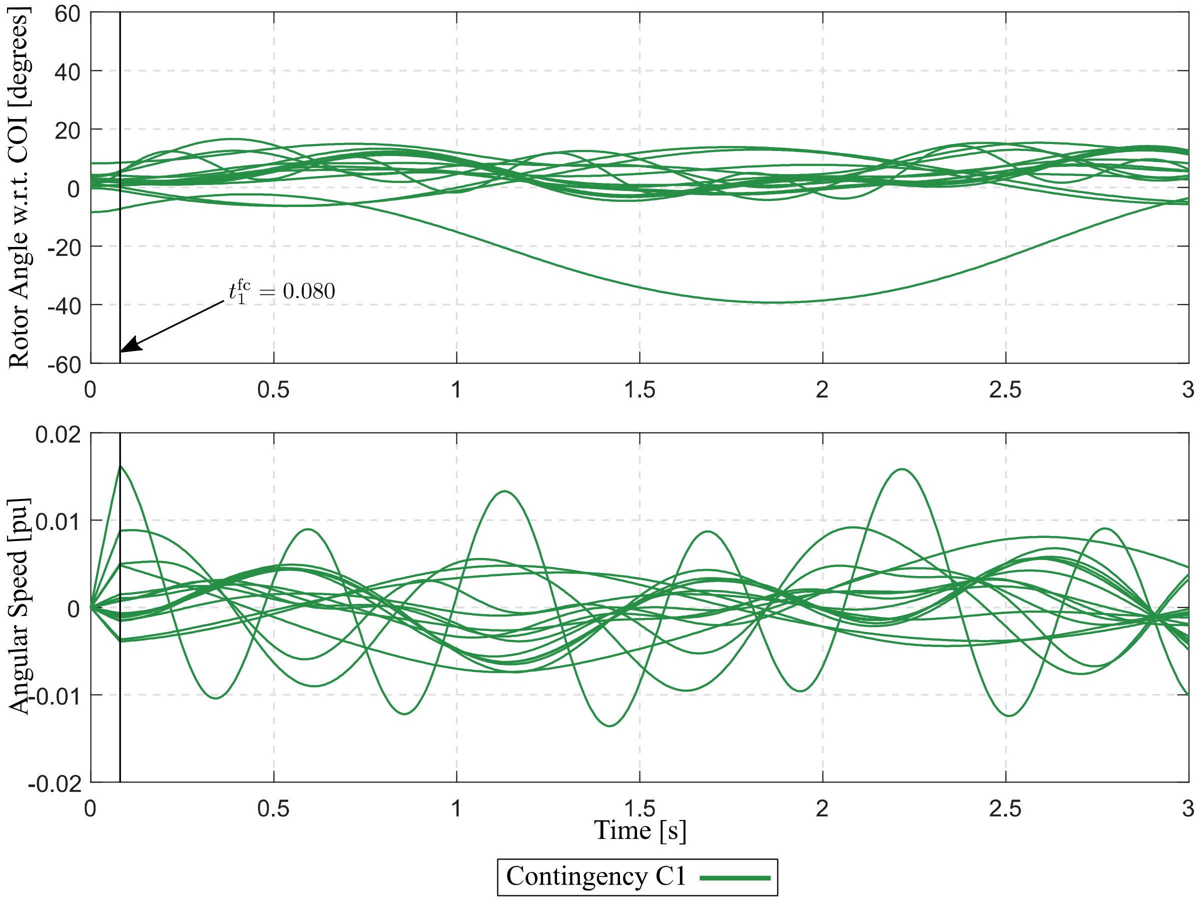

Figure 6.20– Rotor Angle and Angular Speed deviation, 68–bus/16–generators system – one contingency

TSC–OPF without TSC analysis

The TSC–OPF without the TSC is evaluated, the rotor angle deviation with respect to COI and the angular speed are showing in the Figure 6.21, it can be see that the trajectories are instable for the operation point obtained from the TSC–OPF without the TSC to the contingency C1, the previous analysis of the TSC–OPF in the Figure 6.20 for this similar case shown that the trajectories are stable and within the limits, and this analysis prove that the TSC–OPF can be used for this type of problems.

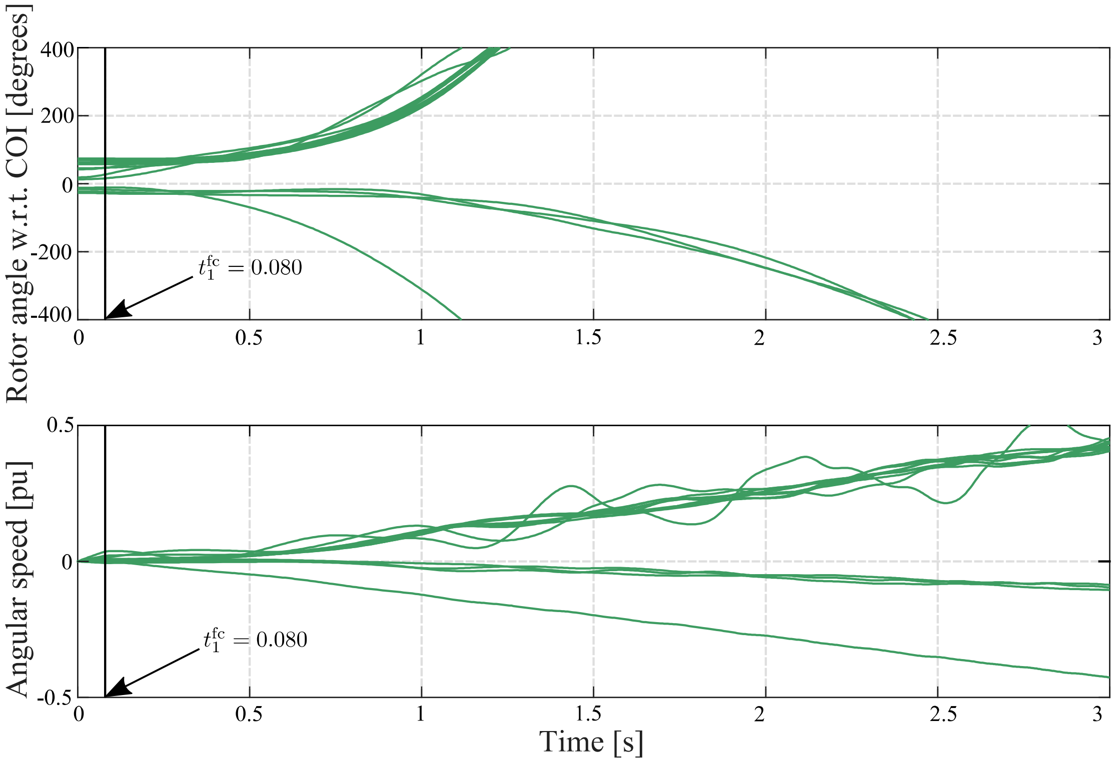

Figure 6.21 – TSC–OPF analysis without TSC 68–bus / 16–generators IEEE system

6.6. IMPORTANT REMARKS

In this chapter was tested four transient stability systems, the first and the second one, were small systems, and the other two were more larger systems, this fact because the small systems has a better response and less computational time when are subjected to various contingencies, and the larger systems are more used to prove the scalability of the model.

The 9–bus/3–generators system, was the more tested, in there three N-1 contingencies are evaluated, and the results from the each of them (increasing one to one), were shown separately, highlighting the generation cost increase of the resulting operation points, and the stable trajectories of the rotor angle with respect to COI and the angular speeds of the generators, the 14–bus/5–generators system, was tested for three N-1 contingencies overall, obtaining a stable and economic point, the stable trajectories of the rotor angle with respect to COI and the angular speeds of the five generators are also shown, proving the efficacy of the MILP model.

In the 39–bus/10–generators system was evaluated two N-1 contingencies at the same time, resulting a stable and economic operating point (including a load shedding cost), the resulting operating point was evaluated on transient stability program, similarly in the 68–bus/16–generators system was studied only one contingency, because the computational time grows exponentially, obtaining a stable an economic operation point, for this contingency, considering the load shedding and increasing the generation cost. A sensibility analysis is also developed to small system, thus proving the efficacy of the model for different problem conditions.

CONCLUSIONS

In this work, the N-1 multi–contingency TSC–OPF problem considering discrete controls using an AC branch flow model was presented. The differential and non–linear algebraic equations used to model the transient stability constraints and the steady-state operation is embedded in the proposed model.

This approach minimizes the generation costs under operational and transient stability constraints. Two solution models were explored in this work: MINLP and MILP. Using the MINLP model we are only able to find the optimal solution for a small-scale test system with a significant computational burden. Due to these limitations, an approach based on a set of efficient linearization techniques was proposed.

The resulting MILP model can be solved using existing off-the-shelf convex optimization solvers. Results using the 9–Bus/3–Generators WSCC, 14–Bus/5–Generators, 39–Bus/10–Generators and 68–Bus/16–Generators IEEE systems show the accuracy, efficiency and scalability of the proposed optimization process, providing transient stable solutions at a minimum generation cost. Refined trajectories of the time-varying variables demonstrate the ability of the proposed TSC–OPF model to guarantee angular stability under different contingencies. Finally, results were validated using a nonlinear time-domain dynamic simulation software.

CONTRIBUTIONS

This dissertation presents the following contributions:

- Two new formulations for the Transient Stability Constrained Optimal Power Flow (TSC–OPF) MINLP model were presented and they were subsequently linearized to a MILP model based on an AC branch flow model.

- A TSC-OPF model that includes the three analysis stages (pre–fault, fault and post–fault) in a single model as shown (CALLE, CASTRONUOVO and LEDESMA, 2013) and the inclusion of discrete variables. The MINLP model was based on an AC branch flow approach and it is presented through a nonlinear formulation found in the literature, which represents an improvement of the method for the subsequent linearization process.

- The inclusion of discrete variables as OLTC tap changers, regulation and shunt elements switched in the steady state stage of the model, guarantees the optimal operation of the EPS in pre-fault stage, keeping the voltages within their limits.

- Using approximations and equivalences to transform the MINLP into a MILP model, that can be solved using off–the–shelf commercial solvers, such as CPLEX (ILOG, 2008) and formulated via mathematical programming languages such as AMPL (FOURER, GAY and KERNIGHAN, 2003).

- The implicit trapezoidal integration rule was used, as seen in (GAN, THOMAS and ZIMMERMAN, 2000), (YUAN, KUBOKAWA and SASAKI, 2003), (CALLE, CASTRONUOVO and LEDESMA, 2013), to integrate the transient stability constraints during fault and post-fault. This implementation is embedded into the model, due its easy formulation and good numerical stability.

- The proposed N-1 multi–contingency assessment considers all contingencies as evaluated independent one of the other, and a single operation point is obtained, which is expected to be stable and economic.

- The computation time of the MINLP respect to the MILP is reduced significantly, and is one of the advantages to obtain a linear or mixed linear programming models. The MINLP can be used to small systems, but for larger systems, an optimal solution may not be found, and will depend on the initial point.

FUTURE WORKS

- The TSC–OPF model via MILP and MINLP approaches can be extended to include other types of stability studies such, as the static or dynamic voltage stability. The voltage stability constraints allows to find the voltage collapse point, making the model more complete. The inclusion of more dynamic constraints in the base model, make the model more restrictive and consequently the computational burden increase.

- The model can be also extended to:

    - Transmission expansion planning problem.
    - A highest order of the synchronous machine model.
    - An application of direct methods as the Lyapunov function into the model.
    - Frequency stability constraints.

REFERENCES

ABHYANKAR, S., GENG, G., ANITESCU, M., WANG, X., & DINAVAHI, V. (2017). Solution techniques for transient stability constrained optimal power flow - part 1. *IET Gen., Trans. & Dist., 11*(12), 3177-3185.

ALSAC, O., BRIGHT, J., PRAIS, M., & STOTT, B. (1990). Further Developments In Lp-Based Optimal Power Flow. *IEEE Transactions On Power Systems, 5*(3), 697-711.

ANDERSON, P., & FOUAD, A. (1977). *Power System Control and Stability.* Iowa: Iowa State University Press, USA.

ARIAS, N. B., TABARES, A., FRANCO, J. F., LAVORATO, M., & ROMERO, R. (2018). Robust joint expansion planning of electrical distribution systems and EV charging stations. *IEEE Trans. Sust. Energy, 9*(2), 884 - 894.

ARREDONDO, F., CASTRONUOVO, E., LEDESMA, P., & LEONOWICZ, Z. (2018). Comparative Implementation of Numerical Integration Methods for Transient Stability Constrained Optimal Power Flow. *IEEE International Conference on Environment and Electrical Engineering (EEEIC / I\&CPS Europe).*

BAKIRTZIS, A. G., BISKAS, P. N., ZOUMAS, C. E., & PETRIDIS, V. (2002). Optimal Power Flow by Enhanced Genetic Algorithm. *IEEE Transactions On Power Systems, 17*(2), 229-236.

BYRD, R. H., J.NOCEDAL, & WALTZ, R. A. (2006). *KNITRO, an integrad package for nonlinear optimization.* New York: Springer.

CAI, H. R., CHUNG, C. Y., & WONG, K. P. (2008). Application Of Differential Evolution Algorithm For Transient Stability Constrained Optimal Powerflow. *IEEE Trans. Power Syst., 23*(2), 719-728.

CALLE, I. A., CASTRONUOVO, E. D., & LEDESMA, P. (2013). Optimal re-dispatch of an isolated system considering transient stability constraints. *Electrical Power and Energy Systems, 44*(1), 728-735.

CHAN, K. Y., LING, S. H., CHAN, K. W., IU, H., & PONG, G. T. (2007). Solving Multi-Contingency Transient Stability Constrained Optimal Power Flow Problems With An Improved Ga. *IEEE Congress on Evolutionary Computation*, 2901 –2908.

CHEN, L., TAKA, Y., & OKAMOTO, H. (2001). Optimal operation solutions of power systems with transient stability constraints. *IEEE Trans. CircSyst I, 30*(2), 327-339.

CHEN, Y., LUO, F., XU, Y., & QIU, J. (2016). Self-adaptive differential approach for transient stability constrained optimal power flow. *IET Generation, Transmission & Distribution*, 3717-3726.

CHRISTIE, R. (1993, August). *University of Washington*. (University of Washington) Retrieved from https://labs.ece.uw.edu/pstca/

DOMMEL, H. W., & TINNEY, W. F. (1968). Optimal Power Flow Solutions. *IEEE Transactions on Power Apparatus and Systems, 87*(10), 1866-1876.

FARIVAR, M., & LOW, S. H. (2013). Branch Flow Model: Relaxations and Convexification - Part I. *IEEE Transactions On Power Systems, 28*(3), 2554-2564.

FOURER, R., GAY, D. M., & KERNIGHAN, B. W. (2003). *AMPL, A Modeling Language For Mathematical.* 2. ed. Pacific Grove: Thomson/Brooks/Cole.

GAN, D., THOMAS, R. J., & ZIMMERMAN, R. D. (2000). Stability-Constrained Optimal Power Flow. *IEEE Tranaction on Power Systems, 15*(2), 535-540.

GENG, G., ABHYANKAR, S., WANG, X., & DINAVAHI, V. (2017). Solution techniquesfor transient stability constrained optimal power flow – part 2. *IET Gen.,Trans. & Dist., 11*(12), 3186–3193.

GRANVILLE, S. (1994). Optimal Reactive Dispatch Through Interior Point Methods. *IEEE Transactions on Power Systems, 9*(1), 136-146.

H. YOSHIDA, K. K., FUKUYAMA, Y., TAKAYAMA, S., & NAKANISHI, Y. (2000). A Particle Swarm Optimization for Reactive Power and Voltage Control Considering Voltage Security Assessment. *IEEE Transactions On Power Systems, 15*(4), 1232-1239.

HISKENS, I. A., & PAI, M. A. (2000). Trajectory Sensitivity Analysis Of Hybrid Systems. *IEEE Trans. Cir. Syst., 47*(2), 204-220.

ILOG. (2008). *CPLEX Optimization subroutine library guide and reference, version 11.0.* Incline: ILOG.

JIN, C., & XIANG, M. (2014). Multi-objective optimal power flow consideringtransient stability based on parallel nsga-ii. *IEEE Trans. Power Syst., 30*(2), 857-866.

KUNDUR, P. (1994). *Power System Stability and Control.* New York: McGraw-Hill.

LAYDEN, D., & JEYASURYA, B. (2004). Integrating security constraints in optimal power flow studies. *IEEE Power Engineering Society General Meeting, 1*, 125-129.

LI, Y. H., YUAN, W. P., CHAN, K. W., & LIU, M. B. (2011). Coordinated Preventive Control Of Transient Stability With Multi-Contingency In Power Systems Using Trajectory Sensitivities. *International Journal of Electrical Power & Energy Systems, 33*(1), 147-153.

LOW, S. H., & FARIVAR, M. (2013). Branch Flow Model: Relaxations and Convexification—Part II. *IEEE Transactions On Power Systems, 28*(3), 2565-2572.

MINANO, R. Z., CUTSEM, T. V., MILANO, F., & CONEJO, A. J. (2010). Securing Transient Stability Using Time-Domain Simulations Within An Optimal Power Flow. *IEEE Tran. Power Syst., 25*(1), 243-253.

MO, N., ZOU, Z. Y., CHAN, K. W., & PONG, T. Y. (2007). Transient Stability Constrained Optimal Power Flow Using Particle Swarm Optimisation. *IET Generation, Transmission Distribution, 1*(3), 476-483.

MONTICELLI, A. J. (1983). *Fluxos De Carga Em Redes De Energia Elétrica.* New York: Edgard Blücher.

MONTICELLI, A., WEN-HSIUNG, & LIU, E. (1992). Adaptive Movement Penalty Method For The Newton Optimal Power Flow. *IEEE Transactions on Power Systems, 7*(1), 334-342.

PAI, M. A., & NGUYEN, T. B. (2003). Dynamic Security-Constrained Rescheduling Of Power Systems Using Trajectory Sensitivities. *IEEE Transactions on Power Systems, 18*(2), 848-854.

PHAN, D., & KALAGNANAM, J. (2014). Some Efficient Optimization Methods for Solving the Security-Constrained Optimal Power Flow Problem. *IEEE Transactions On Power Systems, 29*(2), 863-872.

RAMOS, R. A., KUIAVA, R., FERNANDES, T. C., & PATACA, L. C. (2014, June 20). *IEEE - EESC*. (USP) Retrieved from http://www.sel.eesc.usp.br/ieee/

SAHA, A., BHATTACHARYA, A., DAS, P., & CHAKRABORTY, A. K. (2018). CDO - A New Metaheuristic Algorithm Towards the Solution of Transient Stability Constrained Optimal Power Flow. *International Electrical Engineering Congress (iEECON).*

SANTOS, A., & COSTA, G. D. (1995). Optimal-Power-Flow Solution By Newton'S Method Applied To An Augmented Lagrangian Function. *IEEE Proceedings - Generation, Transmission and Distribution, 142*(1), 33-36.

SUN, D. I., ASHLEY, B., BREWER, B., HUGHES, A., & TINNEY, W. F. (1984). Optimal Power Flow By Newton Approach. *IEEE Transaction on Power Apparatus and Systems, PAS-103*(10), 2864-2880.

TONG, X., LING, C., & QI, L. (2008). A semi-infinite programming algorithm forsolving optimal power flow with transient stability constraints. *Comp.and Applied Math., 217*(47), 432-447.

WÄCHTER, A., & BIEGLER, L. T. (2005). *On the implementation of an interior-point filter line-search algorithm for large-scale nonlinear programming.* Atlanta: v. 106, n. 1.

WEI, H., SASAKI, H. .., KUBOKAWA, J., & YOKOYAMA, R. (1997, June 11). An Interior Point Nonlinear Programming for Optimal Power Flow Problems with A Novel Data Structure. *Proceedings of the 20th International Conference on Power Industry Computer Applications*, 134-141.

WU, Y.-C., DEBS, A. S., & MARSTEN, R. E. (1994). A Direct Nonlinear Predictor-Corrector Primal-Dual Interior Point Algorithm for Optimal Power Flows. *IEEE Transactions on Power System, 9*(2), 876-883.

XIA, S., CHAN, K. W., BAI, X., & GUO, Z. (2015). Enhanced particle swarm optimisation applied for transient angle and voltage constrained discrete optimal power flow with flexible AC transmission system. *IET Generation, Transmission & Distribution*, 61-74.

YANG, Y., LIU, B., QIN, Z., & LIU, H. (2018). Multi-Contingency Transient Stability Constrained Optimal Power Flow Using the Recursive Reduced-order Method and MPI. *International Conference on Power System Technology (POWERCON).*

YANG, Y., LIU, W., DENG, J., LIU, H., WEI, H., & WANG, T. (2017). A parallel approach for multi-contingency transient stability constrained optimal power flow. *IEEE Power & Energy Society General Meeting*.

YANG, Y., QIN, Z., LIU, B., LIU, H., HOU, Y., & WEI, H. (2018). Parallel solution of transient stability constrained optimal power flow by exact optimality condition decomposition. *IET Generation, Transmission & Distribution*, 5858-5866.

YUAN, Y., KUBOKAWA, J., & SASAKI, H. (2003). A Solution of Optimal Power Flow with Multicontingency Transient Stability Constraints. *IEEE Trans. Power Syst., 18*, 1094-1102.

YUMBLA, P. E., RAMIREZ, J. M., & COELLO, C. A. (2008). Optimal Power Flow Subject to Security Constraints Solved With a Particle Swarm Optimizer. *IEEE Transactions On Power Systems, 23*(1), 33-40.

APPENDIX

APPENDIX A. SYSTEMS DATA

The WSCC 9–bus/3–generators, is a classical system used on transient stability studies; the Table A.1 shows the transmission lines data and the Table A.2 shows the bus data.

i	j	R_{ij}	X_{ij}	B_{ij}^{sh}	a_{ij}
1	4	0.00001	0.05760	0.000	1.000
2	7	0.00001	0.06250	0.000	1.000
3	9	0.00001	0.05860	0.000	1.000
4	5	0.01000	0.08500	0.176	0.000
4	6	0.01700	0.09200	0.158	0.000
5	7	0.03200	0.16100	0.306	0.000
6	9	0.03900	0.17000	0.358	0.000
7	8	0.00850	0.07200	0.149	0.000
8	9	0.01190	0.10080	0.209	0.000

Table A.1–Branch Data 9–bus/3–generators System

Type	V_i	θ_i	P_i^{d}	Q_i^{d}	P_i^{g}	Q_i^{g}	g_i^{sh}	b_i^{sh}
SL	1.040	0.000	0.00	0.00	71.60	27.00	0	0
PV	1.025	9.280	0.00	0.00	163.00	6.70	0	0
PV	1.025	4.665	0.00	0.00	85.00	-10.90	0	0
PQ	1.026	-2.217	0.00	0.00	0.00	0.00	0	0
PQ	0.996	-3.989	125.00	50.00	0.00	0.00	0	0.2
PQ	1.013	-3.687	90.00	30.00	0.00	0.00	0	0.1
PQ	1.026	3.720	0.00	0.00	0.00	0.00	0	0
PQ	1.016	0.728	100.00	35.00	0.00	0.00	0	0.1
PQ	1.032	1.967	0.00	0.00	0.00	0.00	0	0

Table A.2–Bus Data 9–bus/3–generators System

The IEEE 14–bus/5–generators system is commonly used in power flow studies, the Table A.3 show the branch data and the Table A.4 shows the bus data of the system.

i	j	R_{ij}	X_{ij}	B_{ij}^{sh}	a_{ij}
1	2	0.01938	0.05917	0.0528	0.000
1	8	0.05403	0.22304	0.0492	0.000
2	3	0.04699	0.19797	0.0438	0.000
2	6	0.05811	0.17632	0.0340	0.000
2	8	0.05695	0.17388	0.0346	0.000
3	6	0.06701	0.17103	0.0128	0.000
6	8	0.01335	0.04211	0.0000	0.000
6	7	0.00001	0.20912	0.0000	0.978
6	9	0.00001	0.55618	0.0000	0.969
8	4	0.00001	0.25202	0.0000	0.932
4	11	0.09498	0.19890	0.0000	0.000
4	12	0.12291	0.25581	0.0000	0.000
4	13	0.06615	0.13027	0.0000	0.000
7	5	0.00001	0.17615	0.0000	0.000
7	9	0.00001	0.11001	0.0000	0.000
9	10	0.03181	0.08450	0.0000	0.000
9	14	0.12711	0.27038	0.0000	0.000
10	11	0.08205	0.19207	0.0000	0.000
12	13	0.22092	0.19988	0.0000	0.000
13	14	0.17093	0.34802	0.0000	0.000

Table A.3–Branch Data 14–bus/5–generators System

Type	V_i	θ_i	P_i^d	Q_i^d	P_i^g	Q_i^g	g_i^{sh}	b_i^{sh}
SL	1.060	0.000	0.00	0.00	232.40	-16.90	0	0
PV	1.045	-1.616	21.70	12.70	40.00	42.40	0	0.2
PV	1.010	-2.529	94.20	19.00	0.00	23.40	0	0.1
PQ	1.070	-7.210	11.20	7.50	0.00	0.00	0	0.2
PQ	1.090	-7.416	0.00	0.00	0.00	0.00	0	0
PV	1.030	-4.880	47.80	-3.90	0.00	12.20	0	0.3
PQ	1.045	-7.416	0.00	0.00	0.00	0.00	0	0
PV	1.038	-4.222	7.60	1.60	0.00	17.40	0	0
PQ	1.026	-8.754	29.50	16.60	0.00	0.00	0	0.2
PQ	1.026	-8.760	9.00	5.80	0.00	0.00	0	0
PQ	1.044	-8.102	3.50	1.80	0.00	0.00	0	0
PQ	1.053	-8.143	6.10	1.60	0.00	0.00	0	0
PQ	1.046	-8.256	13.50	5.80	0.00	0.00	0	0
PQ	1.016	-9.567	14.90	5.00	0.00	0.00	0	0.2

Table A.4–Bus Data 14–bus/5–generators System

The IEEE 39–bus/10–generators system is commonly used in power flow studies, the Table A.5 show the branch data and the Table A.6 shows the bus data of the system.

i	j	R_{ij}	X_{ij}	B_{ij}^{sh}	a_{ij}
1	2	0.0035	0.0411	0.6987	0.0000
1	39	0.0010	0.0250	0.7500	0.0000
2	3	0.0013	0.0151	0.2572	0.0000
2	3	0.0070	0.0086	0.1460	0.0000
2	30	0.0001	0.0181	0.0000	1.0250
3	4	0.0013	0.0213	0.2214	0.0000
3	18	0.0011	0.0133	0.2138	0.0000
4	5	0.0008	0.0128	0.1342	0.0000
4	14	0.0008	0.0129	0.1382	0.0000
5	6	0.0002	0.0026	0.0434	0.0000
5	8	0.0008	0.0112	0.1476	0.0000
6	7	0.0006	0.0092	0.1130	0.0000
6	11	0.0007	0.0082	0.1389	0.0000
6	31	0.0001	0.0250	0.0000	1.0700
7	8	0.0004	0.0046	0.0780	0.0000
8	9	0.0023	0.0363	0.3804	0.0000
9	39	0.0010	0.0250	1.2000	0.0000
10	11	0.0004	0.0043	0.0729	0.0000
10	13	0.0004	0.0043	0.0729	0.0000
10	32	0.0001	0.0200	0.0000	1.0700
12	11	0.0016	0.0435	0.0000	1.0060
12	13	0.0016	0.0435	0.0000	1.0060
13	14	0.0009	0.0101	0.1723	0.0000
14	15	0.0018	0.0217	0.3660	0.0000
15	16	0.0009	0.0094	0.1710	0.0000
16	17	0.0007	0.0089	0.1342	0.0000
16	19	0.0016	0.0195	0.3040	0.0000
16	21	0.0008	0.0135	0.2548	0.0000
16	24	0.0003	0.0059	0.0680	0.0000
17	18	0.0007	0.0082	0.1319	0.0000
17	27	0.0013	0.0173	0.3216	0.0000
19	20	0.0007	0.0138	0.0000	1.0600
19	33	0.0007	0.0142	0.0000	1.0700
20	34	0.0009	0.0180	0.0000	1.0090
21	22	0.0008	0.0140	0.2565	0.0000
22	23	0.0006	0.0096	0.1846	0.0000
22	35	0.0001	0.0143	0.0000	1.0250
23	24	0.0022	0.0350	0.3610	0.0000
23	36	0.0005	0.0272	0.0000	1.0000
25	26	0.0032	0.0323	0.5310	0.0000
25	37	0.0006	0.0232	0.0000	1.0250
26	27	0.0014	0.0147	0.2396	0.0000
26	28	0.0043	0.0474	0.7802	0.0000
26	29	0.0057	0.0625	1.0290	0.0000
28	29	0.0014	0.0151	0.2490	0.0000
29	38	0.0008	0.0156	0.0000	1.0250

Table A.5–Branch Data 39–bus/10–generators System

Type	V_i	θ_i	P_i^{d}	Q_i^{d}	P_i^{g}	Q_i^{g}	g_i^{sh}	b_i^{sh}
PQ	1.072	-9.566	0.00	0.00	0.00	0.00	0	0
PQ	1.045	-10.256	0.00	0.00	0.00	0.00	0	0
PQ	1.020	-10.744	322.00	2.40	0.00	0.00	0	0
PQ	0.987	-10.511	500.00	184.00	0.00	0.00	0	0.1
PQ	0.988	-8.767	0.00	0.00	0.00	0.00	0	0
PQ	0.990	-7.969	0.00	0.00	0.00	0.00	0	0
PQ	0.983	-10.192	233.80	84.00	0.00	0.00	0	0.2
PQ	0.983	-10.683	522.00	176.60	0.00	0.00	0	0.2
PQ	1.046	-9.757	0.00	0.00	0.00	0.00	0	0
PQ	1.014	-5.198	0.00	0.00	0.00	0.00	0	0
PQ	1.004	-6.138	0.00	0.00	0.00	0.00	0	0
PQ	1.095	-6.188	7.50	88.00	0.00	0.00	0	0.1
PQ	1.006	-6.140	0.00	0.00	0.00	0.00	0	0
PQ	0.991	-8.393	0.00	0.00	0.00	0.00	0	0
PQ	0.965	-9.743	320.00	153.00	0.00	0.00	0	0.2
PQ	0.969	-8.564	329.00	32.30	0.00	0.00	0	0.1
PQ	0.984	-9.531	0.00	0.00	0.00	0.00	0	0
PQ	0.996	-10.461	158.00	30.00	0.00	0.00	0	0.2
PQ	0.977	-2.984	0.00	0.00	0.00	0.00	0	0
PQ	0.957	-3.875	628.00	103.00	0.00	0.00	0	0.2
PQ	0.951	-6.520	274.00	115.00	0.00	0.00	0	0.2
PQ	0.951	-1.997	0.00	0.00	0.00	0.00	0	0
PQ	0.949	-1.884	247.50	84.60	0.00	0.00	0	0.1
PQ	0.970	-8.585	308.60	-92.20	0.00	0.00	0	0.1
PQ	0.981	0.084	224.00	47.20	0.00	0.00	0	0.1
PQ	0.991	-6.894	139.00	17.00	0.00	0.00	0	0.2
PQ	0.981	-9.382	281.00	75.50	0.00	0.00	0	0.2
PQ	1.000	-6.638	206.00	27.60	0.00	0.00	0	0.1
PQ	1.003	-4.801	283.50	26.90	0.00	0.00	0	0.1
PV	1.083	-7.940	0.00	0.00	250.00	161.76	0	0
SL	0.980	0.000	9.20	4.60	677.87	221.57	0	0.2
PV	1.094	3.294	0.00	0.00	650.00	206.97	0	0
PV	1.006	1.815	0.00	0.00	632.00	108.29	0	0
PV	0.956	1.888	0.00	0.00	508.00	166.69	0	0
PV	0.954	2.449	0.00	0.00	650.00	210.66	0	0
PV	0.959	7.819	0.00	0.00	560.00	100.17	0	0
PV	0.989	8.075	0.00	0.00	540.00	-1.37	0	0
PV	0.908	0.581	0.00	0.00	830.00	21.73	0	0
PV	1.069	-9.078	1104.00	250.00	1000.00	78.47	0	0.1

Table A.6–Bus Data 39–bus/10–generators System

The IEEE 68–bus/16–generators system is commonly used in power flow studies, the Table A.7 show the branch data and the Table A.8 shows the bus data of the system.

i	j	R_{ij}	X_{ij}	B_{ij}^{sh}	a_{ij}
1	54	0.0001	0.0181	0.000	1.025
2	58	0.0001	0.0250	0.000	1.070
3	62	0.0001	0.0200	0.000	1.070
4	19	0.0007	0.0142	0.000	1.070
5	20	0.0009	0.0180	0.000	1.009
6	22	0.0000	0.0143	0.000	1.025
7	23	0.0005	0.0272	0.000	0.000
8	25	0.0006	0.0232	0.000	1.025
9	29	0.0008	0.0156	0.000	1.025
10	31	0.0001	0.0260	0.000	1.040
11	32	0.0001	0.0130	0.000	1.040
12	36	0.0001	0.0075	0.000	1.040
13	17	0.0001	0.0033	0.000	1.040
14	41	0.0001	0.0015	0.000	1.000
15	42	0.0001	0.0015	0.000	1.000
16	18	0.0001	0.0030	0.000	1.000
17	36	0.0005	0.0045	0.320	0.000
18	49	0.0076	0.1141	1.160	0.000
18	50	0.0012	0.0288	2.060	0.000
19	68	0.0016	0.0195	0.304	0.000
20	19	0.0007	0.0138	0.000	1.060
21	68	0.0008	0.0135	0.255	0.000
22	21	0.0008	0.0140	0.257	0.000
23	22	0.0006	0.0096	0.185	0.000
24	23	0.0022	0.0350	0.361	0.000
24	68	0.0003	0.0059	0.068	0.000
25	54	0.0070	0.0086	0.146	0.000
26	25	0.0032	0.0323	0.531	0.000
27	37	0.0013	0.0173	0.322	0.000
27	26	0.0014	0.0147	0.240	0.000
28	26	0.0043	0.0474	0.780	0.000
29	26	0.0057	0.0625	1.029	0.000
29	28	0.0014	0.0151	0.249	0.000
30	53	0.0008	0.0074	0.480	0.000
30	61	0.0010	0.0092	0.580	0.000
31	30	0.0013	0.0187	0.333	0.000
31	53	0.0016	0.0163	0.250	0.000
32	30	0.0024	0.0288	0.488	0.000
33	32	0.0008	0.0099	0.168	0.000
34	33	0.0011	0.0157	0.202	0.000
34	35	0.0001	0.0074	0.000	0.946
36	34	0.0033	0.0111	1.450	0.000
36	61	0.0011	0.0098	0.680	0.000
37	68	0.0007	0.0089	0.134	0.000
38	31	0.0011	0.0147	0.247	0.000
38	33	0.0036	0.0444	0.693	0.000
40	41	0.0060	0.0840	3.150	0.000
40	48	0.0020	0.0220	1.280	0.000
41	42	0.0040	0.0600	2.250	0.000
42	18	0.0040	0.0600	2.250	0.000
43	17	0.0005	0.0276	0.000	0.000
44	39	0.0000	0.0411	0.000	0.000
44	43	0.0001	0.0011	0.000	0.000
45	35	0.0007	0.0175	1.390	0.000
45	39	0.0000	0.0839	0.000	0.000
45	44	0.0025	0.0730	0.000	0.000
46	38	0.0022	0.0284	0.430	0.000
47	53	0.0013	0.0188	1.310	0.000
48	47	0.0013	0.0134	0.800	0.000
49	46	0.0018	0.0274	0.270	0.000
51	45	0.0004	0.0105	0.720	0.000
51	50	0.0009	0.0221	1.620	0.000
52	37	0.0007	0.0082	0.132	0.000
52	55	0.0011	0.0133	0.214	0.000
54	53	0.0035	0.0411	0.699	0.000
55	54	0.0013	0.0151	0.257	0.000
56	55	0.0013	0.0213	0.221	0.000
57	56	0.0008	0.0128	0.134	0.000
58	57	0.0002	0.0026	0.043	0.000
59	58	0.0006	0.0092	0.113	0.000
60	57	0.0008	0.0112	0.148	0.000
60	59	0.0004	0.0046	0.078	0.000
61	60	0.0023	0.0363	0.380	0.000
63	58	0.0007	0.0082	0.139	0.000
63	62	0.0004	0.0043	0.073	0.000
63	64	0.0016	0.0435	0.000	1.060
65	62	0.0004	0.0043	0.073	0.000
65	64	0.0016	0.0435	0.000	1.060
66	56	0.0008	0.0129	0.138	0.000
66	65	0.0009	0.0101	0.172	0.000
67	66	0.0018	0.0217	0.366	0.000
68	67	0.0009	0.0094	0.171	0.000
27	53	0.0320	0.3200	0.410	0.000

Table A.7–Branch data 68–bus/16–generators System

Type	V_i	θ_i	P_i^{d}	Q_i^{d}	P_i^{g}	Q_i^{g}	g_i^{sh}	b_i^{sh}
PV	1.100	1.983	0.00	0.00	662.01	500.00	0	0
PV	1.100	-1.123	0.00	0.00	489.08	485.07	0	0
PV	1.042	-6.262	0.00	0.00	82.40	-73.70	0	0
PV	1.100	-1.076	0.00	0.00	639.02	357.06	0	0
PV	1.100	-2.303	0.00	0.00	488.82	209.10	0	0
PV	1.100	0.341	0.00	0.00	572.59	500.00	0	0
PV	1.100	1.725	0.00	0.00	454.63	368.09	0	0
PV	1.100	0.469	0.00	0.00	475.31	195.39	0	0
PV	1.100	-2.569	0.00	0.00	597.12	148.60	0	0
PV	1.066	1.495	0.00	0.00	427.50	486.41	0	0
PV	1.100	4.033	0.00	0.00	800.00	500.00	0	0
PV	1.100	-1.462	0.00	0.00	872.14	500.00	0	0
PV	0.925	-2.390	0.00	0.00	1750.00	-223.00	0	0
PV	0.800	5.064	0.00	0.00	1194.52	-34.94	0	0
PV	0.800	6.518	0.00	0.00	1113.37	-87.99	0	0
SL	0.800	0.000	0.00	0.00	1250.00	-471.79	0	0
PQ	0.960	-6.118	6000.00	300.00	0.00	0.00	0	0.5
PQ	0.858	-3.132	2470.00	123.00	0.00	0.00	0	0.4
PQ	1.100	-4.722	0.00	0.00	0.00	0.00	0	0.2
PQ	1.100	-5.892	680.00	103.00	0.00	0.00	0	0
PQ	1.069	-6.842	274.00	115.00	0.00	0.00	0	0.2
PQ	1.067	-3.325	0.00	0.00	0.00	0.00	0	0
PQ	1.089	-3.752	248.00	85.00	0.00	0.00	0	0.2
PQ	1.091	-8.481	309.00	-92.00	0.00	0.00	0	0
PQ	1.086	-4.337	224.00	47.00	0.00	0.00	0	0.2
PQ	1.100	-8.112	139.00	17.00	0.00	0.00	0	0
PQ	1.102	-9.338	281.00	76.00	0.00	0.00	0	0.2
PQ	1.100	-7.729	206.00	28.00	0.00	0.00	0	0
PQ	1.100	-6.295	284.00	27.00	0.00	0.00	0	0.2
PQ	1.031	-5.103	0.00	0.00	0.00	0.00	0	0
PQ	1.031	-4.312	0.00	0.00	0.00	0.00	0	0
PQ	1.042	-0.738	0.00	0.00	0.00	0.00	0	0
PQ	1.027	-3.409	112.00	0.00	0.00	0.00	0	0.2
PQ	0.999	-6.067	0.00	0.00	0.00	0.00	0	0
PQ	1.044	-7.914	0.00	0.00	0.00	0.00	0	0
PQ	0.987	-4.856	102.00	-19.46	0.00	0.00	0	0
PQ	1.085	-8.700	0.00	0.00	0.00	0.00	0	0
PQ	1.025	-5.475	0.00	0.00	0.00	0.00	0	0
PQ	0.955	-17.369	267.00	12.60	0.00	0.00	0	0
PQ	1.063	-8.235	65.63	23.53	0.00	0.00	0	0
PQ	0.881	3.607	1000.00	250.00	0.00	0.00	0	0.5
PQ	0.802	5.027	1150.00	250.00	0.00	0.00	0	0
PQ	0.966	-12.978	0.00	0.00	0.00	0.00	0	0
PQ	0.966	-13.252	267.55	4.84	0.00	0.00	0	0.2
PQ	1.022	-12.144	208.00	21.00	0.00	0.00	0	0
PQ	0.995	-9.077	150.70	28.50	0.00	0.00	0	0
PQ	1.062	-9.168	203.12	32.59	0.00	0.00	0	0
PQ	1.070	-9.873	241.20	2.20	0.00	0.00	0	0
PQ	0.972	-10.302	164.00	29.00	0.00	0.00	0	0
PQ	0.991	-9.887	100.00	-147.00	0.00	0.00	0	0
PQ	1.028	-12.792	337.00	-122.00	0.00	0.00	0	0
PQ	1.074	-8.672	158.00	30.00	0.00	0.00	0	0
PQ	1.040	-6.128	252.70	118.56	0.00	0.00	0	0
PQ	1.062	-3.410	0.00	0.00	0.00	0.00	0	0
PQ	1.059	-7.573	322.00	2.00	0.00	0.00	0	0
PQ	1.031	-8.183	200.00	73.60	0.00	0.00	0	0
PQ	1.020	-7.273	0.00	0.00	0.00	0.00	0	0
PQ	1.019	-6.924	0.00	0.00	0.00	0.00	0	0
PQ	1.015	-8.009	234.00	84.00	0.00	0.00	0	0.5
PQ	1.015	-7.959	208.80	70.80	0.00	0.00	0	0.4
PQ	1.008	-5.571	104.00	125.00	0.00	0.00	0	0.3
PQ	1.018	-7.152	0.00	0.00	0.00	0.00	0	0
PQ	1.018	-7.089	0.00	0.00	0.00	0.00	0	0
PQ	0.928	-7.334	9.00	88.00	0.00	0.00	0	0
PQ	1.020	-7.426	0.00	0.00	0.00	0.00	0	0
PQ	1.034	-8.099	0.00	0.00	0.00	0.00	0	0
PQ	1.061	-9.312	320.00	153.00	0.00	0.00	0	0
PQ	1.087	-8.380	329.00	32.00	0.00	0.00	0	0.5

Table A.8–Bus Data 68–bus/16–generators System

APPENDIX B. REDUCE NETWORK CALCULATION

For the contingency C1 and as seen in the Figure 3.2, after the load flow calculation, the loads are converted in equivalent admittances:

$$Load\ A: Y_{L5} = 1.2610 - j0.5044$$

$$Load\ B: Y_{L6} = 0.8777 - j0.2926$$

$$Load\ C: Y_{L8} = 0.9690 - j0.3391$$

The generator internal voltages and their initial angles are:

$$E_1\angle\delta_1 = 1.0566\angle 2.2717°$$

$$E_2\angle\delta_2 = 1.0502\angle 19.7315°$$

$$E_3\angle\delta_3 = 1.0170\angle 13.1752°$$

The matrix values are shown in the next tables:

Node	1	2	3	4	5	6	7	8	9
1	-j8.445	0	0	j8.445	0	0	0	0	0
2	0	-j5.485	0	0	0	0	j5.48	0	0
3	0	0	-j4.168	0	0	0	0	0	0
4	j8.445	0	0	3.30-j30.39	-1.36+j11.60	-1.94+j10.51	0	0	j4.16
5	0	0	0	-1.36+j11.60	3.81+j17.84	0	-1.18+j5.97	0	0
6	0	0	0	-1.94+j10.51	0	4.10+j16.13	0	0	-1.28+j5.58
7	0	j5.485	0	0	-1.18+j5.97	0	2.80-j24.93	-1.61+j13.69	0
8	0	0	0	0	0	0	-1.61+j13.69	3.74-j23.64	-1.15+j9.78
9	0	0	j4.168	0	0	-1.28+j5.58	0	-1.15+j-.78	2.43-j19.25

Table B.1 – Y matrix on pre-fault network

Node	1	2	3	4	5	6	7	8	9
1	-j8.445	0	0	j8.445	0	0	0	0	0
2	0	-j5.485	0	0	0	0	0	0	0
3	0	0	-j4.168	0	0	0	0	0	0
4	j8.445	0	0	3.30-j30.39	-1.36+j11.60	-1.94+j10.51	0	0	j4.16
5	0	0	0	-1.36+j11.60	3.81+j17.84	0	0	0	0
6	0	0	0	-1.94+j10.51	0	4.10+j16.13	0	0	-1.28+j5.58
7	0	0	0	0	0	0	0	0	0
8	0	0	0	0	0	0	0	3.74-j23.64	-1.15+j9.78
9	0	0	j4.168	0	0	-1.28+j5.58	0	-1.15+j-.78	2.43-j19.25

Table B.2 – Y matrix on fault network

Node	1	2	3	4	5	6	7	8	9
1	-j8.445	0	0	j8.445	0	0	0	0	0
2	0	-j5.485	0	0	0	0	j5.48	0	0
3	0	0	-j4.168	0	0	0	0	0	0
4	j8.445	0	0	3.30-j30.39	-1.36+j11.60	-1.94+j10.51	0	0	j4.16
5	0	0	0	-1.36+j11.60	3.81+j17.84	0	0	0	0
6	0	0	0	-1.94+j10.51	0	4.10+j16.13	0	0	-1.28+j5.58
7	0	j5.485	0	0	0	0	1.61+j18.95	-1.61+j13.69	0
8	0	0	0	0	0	0	-1.61+j13.69	3.74-j23.64	-1.15+j9.78
9	0	0	j4.168	0	0	-1.28+j5.58	0	-1.15+j-.78	2.43-j19.25

Table B.3 – Y matrix on post-fault network

Using the Kron reduction, the obtained reduced network to the three stages of study are:

Node	**1**	**2**	**3**
1	0.846-j2.988	0.287+j1.513	0.210+j1.226
2	0.287+j1.513	0.420-j2.724	0.213+j1.088
3	0.210+j1.226	0.213+j1.088	0.277-j2.368

Table B.4 – Y matrix on pre-fault reduced network

Node	**1**	**2**	**3**
1	0.657-j3.816	0.000+j0.000	0.070+j0.631
2	0.000+j0.000	0.000-j5.486	0.000+j0.000
3	0.070+j0.631	0.000+j0.000	0.174-j2.796

Table B.5 – Y matrix on fault reduced network

Node	**1**	**2**	**3**
1	1.181-j2.229	0.138+j0.726	0.191+j1.079
2	0.138+j0.726	0.389-j1.953	0.199+j1.229
3	0.191+j1.079	0.199+j1.229	0.273-j2.342

Table B.6 – Y matrix on post-fault reduced network